Thalamocortical Innervation of GABAergic Interneurons in Mouse Primary Vibrissal Somatosensory Cortex

PhD Thesis

in partial fulfilment of the requirements
for the degree Dr. rer. nat.
in the Neuroscience Program
at the Georg August University Göttingen,
Faculty of Biology

submitted by

Michael Daan Feyerabend

born in

Munich, Germany

2019

Abstract

Interneurons utilizing gamma-aminobutyric acid (GABA) as primary neurotransmitter are thought to play a key role in neocortical processing. Their striking diversity has been in focus of numerous studies for decades. However, with the exception of fast spiking cells, their possible innervation by thalamocortical afferents (TCAs) has rarely been looked at systematically. This project investigates the innervation of somatostatin (SST) and vasoactive intestinal polypeptide (VIP) expressing cells throughout all layers of the mouse barrel cortex by its two dominant thalamic input sources: the ventral posteromedial nucleus of the thalamus (VPM) and the medial part of the posterior thalamic nuclear group (POm). Understanding how GABAergic interneurons are recruited by thalamocortical circuits is crucial to understand their overall role in neocortical processing. Our aim is thus to characterize the extension of inputs in a cell type and layer specific manner assessing efficacy and other synaptic properties. We use optogenetics combined with in-vitro whole cell recordings of animals aged P42 – P58. Channelrhodopsin-2 (ChR2) expression is achieved by stereotactic injections of an adeno-associated virus. Our data show a strong and almost ubiquitous thalamic innervation of VIP cells by both POm and VPM across all layers. Input of SST cells is comparatively weak, but also occurs frequently throughout the cortical depth. Cell type identity has at best a minor influence on the likelihood of receiving direct input from either nucleus. Two findings stand out: 1) VIP cell recruitment, which was thought to be predominantly driven by corticocortical or neuromodulatory inputs is also possible by bottom-up circuits. 2) SST cells are also innervated by POm afferents.

A mi cielo querido,

Michelle Jiménez Sosa,

de repente convertiste mi vida en un cuento,

y el sueño sigue,

te amo.

”We learn who we are in practice not in theory -by testing reality, not looking inside”

Herminia Ibarra

Professor of Organizational Behavior at London Business School

Declaration

I, Michael Feyerabend, hereby certify that the present thesis has been written independently and with no other sources and aids than quoted. All results presented here were the fruit of my own labor unless stated otherwise.

.....
Gøttingen, 31.09.19

Abbreviations

Acronym	Explanation
4-AP	4-aminopyridine
5-HT	5-hydroxytryptamine (also referred to as serotonin)
AAV	adeno-associated virus
ACSF	artificial cerebral spinal fluid
AHP	afterhyperpolarization
AP	action potential
BS	burst spiking
CA	continuous adapting
CB	calbindin
CC	current clamp
CCK	cholecystokinin
CF	correction factor
ChR2	Channelrhodopsin-2
CR	calretinin
DAPI	4,6-diamidino-2-phenylindole
EPSP	excitatory postsynaptic potential
FS	fast spiking
GABA	gamma-aminobutyric acid
GAD	glutamic acid decarboxylase
HC	hippocampus
IQR	interquartile range
IS	irregular spiking
ISI	interspike interval

Acronym	Explanation
L	layer
LAMP	lysosome associated membrane protein
LED	light-emitting diode
LTS	low threshold spiking
MC	Martinotti cell
NA	numerical aperature
PB	phosphate buffer
PC	pyramidal cell
PFA	paraformaldehyde
POm	medial part of the posterior thalamic nuclear group
PV	parvalbumin
RNA	ribonucleic acid
RS	regular spiking
RSNP	regular spiking non pyramidal
SST	somatostatin (in the literature occasionally referred to as SOM)
TB	Tris buffer
TBS	Tris-buffered saline
TBST	Tris-buffered saline with Triton X 100
TCA	thalamocortical afferent
tdTomato	tandem dimer Tomato
TTX	tetrodotoxin
VC	voltage clamp
VIP	vasoactive intestinal polypeptide
VPM	ventral posteromedial nucleus of the thalamus
YFP	yellow fluorescent protein

Contents

Introduction

One of the major goals of neuroscience is to understand how information is represented and processed in the central nervous system. The cerebral cortex has a prominent role in this context, since it is the principal material constituent for higher cognitive functions like conscious perception, attention, working memory, decision making and many more. For more than 100 years modern science has tried to further illuminate and understand the structural particularities of the cortex to gain insight in the physiological mechanism(s) of the mind. Pioneering work by early neuroanatomists like Nissl, Ramon y Cajal, Brodmann, von Economo, to name a few, uncovered a daunting amount of diversity and complexity on the cellular and histological scale, which is unparalleled in the human body. A fundamental tenet of neuroscience is that these vastly different components of cortex reflect an extraordinary division of labor required for proper mental functioning. Comparisons across species and anatomical areas, for example, suggest that an increase in cognitive capacity goes in parallel with an expansion and stronger differentiation of cortex, which is also accompanied by more cell diversity. Sorting and disentangling these cells into meaningful or otherwise useful categories, types or components is an ongoing effort.

1.1 Historical overview and state of the field

1.1.1 First steps in understanding neuronal diversity in the neocortex

Anatomical properties of single cells (i.e. shape, extent of neurites, etc.), also referred to as morphology, were the first manifest features used to distinguish neurons from one another. After the establishment of new staining techniques in the second

half of 19th century, researchers soon realized that cortical neurons can be divided into projection cells – also called pyramidal cell (PC) due to their triangular shaped somata– with an axon that extents beyond the local cell assembly and interneurons whose postsynaptic targets are confined to the local network (Ramon y Cajal, 1899; Ramón y Cajal, 1911). This distinction has further weight by the fact that interneurons generally have a dendritic tree with substantially less protrusion known as spines. Even though interneurons make up a minority of cortical neurons, they seem to reach a diversity much greater than the numerous PCs. Consequently, they have been in the field's focus from early stages and following generations of neuroanatomists kept adding to their description (Lorente de Nó, 1933, 1934; O'Leary, 1941; Sholl, 1953). We know now, that interneurons and projecting cells are not only distinct in their morphology, but their physiological effect on their postsynaptic partners is profoundly different. With some minor exceptions (e.g. spiny stellate cells in LIV of some primary sensory cortices), PCs mediate excitation, whereas interneurons have an inhibitory effect. This relationship was already suspected by researchers in the early 1960s: Andersen et al. (1964), for example, accurately predicted that basket cells of the hippocampus (HC) mediate feed-forward inhibition. In addition, early electronmicroscopy suggested that symmetric synapses, rightfully thought to be inhibitory, are made by interneurons (Colonnier, 1964, 1965). Around the same time, gamma-aminobutyric acid (GABA) was discovered to be the key inhibitory neurotransmitter in the cortex (Krnjević and Phillis, 1963). Immunohistochemistry stainings against the gamma-aminobutyric acid (GABA) synthesizing enzyme glutamic acid decarboxylase (GAD), ultimately confirmed the inhibitory nature of sparsely and aspiny interneurons in various mammals (Ribak, 1978; Hendrickson et al., 1981). Nowadays, when referring to the cortex the terms interneuron, GABAergic and aspiny cell are often used interchangeably, even though these features are conceptually independent from each other.

The field of neuronal diversity progressed steadily by expanding into the domains of neuronal biochemistry and electrophysiology. The investigation of intrinsic electrical properties of neurons was rendered possible by the use of intracellular recordings pioneered by Ling and Gerard (1949) and subsequently applied in the central nervous

system in the living cat spinal chord (Brock et al., 1952; Coombs et al., 1955). Similar techniques and approaches were applied to the neocortex in the subsequent years (Li and Jasper, 1953; Creutzfeldt et al., 1964). It became apparent that neurons differ in various intrinsic properties such as their sensitivity to electrical stimulation, action potential (AP) shape, presence and shape of afterhyperpolarizations (AHPs) and accommodation of spiking frequency, which reflects differences in features of the cell membrane like the extension of its surface and ion channel composition. For example, Mountcastle et al. (1969) made the observation of cells with ”thin” spikes (the field later adopted the term fast spiking[fast spiking]), which they rightly attributed to interneurons. An important methodological innovation in this context was the use of the acute in-vitro slice preparations (first established for HC and later adopted for neocortex [Skrede and Westgaard, 1971; Schwartzkroin and Prince, 1976]). Preparations were easier to obtain and maintain, while neurons became more accessible. This innovation led to the detailed description of different firing patterns and the pharmacological dissection of underlying ion channels (Ogawa et al., 1981; Connors et al., 1982; McCormick et al., 1985). In addition, in-vitro investigations made it possible to relate electrophysiology to morphological identified types, visualized by intracellular dyes (Gutnick and Prince, 1981; Horikawa and Armstrong, 1988). Later on, sharp electrodes were replaced by the whole-cell patch-clamp technique (Hamill et al., 1981), which allowed selective targeting of cells with differently shaped somata. This innovation made it possible to avoid recording from the abundant excitatory cells. Another major advancement was the development of better staining techniques relying on the binding by antibodies (Coons et al., 1941). This technique enabled stainings of cells according to their protein expression like utilizing the inhibitory neurotransmitter GABA as mentioned before. The creation of very specific and inexhaustible antibodies, like via the hybridoma fusion technique, revealed a remarkable diversity in antigens, specific to varying groups of neurons (McKay and Hockfield, 1982). ”Marker” proteins for staining different cell populations were established. Obvious candidates were neurotransmitters known to be synthesized in the cortex like acetylcholine (Eckenstein and Thoenen, 1982). But also many functionally obscure secretory peptides were found to stain different sets of neocortical neurons: for example, vasoactive intestinal polypeptide (VIP, [Larsson et al.,

1976; Fuxe et al., 1977]), somatostatin (SST, [Parsons et al., 1976]), cholecystokinin (CCK, [Straus et al., 1977]). These populations are predominantly GABAergic; some of them overlapping, but each having a unique distribution (Hendry et al., 1984; Kosaka et al., 1987).

1.1.2 Major breakthroughs and establishment of three main subpopulations

Observations by different disciplines converged into major breakthroughs, starting the second half of 1980s. McCormick et al. (1985) confirmed that neocortical FS cells are sparsely spiny GABAergic interneurons and not PCs. Soon after, it was shown that the marker parvalbumin (PV), a calcium buffer protein, is expressed in a high fraction of GABAergic interneurons (Celio, 1986). One year later, Kawaguchi et al. (1987) were able to tie together traits in domains of biochemistry, physiology and anatomy for the first time and showed that FS basket cells of the HC are positive for PV. In fact, the co-occurrence of PV and the FS phenotype turned out to be very robust and holds true in various anatomical areas and species (see, for example, Zaitsev et al. [2005] in non-human primates). From this fact it can be inferred that PV positive chandelier cells (Szentágothai, 1975; DeFelipe et al., 1989) also must be of the FS class, which was later confirmed (Buhl et al., 1994; Kawaguchi, 1995). Other interneuron populations came into focus, in the hope to find similar cohesive groups. Another calcium buffer protein, calbindin (CB), was found to be present in an almost non-overlapping set of interneurons (Hendry et al., 1989; Celio, 1990; van Brederode et al., 1991). Electrophysiological investigations associated them with an unique set of properties called low threshold spiking (LTS), which is characterized by a depolarized resting membrane potential, a small rheobase and rebound spiking upon hyperpolarizing current injections (Kawaguchi, 1993). In addition, they showed firing patterns previously associated with excitatory cells. Namely, burst spiking (BS), which is characterized by multiple spikes at threshold stimulation, and regular spiking, hence these interneurons were called regular spiking non pyramidal (RSNP, [Kawaguchi and Kubota, 1996; Cauli et al., 2000; Wang et al., 2004; Karagiannis et al., 2009]). In most species there is a consider-

able overlap between cells positive for CB and SST, another marker that barely colocalizes with PV (Rogers, 1992; Kawaguchi and Kubota, 1996; Kosaka et al., 1987). Furthermore, they both are associated with the Martinotti cell (MC) morphology (Martinotti, 1889; Wahle, 1993; Condé et al., 1994; Kawaguchi and Kubota, 1996; Wang et al., 2004). Eventually, a third non-overlapping population of cells with shared features emerged: a group of vertically oriented bipolar or bitufted interneurons. These cells commonly express VIP and are also associated to another calcium binding protein, called calretinin (CR, [Connor and Peters, 1984; Jacobowitz and Winsky, 1991; Rogers, 1992; Condé et al., 1994]). Their smaller numbers and delayed momentum in recognizing them as a distinct category, led to fragmented or late characterizations (Kawaguchi, 1995; Kawaguchi and Kubota, 1996; Cauli et al., 1997; Porter et al., 1998; Cauli et al., 2000). Their firing pattern has also been described as RSNP (Kawaguchi, 1995; Kawaguchi and Kubota, 1996; Cauli et al., 1997; Karagiannis et al., 2009) as well as BS (Kawaguchi and Kubota, 1996; Karagiannis et al., 2009). Some studies gave them the unique description of irregular spiking (IS), which is marked by strong adaptation and variable interspike intervals (ISIs, [Cauli et al., 1997; Porter et al., 1998]).

The two last mentioned subpopulations of GABAergic interneurons are not as cohesive as for the PV-FS-Chandelier/basket cells, which is also reflected in their delineation by respective markers. Their firing patterns show a greater diversity and appropiate markers can deviate between species. Furthermore, there are many types of interneurons, which are not associated to the three aforementioned groups, but yet have a claim on being part of an exhaustive taxonomy. They were also described electrophysiologically: prominent examples are the late spiking neurogliaform and other cells close to the pial surface (Kawaguchi, 1995; Hestrin and Armstrong, 1996; Chu et al., 2003). The field progressed massively with the advent of modern molecular biology. Genetic manipulations, pioneered and mastered in mice, enabled targeting and manipulation of neurons in living tissue. The mouse has become the most popular model organism in biomedical research and, henceforth, if not stated specifically otherwise, this section refers to the condition in the mouse. This caveat applies particularly in regard to markers. Mice, show a considerable collocalization of SST and CR due to CR-positive MCs

(Xu et al., 2006); an important difference that has not been found in the phylogentically close rats (Gonchar and Burkhalter, 1997). Consequently, SST and VIP are used as markers of choice for the cell populations introduced in the previous paragraph. The generation of transgenic lines (like Oliva et al. [2000]; Tamamaki et al. [2003]; Chattopadhyaya et al. [2004]; Ma et al. [2006]) allowed the characterization of more infrequent interneurons and created new insights in diversity, connectivity and function of known subpopulations. A more recent addition to the methodological tool box was the utilization of the cre-lox system, providing many driver lines for conditional expression of fluorescent or otherwise useful proteins (Srinivas et al., 2001; Hippenmeyer et al., 2005; Taniguchi et al., 2011). Hence, there has been an explosion of papers investigating interneurons in the last 20 years and the rest of the subsection can only refer to most pertinent developments. Noteworthy here, are two new distinct types in the SST cell population: first, there has been the description of a non-MC (nMC) with similarities to the FS phenotype (Ma et al., 2006; Xu et al., 2013). Besides that, a long range projecting GABAergic cell, expressing the neuronal version of nitric oxide synthase, has been described (Tomioka et al., 2005; He et al., 2016). In addition, interneurons not belonging to either the PV or SST population were found to form a third very heterogeneous group, that also contains VIP cells with a common developmental origin from the caudal ganglionic eminence (Miyoshi et al., 2010). Furthermore the 5-hydroxytryptamine (5-HT) receptor subunit 3A was found to be a genetic marker signifying this lineage and a comprehensive taxonomy of neocortical GABAergic interneurons was achieved (Lee et al., 2010; Vucurovic et al., 2010). Additional efforts were made to improve the taxonomy by further differentiation, which led to the question of how to define a cell type (see the Petilla convention, Ascoli et al. [2008]). However, until now, no consensus has been reached on appropriate criteria for a newly introduced cell type (see DeFelipe et al. [2013], for example, for morphological categorization). The recent years provided a plethora of studies introducing more and more morphological and physiological distinctions (see examples like Xu et al. [2006]; Li and Huntsman [2014]; Jiang et al. [2015]; Schuman et al. [2019]). High-throughput strategies are the current peak of this development: Markram et al. (2015), for example, report of 9 morphological and 10 electrophysiological types for inhibitory cells in rat somatosensory cortex; whereas

in mouse visual cortex even 19 and 13 of the aforementioned types have been distinguished (Gouwens et al., 2019). It is an open question which features on which level of abstraction will be helpful in generating insights into neocortical function. Many neuronal properties are likely acquired by random or otherwise opaque processes during genesis and maturation. These characteristics must be inherently variant with distributions that are continuous or with fuzzy broders. Transcriptomic analysis of single cells, for example, seemed a promising tool in understanding cellular diversity (Tasic et al., 2016), but has not led to improved cell markers. Most protein expression profiles and resulting cell traits might lack the required stability for a taxonomic classification due to changes according to demands of the network. The best results in specifically targeting a cohesive set of cells has been achieved by reporter systems using either dual recombination approach (He et al., 2016; Paul et al., 2017).

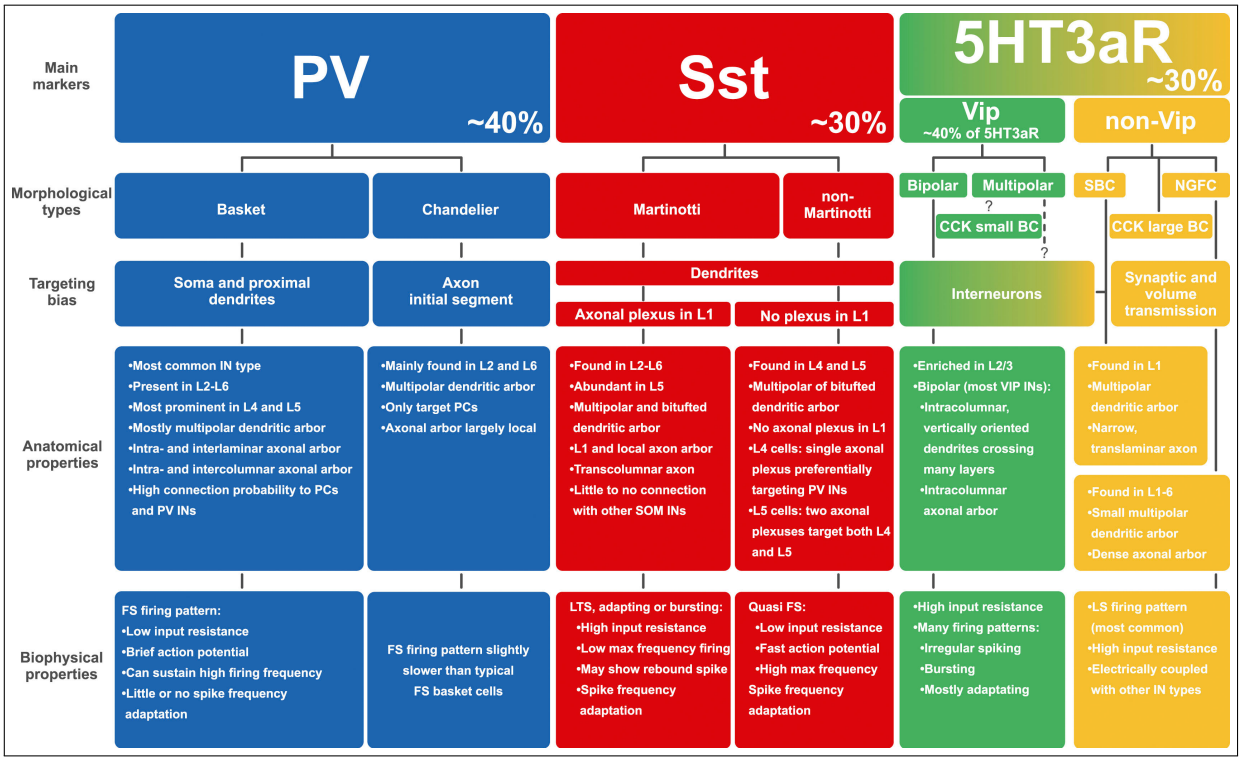

Figure 1.1. Current taxonomy of murine neocortical GABAergic interneurons.
Three big subpopulations can be identified by the expression of PV, SST and VIP, which can be further subdivided. Diversity of cells derived from caudal ganglionic eminence (green and yellow) is poorly understood, but VIP cells form the most coherent and distinct subgroup. A summary of the anatomical and electrophysiological properties of the subpopulations is given. Not all, but most of them, are referred to in this work. Targeting bias is going to be discussed later in 1.1.4; adapted from Tremblay et al. (2016).

1.1.3 Barrel cortex as a model system: thalamic afferents, intracortical circuitry and function

Since the inception of modern neuroscience, the neocortex has been a prominent object of investigation. As in the field of cell diversity, anatomical observations led the way in understanding physiology. The neocortex can be divided into horizontal segments, also called layers (Ls), distinguishable by cellular density and composition (Ramón y Cajal, 1898). The cytoarchitectonic make-up, systematically described by Brodmann (1909) and von Economo (1927), changes throughout neocortex at the expense and respective gain of different layers. This diversification strongly suggests a considerable amount of functional division or specialization and is in line with the ”localization theory”, which emerged out of observations from cortical lesions of clinical cases throughout the 19th century. An excellent example of this specialization are the primary sensory cortices. The thalamus dorsalis is the major relay of afferent nerve fibers to neocortex. Early anatomical evidence demonstrated, that some thalamic nuclei, tied to a specific modality, project into restricted cortical areas, where they predominantly terminate in a pronounced LIV (Lorente de Nó, 1938). Consequently, these projections were prime candidates for passing information from the senses into the neocortex. Physiological experiments in the sensory systems of cats and monkeys confirmed this relationship functionally. Moreover, the evoked responses were clustered in a stereotypical topographic fashion; representing the perceptual space of the respective modality (Morison and Dempsey, 1941; Marshall et al., 1941; Talbot and Marshall, 1941). For example, mechanically stimulating the front paw only elicits primary responses in cells of a small area and nowhere else. This line of research was continued by Hubel and Wiesel (1962) in the visual and Mountcastle (1957) in the somatosensory system. These studies led to a much better understanding of the functional organization of cortex. The detailed mapping of cellular responses to certain stimulus features, also refereed to as tuning, led to the development of an important concept known as the ”cortical column”. Neurons within a certain extend of cortex have similar tuning. Hence, it has been postulated, that cortex is comprised of many parallel vertical modules, each of which being functionally specialized in processing a certain

fraction or feature of the stimulus (Mountcastle, 1957).

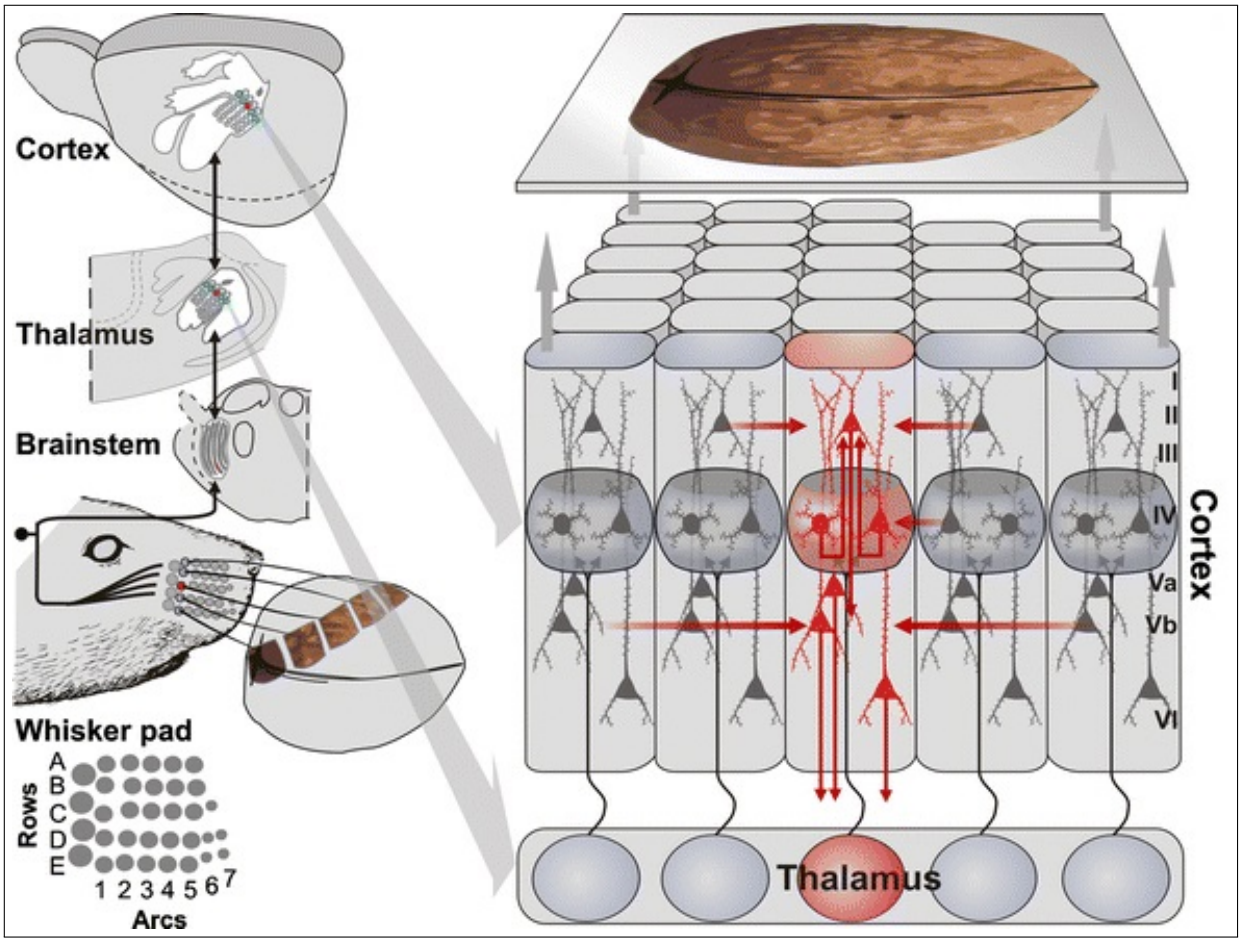

Figure 1.2. Schematic explaining the rodent vibrissal somatosensory pathway
Sensory information obtained from the whiskers of the animal is relayed through brainstem and thalamus to the primary vibrissal somatosensory cortex. Dense patches of neuropile in LIV, also called ”barrels”, delineate the cortical column. Each module can be assigned to one primary whisker (exemplified by red coloring of a single module) and the barrel field as a whole is a somatotopic representation of the whisker pad. This relationship is derived by a highly parallel labeled line design of the sensory pathway. Basic aspects of intracolumnar circuitry are discussed at the end of the subsection; adapted from Schubert et al. (2007).

The primary vibrissal somatosensory cortex of rodents first described by Woolsey and Van der Loos (1970) soon became a popular model system to understand and refine the concept of the cortical column and its anatomy. It is marked by dense patches of tissue in LIV. Their particular shape is reminiscent to barrels and gives the area its second name. Tangential sectioning of the flattened cortex reveals, that the barrel field contains a topographic representation of the whiskers on the animals snout with each

barrel receiving a discrete portion of thalamic afferents (Killackey, 1973). Furthermore, the strict separation of downstream sensory inputs was also found to be present in its main thalamic relay nucleus, the ventral posteromedial nucleus of the thalamus (VPM), and further downstream in the brain stem (Van Der Loos, 1976; Belford and Killackey, 1979; Veinante and Deschênes, 1999). Naturally, thalamocortical afferents (TCAs) of the VPM, as conveyor of sensory information, branch heavily in LIV and to a lesser extent in upper LVI (Jensen and Killackey, 1987; Bernardo and Woolsey, 1987). In addition, some studies also report labeling in LI (see for example Bernardo and Woolsey [1987] or Lu and Lin [1993]). Next to the well-organized and already described pathway, the medial part of the posterior thalamic nuclear group (POm) was found to be another considerable, but ambigious thalamic projection (Koralek et al., 1988) : for one, it receives several inputs from sensory brainstem nuclei (Peschanski, 1984; Chiaia et al., 1991; Veinante and Deschênes, 1999), but responds surprisingly poorly to whisker stimulation (Diamond et al., 1992). Furthermore, it has been implicated in whisker movement and receives stronger corticofugal input from sensory and motor areas (Sharp, 1984; Hoogland et al., 1987). In addition, it targets several other cortical areas and individual POm projections are suggested to be more heterogeneous than lemniscal fibers (Zhang and Deschenes, 1998; Ohno et al., 2012). There have been reports of other sensory pathways, which have only been observed in rats so far and are not further discussed here (Pierret et al., 2000; Yu et al., 2006). The projections of both nuclei have a nearly complementary profile in a multiple sense (see 1.3): not only are fibers from the POm innervating LVa and LI (Herkenham, 1980; Koralek et al., 1988; Lu and Lin, 1993; Wimmer et al., 2010), but they also reach into the less dense neuropile between the barrels also known as the septum (Kim and Ebner, 1999). Furthermore, POm is relaying multi-whisker information, whereas VPM cells are naturally tuned to their primary whisker (Veinante and Deschênes, 1999). This duality of TCAs is found in other modalities as well. Already Lorente de Nó (1938) made the conceptual distinction between ”specific” projections, represented by the VPM, in contrast to ”non-specific” ones, which the POm can be attributed to. However, synapses of the respective nuclei do not show differences on the ultrastructural level (Lu and Lin, 1993).

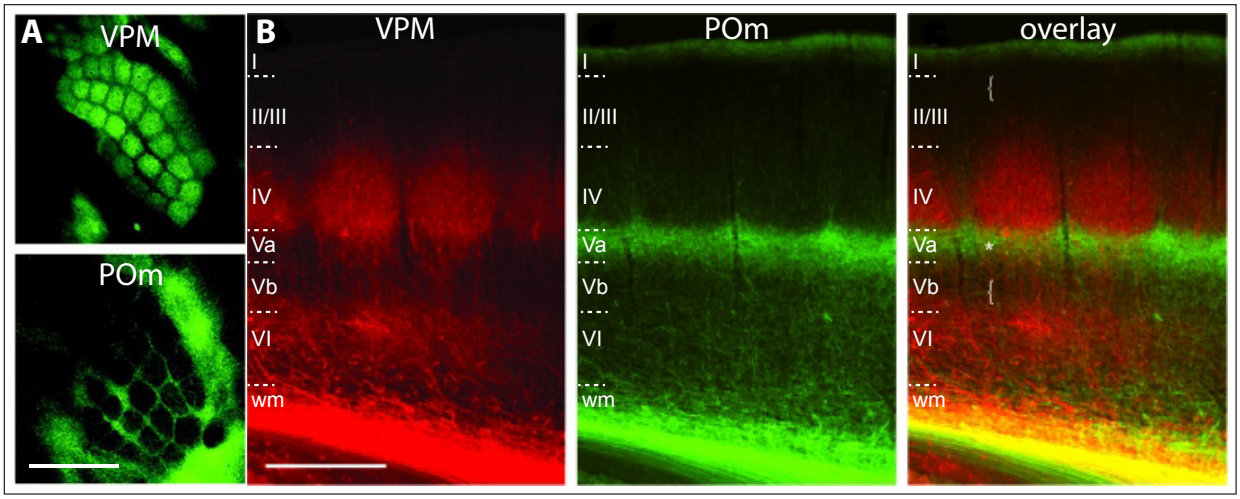

Figure 1.3. Complementary innervation of barrel cortex by VPM and POm
Depictions of different tracings illuminating the two thalamocortical projection patterns. **A** Tangential sections through the barrel field. The upper image is obtained from a VPM injection, whereas the lower one is from POm. Barrels are clearly visible in both, but with an inversion in the signal profile; scale bar = 1 mm **B** Panel of images with coronal orientation. TCAs target different layers: VPM fibers are most abundant in LIV and the LVb/LVI border, whereas POm projections show prominent signal in LI and LVa. White brackets indicate segments of sparse thalamic innervation, asterisk indicates potential overlap between the two pathways at the LIV/LVa border; scale bar 500 µm adapted from Wimmer et al. (2010).

The straightforward structure of the barrel cortex also encouraged further mapping of intracortical circuitry. As mentioned before, the barrel in LIV has been considered as the first processing unit of incoming sensory information. Its dense lemnsical innervation is reflected in an isolation of local extra-barrel inputs. Dendrites of LIV excitatory cells, for example, have a strong bias towards the barrel and the high connectivity between cells drops steeply at the septum (Simons and Woolsey, 1984; Lübke et al., 2000; Petersen and Sakmann, 2000; Staiger et al., 2004a). Interestingly, even in LIV the thalamocortical synapses are only a minority of the excitatory connections (Lu and Lin, 1993). This observation led to the believe that, next to further processing, LIV also has to act as an amplifier of sensory signals (Feldmeyer et al., 1999), which has been challenged more recently (Bruno and Sakmann, 2006). As the next step of processing, these signals are then supposed to be relayed to neurons of LII/III (Feldmeyer et al., 2002). This activity is then passed on further to infragranular layers (Thomson et al., 2002), which are thought of as the output compartment of the cortical column. They contain a high fraction of PCs that project subcortically (Hattox and Nelson, 2007).

The sequential flow of excitation and its underlying connectivity is also known as the cannonical microcircuit, which has been observed across several modalities and mammalians. The most prominent work in this context was done by Douglas and Martin (1991) in the cat visual cortex.

Tuning and receptive fields revealed by whisker stimulation in-vivo was done in a similar manner to earlier work mentioned before (Welker, 1976; Simons, 1978). However, it was unclear, how whisking sensation can best be described and encoded in more abstract but meaningful features. Hence, various means of stimulation have been used to map responses in cortical and thalamic cells (Simons and Carvell, 1989; Brecht and Sakmann, 2002; Wilent and Contreras, 2005). Many response features like latency of suprathreshold events or excitatory postsynaptic potentials (EPSPs) correlate well with the lemniscal projection pattern (Armstrong-James et al., 1992; Zhu and Connors, 1999). In addition, in-vivo dual recordings revealed that cells in infragranular cortical layers are also directly activated by the VPM with latencies comparable to LIV cells (Constantinople and Bruno, 2013). These layers also harbor cells, which show a substantial increase of their firing rate, but individually do not seem to be driven by conventional stimulus features (de Kock and Sakmann, 2009). Activity in LII/III, on the other hand, is sparse and less driven by sensory stimulation, while subthreshold responses retain the overall tuning of the column (Brecht et al., 2003; Kerr et al., 2007; de Kock and Sakmann, 2009). The lemniscal and paralemniscal pathway seem to encode different stimulus features when a more naturalistic stimulation is used (Ahissar et al., 2000). Intracortical circuitry suggests that the two pathways are also processed separately within the cortical column (Bureau et al., 2006). In this line of research, Jouhanneau et al. (2014) identified a subpopulation of LII/III cells, which can be driven by POm fibers and strongly respond to multi-whisker stimulation in a distinct manner. More recently, the integrative function of POm was given more focus: Groh et al. (2013) showed it to receive additional cortical feedback in vivo. Furthermore, Urbain et al. (2015) achieved first recordings in awake and behaving mice, while monitoring whisking and cortical state. Their data suggests that POm is much less driven by sensory input as previously thought.

1.1.4 Possible diversity in neocortical interneuron function

A self-evident function of inhibition is the prevention of runaway cortical activity. Considering the massive recurrent connectivity and various afferents of the neocortex, this task has to be particularly challenging. Besides, inhibition has also been implicated to have a more direct role in processing: sculpting or sharpening activity patterns of excitatory cells (Morrone et al., 1982; Wehr and Zador, 2003). A delicate mismatch of inhibition and excitation, in either time and strength, is thought to enable more effective processing with a higher dynamic range. Indeed, excitation is readily and consistently accompanied by correlated inhibition be it due to sensory stimulation or spontaneous activity (Wehr and Zador, 2003; Okun and Lampl, 2008; Haider et al., 2013; Xue et al., 2014). To serve the mentioned functions, interneurons would require to be more broadly tuned. Many early in-vivo studies are in line with these concepts. FS are reported to respond with less selectivity in their respective modality (Simons, 1978; Bruno and Simons, 2002; Wu et al., 2008), which was later also shown in PV cells (Ma et al., 2010; Hofer et al., 2011; Li et al., 2015) and in some cases for GABAergic cells in general (Sohya et al., 2007; Kerlin et al., 2010). Furthermore, Bock et al. (2011) suggested that convergent inputs by differently tuned excitatory cells are the underlying structural basis for broader receptive fields in interneurons. Indeed, both PV and SST cells are well-connected to the local network, with little preference in regard of both output and input (Packer and Yuste, 2011; Fino and Yuste, 2011; Inan et al., 2013). PV cells seem to be particularly unselective in their targeting, having synapses to others of their kind and even themselves (Tamás et al., 1997; Bacci et al., 2003), whereas SST cells do not seem to be connected to each other (Beierlein et al., 2003; Pfeffer et al., 2013). The PV and SST populations are thought to have different roles in inhibiting the local network. First of all, they are known to target different subcellular domains of their postsynaptic excitatory cells: with PV cells having a more direct effect on AP generation by targeting the soma (Kawaguchi and Kubota, 1993), whereas the ascending axon of MCs hints at inhibitory control of inputs at the distal dendrite (Murayama et al., 2009). In addition, simultaneous recordings in-vitro have revealed differences in functional circuitry and dynamics of synaptic input (Thomson et al., 1996; Markram et al., 1998; Gupta et al., 2000). It was shown that higher frequency inputs to FS/PV

cells are depressing, but less so than synapses between excitatory cells (Reyes et al., 1998; Galarreta and Hestrin, 1998). EPSPs onto LTS/SST cells, on the other hand, facilitate (Gupta et al., 2000; Silberberg and Markram, 2007). These findings hint at how the inhibition mediated by the two cell types might differ. Two different delivery mechanisms of inhibition are distinguished: for one, feed-forward inhibition keeping excitation by distant afferents like sensory input in check and lateral inhibition dampening recurrent activity of the local network. PV seem to provide fast and temporal precise inhibition, being more associated with feedforward pathways. Whereas SST cells, given a more sustained stimulation, are powerful inhibitors of local excitatory cells (Silberberg and Markram, 2007; Kapfer et al., 2007; Berger et al., 2009). Furthermore, SST cells in the barrel field are reported to be inhibited by sensory stimulation, suggesting an antagonistic relationship to feedforward pathways (Gentet et al., 2012). More recent in-vivo studies investigated how stimulating the two populations effects tuning of excitatory cells, but showed mixed results (Wilson et al., 2012; Atallah et al., 2012; Lee et al., 2014). There is also an increasing amount of evidence, that PV cell connectivity allows the formation of specialized subnetworks in concert with excitatory cells. Runyan et al. (2010), for example, report that tuning in PV cells shows the same amount of variability as in excitatory cells. In addition, several studies have indicated that PV cells form differentiated subnetworks and fine tune their synaptic weights along their excitatory targets (Yoshimura and Callaway, 2005; Donato et al., 2013; Xue et al., 2014; Khan et al., 2018). Furthermore, single PV cells have a comparatively high influence onto connected excitatory cells, whereas inputs by SST cells are more convergent and exert their influence as a group (Safari et al., 2017).

Studies on VIP cells suggest them to have a unique role. Anatomical evidence from HC and neocortex implicate them to inhibit other interneurons (Gulyás et al., 1996; Staiger et al., 2004b; Dávid et al., 2007). More functional studies in slices confirmed and refined this notion. They revealed that VIP cells are capable of reducing activity of SST cells within and outside their home layer (Férézou et al., 2002; Lee et al., 2013; Pfeffer et al., 2013; Jiang et al., 2015; Walker et al., 2016). Interestingly, many studies have shown that VIP in various neocortical areas are strongly driven by associative or neuromodulatory input and are very likely to be a mediator of disinhibition of the lo-

cal excitatory network (Lee et al., 2013; Pi et al., 2013; Fu et al., 2014; Zhang et al., 2014). In the recent years, this circuit motive became a popular object of investigation (Jackson et al., 2016; Muñoz et al., 2017; Williams and Holtmaat, 2018). However, there is also considerable evidence that VIP cells can inhibit excitatory cells directly (Caputi et al., 2009; Garcia-Junco-Clemente et al., 2017; Zhou et al., 2017), raising the question if their net effect is consistently disinhibitory throughout different contexts like cortical state.

Targeting specific subpopulations in in-vivo experiments has only recently been rendered possible with the development of 2-photon microscopy (Margrie et al., 2003; Stosiek et al., 2003; Helmchen and Denk, 2005). Consequently, most of these studies are limited to supragranular layers and in-vivo function of deeper GABAergic interneurons is largely unknown. In-vivo experiments are challenging to implement and have a plethora of known and unknown interfering factors, which are difficult to control. Nevertheless, different cell types should be ultimately determined by their functional repertoire. Therefore, further breakthroughs in a better taxonomy are likely to be seen from this line of research. An illustrative example in this context is Muñoz et al. (2017), who report of two types of MCs with minor morphological differences, but opposite response profiles to whisker stimulation.

1.1.5 Thalamocortical innervation of GABAergic interneurons in barrel cortex

The question arises, if and which GABAergic interneurons receive thalamocortical innervation. First evidence for the presence of such connections was obtained by electron microscopy studies, which lacked the means to further identify the respective cell (Hersch and White, 1981; White and Rock, 1981). However, these early studies already hinted at a considerable variety in input strength (Keller and White, 1987). More refined conclusions could be made with the advent of the aforementioned markers and better understanding of neuronal diversity. It became apparent, that PV cells, most abundant in LIV, receive strong input from VPM (Staiger et al., 1996a). This finding was an affirmation that FS interneurons are mediators of a powerful and swift feed-forward inhibition of afferent inputs; found both in-vivo and in-vitro (Simons, 1978; Swadlow, 1989;

Agmon and Connors, 1992), similar to findings in the HC decades before. A plethora of studies further investigated the details and functional implications of this mechanism: showing that thalamocortical recruitment of PV cells is even faster and stronger than of L4 excitatory cells (Gibson et al., 1999; Porter et al., 2001; Beierlein et al., 2003; Sun et al., 2006; Cruikshank et al., 2007; Hull et al., 2009).

Data on innervation of other types of inhibitory cells is more complicated and inconclusive. Straightforward anatomical evidence is relatively rare: Notably, VIP cells in rat barrel cortex receive synapses from VPM projections (Staiger et al., 1996b). A recent report in mice by Wall et al. (2016) shows VIP cells to receive inputs by both VPM and POm. Interestingly, they also report comparable input magnitudes for SST and PV cells, which raises the question of how these data relate to function. A majority of slice studies in rats and mice, for example, report that SST and LTS cells are much less responsive to thalamocortical stimulation than PV cells (Gibson et al., 1999; Beierlein et al., 2003; Cruikshank et al., 2010; Tuncdemir et al., 2016). However, Tan et al. (2008) report that SST cells in L5 can by recruited by thalamocortical fibers given persistent stimulation. In addition, Porter et al. (2001) show that also non-FS cells in rats can mediate feed-forward inhibition upon stimulation of TCAs. To sum up, it is unclear if and how SST cells are involved in first order sensory processing.

Slice studies with VIP cells have not been published, but some reports hint at the possible nature of their innervation. Porter et al. (2001) report that more than half of non-CB RSNP are recruited upon TCAs stimulation. In mice, Lee et al. (2010) showed that cells in LII/III and LIV targeted via 5-HT3aR-EGFP line also receive direct synaptic input, potent enough to elicit APs. However, it is unclear if these cells are VIP cells or some other type of interneurons. Neurogliaform cells, for example, are also reported to receive thalamic input (Chittajallu et al., 2013); as do other cells of the non-VIP subgroup (Zhu and Zhu, 2004). Very recently, studies in respect of innervation by POm have also been published showing some similarity to the lemniscal pathway. POm activity seem to primarily drive VIP and PV cells, whereas SST cells are innervated weakly or not at all (Audette et al., 2017; Williams and Holtmaat, 2018).

1.2 Aim of the thesis

The objective of this thesis is to clarify which subpopulations of inhibitory interneurons in vibrissal somatosensory cortex receive projections from main thalamic afferents (either VPm or POm). Furthermore, we want to investigate the properties of underlying synaptic connections and gain insight into how direct recruitment of inhibition effects sensory processing.

Connectivity is a feature often neglected when categorizing neocortical GABAergic interneurons into distinct subgroups. Recent advances in the retina demonstrated that mapping the circuitry of cells can be a valuable tool in understanding their present diversity (Seung and Sümbül, 2014). We aim to understand the present diversity within defined subpopulations of GABAergic interneurons in greater detail by considering thalamocortical input. Since the extensive innervation of PV interneurons is well-established, the project's focus is on SST and VIP expressing cells.

Material and Methods

2.1 Mouse lines and stereotactic injections

Targeting of GABAergic interneuron populations was achieved by selective expression of the red fluorescent protein tandem dimer Tomato (tdTomato) via the cre-lox system. All animals used were heterozygous offspring of the respective cre driver line crossed with the reporter line Ai9 (Madisen et al., 2010; Taniguchi et al., 2011). All mouse lines were acquired from The Jackson Laboratory (Bar Harbor, USA). For proper nomenclature of the strains used, see appendix A.1. Animals were kept on a 12 hour light-dark cycle and with an ad libitum standard diet. All experiments were conducted in accordance with the German Animal Welfare Act and corresponding EU legislation. Expression of Channelrhodopsin-2 (ChR2, first described by Nagel et al. [2003]) was achieved by transduction via adeno-associated viruss (AAVs) obtained from the Vector Core of the University of Pennsylvania (Philadelphia, USA). The variant used in this study contained the H134R mutation (Lin et al., 2009) and was directly coupled to the enhanced version of yellow fluorescent protein (YFP) as a fusion protein. A detailed description of the used vectors and their original titer is given in A.2. All obtained viruses were aliqouted on ice 1:4 in sterile phosphate buffer (PB), under a laminar flow hood into batches of 5–10 µl each. Aliquots were not used more often than 2-3 times to ensure that consecutive thaw-freeze cycles did not lower the titer drastically.

For a detailed description of stereotactic virus injection, see Cetin et al. (2006). Before the surgery mice of both sexes at postnatal day 21-28 were injected intraperitoneally (30 µl per 10 g body weight) with buprenophen (Temgesic; RB Pharmaceuticals, Mannheim, Germany; diluted 1:14 in sterile saline) for analgesia. After 15-20 min

mice then were anesthetized with isofluran (FORENE, AbbVie, North Chicago, USA) and placed on a heating plate set at 37 ℃ (ATC 1000; WPI, Sarasota, USA) with their head mounted in a stereotactic frame (David Kopf Instruments, Tujunga, USA). To prevent drying of the eyes an ointment was applied. The snout was placed in a constant flow of oxygen, infused with 1-3 % isofluran by a vaporizer (Harvard Apparatus, Holliston, USA) for continuous anesthesia. The animal's breathing frequency and depth were monitored throughout the surgery and the concentration of isofluran adjusted accordingly. Excess isofluran was absorbed by carbon filtering (Harvard Apparatus, Holliston, MA). After shaving of the head, the scalp was injected with lidocain (2%, Xylocain, AstraZeneca, London, England)) for local anesthesia. An incision was made after a few minutes of waiting and the fascia between bone and skin were removed. Then, the rostrocaudal angle of the head was adjusted until lambda and bregma had the same z-coordinates. The cranial windows for both hemispheres were made at the respective coordinates with a dental drill (Osada Success 40, Osada, Tokyo, Japan). The injection coordinates were taken from the Paxinos mouse atlas (see [Franklin and Paxinos, 2001]; VPM: 1.7, 1.75, -3.25; POm: 2.16, 1.25, -3.00, axis: anterior-posterior, medial-lateral, dorsal-ventral, all in mm) and multiplied by a correction factor (CF) to account for the smaller skull size of juvenile animals. The CF was calculated by the ratio of measured distance between bregma and lambda and 4.2 mm. For correction on the dorsal-ventral axis the term $\frac{2}{3}$(1-CF) was added to the factor due to uneven growth along the body axes. Sterile saline was regularly applied to the cranial window to keep the exposed tissue moist. Prior to surgery, injection pipettes were made from glass capillaries (GB150F-8B, Science Products, Hofheim, Germany) with a horizontal puller (P-97, Shutter Instruments, Novato, USA). The two-step program was optimized to provide tips with maximally long and thin tapering, which were then trimmed under a microscope to have an opening of 20–25 µm. Pipettes were front-filled with the virus solution and mounted in the injection holder of the stereotactic frame. Approximately 100–150 nl of virus solution was delivered at the respective depth by pressure injection (standard parameters: 3 psi, 250 ms; on PDES-02Dx, npi electronics, Tamm, Germany). After a resting period of several minutes, pipettes were removed and the head was sutured. After removing them from the frame animals slowly woke up on the heat-

ing plate and placed in a fresh cage. For post-operative care animals were injected two more times with buprenophen at 4 and 8-10 hours after the surgery.

2.2 In-vitro electrophysiology and optogenetic stimulation

2.2.1 Solutions and preparation

3 to 4 weeks after the injection, animals were used for in-vitro experiments with acute slices. Animals were anesthetized by isofluran and then decapitated. Their brain was quickly removed and placed into iced high-sucrose preparation solution (see A.3 for detailed composition). All solutions, used for electrophysiological recordings, were prepared with ultrapure water obtained with a Milli-Q system (Merck Millipore, Burlington, USA). Both cutting and recording solutions were prepared fresh from 10X stocks, with $NaHCO_3$ added separately, and constantly perfused with carbogen gas (95 % CO_2 5% O_2). After waiting for a minute, hemispheres were separated and cut according to Agmon and Connors (1991) to obtain thalamocortical slices. Tissue blocks were fixed into the buffer tray of a vibratome (Leica VT1200 S, Leica Biosystems, Nussloch, Germany). 300 µm thick slices containing the barrel field of the primary somatosensory cortex were collected as soon as the HC was visible and transferred to recording solution, which ionic composition is close to extracellular conditions in-vivo. Hence, this solution is also referred to as artificial cerebral spinal fluid (ACSF); see A.3 for its detailed composition. After cutting, slices were rested for 30 min at 37 °C.

Cells were recorded from with two different kinds of intracellular solutions: either based on K^+-gluconate, which is closer to the actual physiological conditions of the cell, or based on Cs^+-$MeSO_4$, which eases the attenuation of distal synaptic inputs by unselectively blocking of K^+-channels (Adelman, 1966; Stuart and Spruston, 1998). Aliqouts of 0.5 ml intracellular solution were made in bulk as follows: After adding the respective substances (specified in A.3), the pH of solutions were carefully adjusted to 7.4 by adding either KOH or CsOH, while monitored with a pH-meter (Lab 850, Schott instruments, Mainz, Germany). Then, the solution's osmolarity was assessed with a OSMOMAT 030 (gonotec, Berlin, Germany) and adjusted to 300 mOsm by adding

sucrose. Aliquots were sterile filtered and frozen at –20 °C. Shortly before experiments, an aliquot was thawed and 0.5% biocytin (Sigma-Aldrich, St. Louis, USA) was added for labeling of the recorded cell (Horikawa and Armstrong, 1988; Marx et al., 2012). Before filling of the patch pipette, solution was passed through an additional syringe filter (Rotilabo, Carl Roth, Karlsruhe, Germany; polytetrafluoroethylene, sterile, pore size 0.2 µm).

2.2.2 Set-up and whole-cell recordings

Recordings were made with an single electrode patch-clamp amplifier (SEC-05; npi electronics) connected to a low noise headstage (Hamill et al., 1981). To avoid series resistance errors, measurements were made in discontinuous mode with a switching frequency above 20 kHz and a 1/4 duty cycle. The amplifier included a low pass Bessel filter with the corner frequency set to 3 kHz. In addition, signals were also subjected to a filter module (DPA-2FX; npi electronics) with manual offset correction and a single pole lowpass filter with corner frequency of 20 kHz. Ultimately, recordings were digitized at 20 kHz by an AD-Converter (CED Power1401, CED Limited, Cambridge, England). Tissue and single cells were visualized with an upright microscope (Axio Examiner A1, Carl Zeiss Microscopy, Jena, Germany) using two different objectives: a 2.5x (EC Plan-Neofluar 2.5x, = 0.075, working distance = 9.5 mm, Carl Zeiss Microscopy) and a 40x water immersion objective (LUMPlanFI W/IR, NA = 0.80, working distance = 3.3 mm, Olympus Corporation, Tokyo, Japan). For brightfield microscopy with infrared light, a halogen lamp (housed in HBO 100 illuminator, Carl Zeiss Microscopy) was filtered and coupled into a Dodt gradient contrast system (Dodt et al., 1998). Epifluorescence was enabled with light of a mercury arc lamp (HXP 120 C, Carl Zeiss Microscopy) that was filtered by a dichoric mirror. Light of both optical paths was ultimately captured by a CCD camera (INFINITY3S-1UR, Lumenera corporations, Ottawa, Canada). Micromanipulators (SM5, Luigs & Neumann, Ratingen, Germany) were used for moving the headstage and recording chamber to control patch pipette and image plane. Most parts of the set-up were mounted on an IsoStation vibration isolated workstation (Newport Corporation, Irvine, USA) and placed within a Faraday cage. Constant perfusion with recording solution was achieved by a peristaltic pump (Minipuls 3, Gilson, Middle-

ton, WI) at a rate of about 2 ml min^{-1}. Before entering the recording chamber, ACSF was heated up at 34 °C with a heating pen and maintained in the recording chamber with a temperature controller (TC05, Luigs and Neumann). To prevent noise, electrical components were individually connected to ground.

Pipettes were made shortly before experiments with a horizontal puller (P-1000, Shutter Instruments) using 4 cycles. When immersed into the recording solution pipettes had a resistance of 6 MΩ–10 MΩ. After immersion, slight positive pressure was applied through the tip. Then, slow capacitance compensation was done manually, when the pipette was in proximity to the slice surface. The target cell was approached swiftly at an horizontal angle of about 45°. After dimpling of the membrane, the pressure was reversed and the amplifier switched to voltage clamp (VC) with a command voltage of –60 mV. Pipette tip and membrane then usually formed a tight seal of a resistance beyond 1 GΩ. Renewed manual compensation of the capacitance was done according to 1 s long hyperpolarizing 100 pA current pulses. Stimulation was applied via a gating unit (GIA-05X; npi electronics). Acquisition protocols were designed by Martin Möck and Mirko Witte in Signal 5 (CED Limited). Measured values were not corrected for liquid junction potential. Based on Barry (1994), these are estimated to be +14 mV for Cs^+-based intracellular solution and +16 mV K^+-based solution.
Optogenetic stimulation was applied with a solid state laser (λ = 473 nm, DL-473, Rapp OptoElectronic, Hamburg, Germany). The laser output was coupled into the microscope via a glass fiber light cable (200 µm, NA = 0.22) and a beam combination cube containing a dichroic mirror for the appropriate wave length (all Rapp OptoElectronic).

2.2.3 Experimental protocols and analysis of recordings

All electrophysiological measurements were made in current clamp (CC), if not specifically stated otherwise, and analyzed by custom scripts developed by Martin Möck in Signal 5. Subthreshold intrinsic properties (except rectification index and rheobase) were obtained from 10 iterations of a one second stimulation with -10 pA or, alternativly, -50 pA if necessary for a dependable response. The resting membrane potential V_m (in absolute voltage) is measured as the average prestimulus membrane voltage.

The input resistance R_{in} is determined according to Ohm's law by the potential change measured from rest to highest deflection. The time constant τ was extracted from the average of the same traces. It is calculated as the time in milliseconds, at which 63% of the change in voltage (according to highest deflection) is reached. For this, an exponential fit of the course of the membrane voltage from stimulus onset to highest deflection was used (provided $R^2 \geq 0.9$). The sag index is calculated as follows: change of membrane potential reached at the highest deflection minus change at steady state, divided by the former. It is a measure of slow rectification given in % and is attributed to a hyperpolarization-activated cation current, referred to as I_h (McCormick and Huguenard, 1992). The rheobase is defined as the value of a 1 s long current step as the minimal stimulation sufficient to evoke a single AP or burst in case of BS cells. The AP threshold is defined as the membrane potential at which the slope of the upstroke AP reaches 10 % of the maximum slope of the rising phase. The AP width was determined by the time passed from the half-amplitude and back to the same membrane potential during repolarization. The AHP amplitude was calculated by the difference between threshold and the peak of the hyperpolarization after the AP. The firing pattern of a neuron was assessed by an increasing stimulation of 1 s long current pulses with an increment of 10 pA until the cell appeared to be saturated by either no further increase in spiking or prominent fluctuations of AP amplitudes. The 10:01 adaptation ratio was calculated as 1 minus the ratio of the average AP counts of the first tenth of the spike train and the last tenth. The introduction of the first term is necessary to accommodate some cases of BS cells, which cease to fire APs in the late segment of the stimulation.

After assessment of intrinsic properties, tetrodotoxin (TTX, 1 µM) and 4-aminopyridine (4-AP, 100 µM) were washed in by bath application (Petreanu et al., 2009; Cruikshank et al., 2010). TTX blocks most voltage-gated Na^+-channels and thus hinders neurons to generate APs, whereas 4-AP selectively blocks K_v1 channels. The application of both drugs is used to ensure that measured postsynaptic events are due to direct innervation of transduced fibers onto the recorded cell. Given sufficient stimulation, the ChR2-mediated depolarization is strong enough to directly activate presynaptic Ca^{2+}-channels and triggers vesicle release despite the absence of APs. In order to facili-

tate this mechanism, the fast repolarization of the cell membrane is hampered by the blockade of K_v1 channels. Since postsynaptic depolarizations, on the other hand, are unable to lead to spiking in cortical cells, EPSPs in recorded cells are solely caused by ChR2-positive fibers and not by the local network. Responses recorded under these conditions are also referred to as mono-synaptic, in the sense that stimulation propagates through only one synapse and all responses are due to direct inputs. Intensity of stimulation was increased in a step-wise manner, with at least three repetitions at each level at an inter-stimulus intervals of either 5 or 15 s. The different conditions did not have an effect on variability of amplitude or latency of the responses, which would have hinted at different recruitment of ChR2 by desensitization, and were consequently pooled. Intensity level started at subthreshold levels (approximately 10–30 µW) and were increased in a step wise manner, which could reach up to 50 mW. Intensity of transmitted light passing the objective was regularly measured in dry conditions with a photometer (PowerMax Wand UV/VIS Quantum, Coherent, Santa Clara, USA). Given loss through scattering in recording solution (see Yizhar et al. [2011]) and other factors, absolute values of intensity should not be interpreted as actual strength of stimulation and are primarily used for comparisons within the same conditions. The holding current applied to the cells was adjusted manually to a baseline membrane potential of 70 mV. The first postsynaptic events that reliably followed a 1 ms light flash within a consistent time window (latency range of 1.5 ms) were considered threshold stimulation of transduced fibers. To ensure that an unresponsive cell was in fact due to a lack of input and not other factors like weak expression, a positive control in the same slice or hemisphere was obtained. Reflections visualized via the camera, showed a circular area of distinct illumination with a diameter of about 95 µm, which is estimated to be the field of stimulation. Response latencies were quantified as time difference between stimulus onset and the time point in which the membrane voltage passes 3 times the standard deviation of baseline fluctuations at the prestimulus membrane potential. The end of the responses was determined by the return of the membrane voltage back to threshold level. The amplitude was calculated as the maximum deviation of the membrane voltage within the first 50 ms of stimulus onset. The integral was determined by the area delineated by course of the membrane voltage during the response and the

baseline resting potential. The time to peak or rising time is calculated by the time difference between crossing of the threshold and time point of the amplitude. All statistical analysis was done in SigmaPlot 13 (Systat Software, San Jose, USA). If not specifically stated otherwise the significance test used was a Mann-Whitney Rank Sum Test and was uncorrected for multiple comparisons.

2.3 Stainings, imaging and analysis

After in-vitro experiments, slices were fixed overnight in a solution of 4% paraformaldehyde (PFA) and picric acid at 4 ℃. The detailed composition of each solution used is given in A.4 and the following procedures were carried out at room temperature, if not specifically stated otherwise. Slices were washed in PB several times until they were completely destained of the yellow picric acid. Then they were transferred into a saline solution by first washing them 15 min with Tris buffer (TB) buffer, followed by washing in Tris-buffered saline (TBS) for 15 min. For permeabilization they were washed two times for 15 min each in TBS with additional 0.5% Triton-X 100 (TBST). In some POm injections the YFP signal was immunhistochemically amplified. In these cases, slices were incubated for 90 minutes in TBST with additional blocking agents, to limit unspecific binding of primary and secondary antibody. Then, slices were incubated for 2-3 days at 4–8 ℃ in a solution of the same composition as in the previous step, but with the addition of goat polyclonal antiGFP (abcam, Cambridge, UK; original concentration 0.5 mg ml^{-1} diluted 1:4000). Further on, slices were washed for five times each 15 minutes in TBST. For staining of biotin and optional amplification with the secondary antibody, streptavidin conjugated to the fluorophore Alexa633 (life technologies, Carlsbad, USA) and donkey anti goat coupled to Alexa488 was added and incubated for 4 hours. After that, slices were washed again 3 times in TBST and transferred in TBS. Then, cell nuclei were stained with 4,6-diamidino-2-phenylindole (DAPI, life technologies; 5 mg ml^{-1}, diluted 1:1000) for 5 min, washed one time in TBS and two times in TB and ultimately mounted with aqua polymount (Polysciences, Warrington, USA) on specimen slides with 0.08–0.12 mm thick cover slips (Menzel, Thermo Scientific, Waltham, USA).

For evaluation of cellular morphology and the thalamocortical injection pattern, partial image stack acquisitions of the barrel field were made with a confocal microsope (TCS SP2, Leica Microsystems, Wetzlar, Germany) using a 40x oil-immersion objective. Single tiles of confocal image stacks were stitched either manually in arivis vison4d (arivis, Munich, Germany) or automatically with an ImageJ-plugin (Schneider et al., 2012). Specificity of injections was evaluated by vertical plot profile of YFP-ChR2 signal along the cortical column. For this purpose, sum projections of confocal image stacks were used. Single cells, which showed sufficient completeness of neuronal arborizations, were selected for reconstruction. Morphology was reconstructed manually in Neurolucida (MBF Bioscience, Williston, USA) from acquired image stacks. No shrinkage correction due to fixation of the tissue was applied. Post-processing for display of images was done in ImageJ, whereas intracellular stainings were enhanced by non-linear adjustments in Adobe Photoshop (Adobe, San Jose, USA).

Results

3.1 Characterization of cells targeted by cre-reporter lines

The targeting of specific subpopulation of GABAergic interneurons is achieved by the use of cre reporter lines. This study is aimed to reach a sample that represents in-group diversity of both VIP and SST cells accurately while retaining a sufficient sample size for all cortical layers. Neuronal diversity is assessed by features of intrinsic electrophysiological properties and morphology. This study also sets out to investigate the relationship of further subpopulations of GABAergic interneurons and putative thalamocortical input. The first section of this chapter addresses two questions: First, are there apparent sub-groups within either VIP or SST cells and, second, are the features of recorded cells in agreement with previous reports of the respective populations? In this study cells were recorded from with K^+ and Cs^+-based intracellular solution. Characterization of firing patterns with the latter is of limited use, since Cs^+ blocks a substantial fraction of K^+-channels. Hence, only morphology and basic subthreshold properties can be used to pinpoint the identity of cells patched with this solution.

VIP-cre positive cells

Their firing pattern is predominantly continuous adapting (CA), meaning that ISIs gradually increase over time until the end of the stimulus. Some cells, however, also show occasional interruptions by spike intervals with unusual length and seemingly random occurrence also known as IS. In addition, there is another minority of BS cells, which are defined by the occurrence of several spikes at rheobase. Examples for the de-

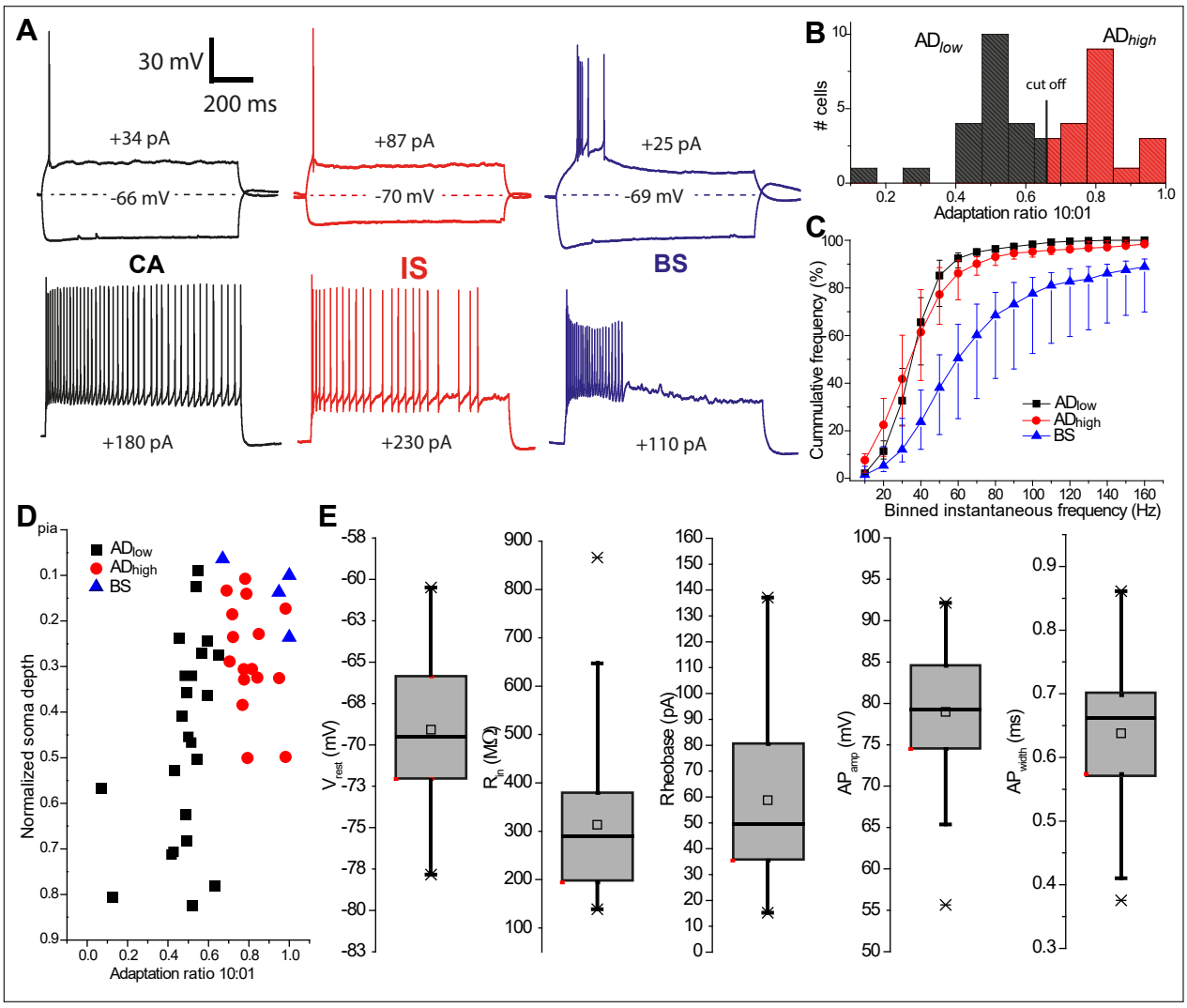

Figure 3.4. Intrinsic properties of VIP cells recorded with K^+-based intracellular solution
A Examples of cells with archetypical firing pattern associated with VIP cells. Hyperpolarizing current step in all cells is –100 pA. **B** Histogram of spike adaptation ratio of non-BS VIP cells. The two peaks in the distribution suggests that there are two populations with different adaptation behavior, here referred to as AD_{low} and AD_{high}. AD_{low} has a high content of continuous adapting (CA) cells, whereas AD_{high} has a high content of cells, which are IS or a blend of said firing patterns. Hence, the introduced color code is extended to the two new categories. **C** Dynamic frequency range of the three different firing pattern phenotypes. Plot indicates the median of the cumulative fraction of the total instantaneous frequency. Data is resampled into 10 Hz bins. Error bars mark the interquartile range (IQR). **D** Scatter plot showing the relationship between adaptation ratio and normalized depth of the soma. BS and AD_{high} cells are concentrated in the upper half. **E** Distributions of selected intrinsic electrophysiological properties irrespective of firing pattern. Averages are indicated by small hollow squares.

scribed firing patterns can be seen figure 3.4A. Distinguishing between CA and IS is not feasible in 14.6%, of cells, since irregularities in spiking vary from subtle to obvi-

ous. A recent rigorous study of VIP firing patterns used a new classification scheme relaying on quantified parameters (Prönneke, 2016). To make the presented data more comparable with this work and to assign all VIP cell firing patterns, the described categories were abolished in favor of grouping non-BS cells according to their adaptation ratio. This approach revealed the presence of two subgroups with little overlap (see figure 3.4B): low adapting cells (AD_{low}) with a high fraction of CA cells (91.3%) and highly adapting cells (AD_{high}), approximating a BS phenotype with very short ISIs at the beginning of the stimulus and strong adaptation. This last category has a higher fraction of IS cells (35.3%) and those that are in-between IS and CA (also 35.3%). The two groups showed subtle differences in the dynamic frequency range visualized in 3.4C). Highly adapting cells have a bigger proportion of frequencies at the poles of the distribution; meaning 10 Hz and below as well as spikes over 160 Hz. The BS group, on the other hand, has a very distinctive distribution with the median cell having a high share (about 15%) of frequencies above 160 Hz. Intrinsic properties in the spike or sub-threshold domain are independent of firing pattern (data not shown). Soma location and firing pattern, however, show a clear interaction with BS and AD_{high} cells only being present in the upper half of the cortical column (see 3.4 subfigure D). Furthermore, recordings with K^+-based intracellular solution show that VIP cells have on average a high input resistance (300 MΩ) and a low rheobase (59.0 pA). Their action potential width (median:0.66 ms) and amplitude (median:78.0 mV) is similar to excitatory cells (see figure 3.4E).

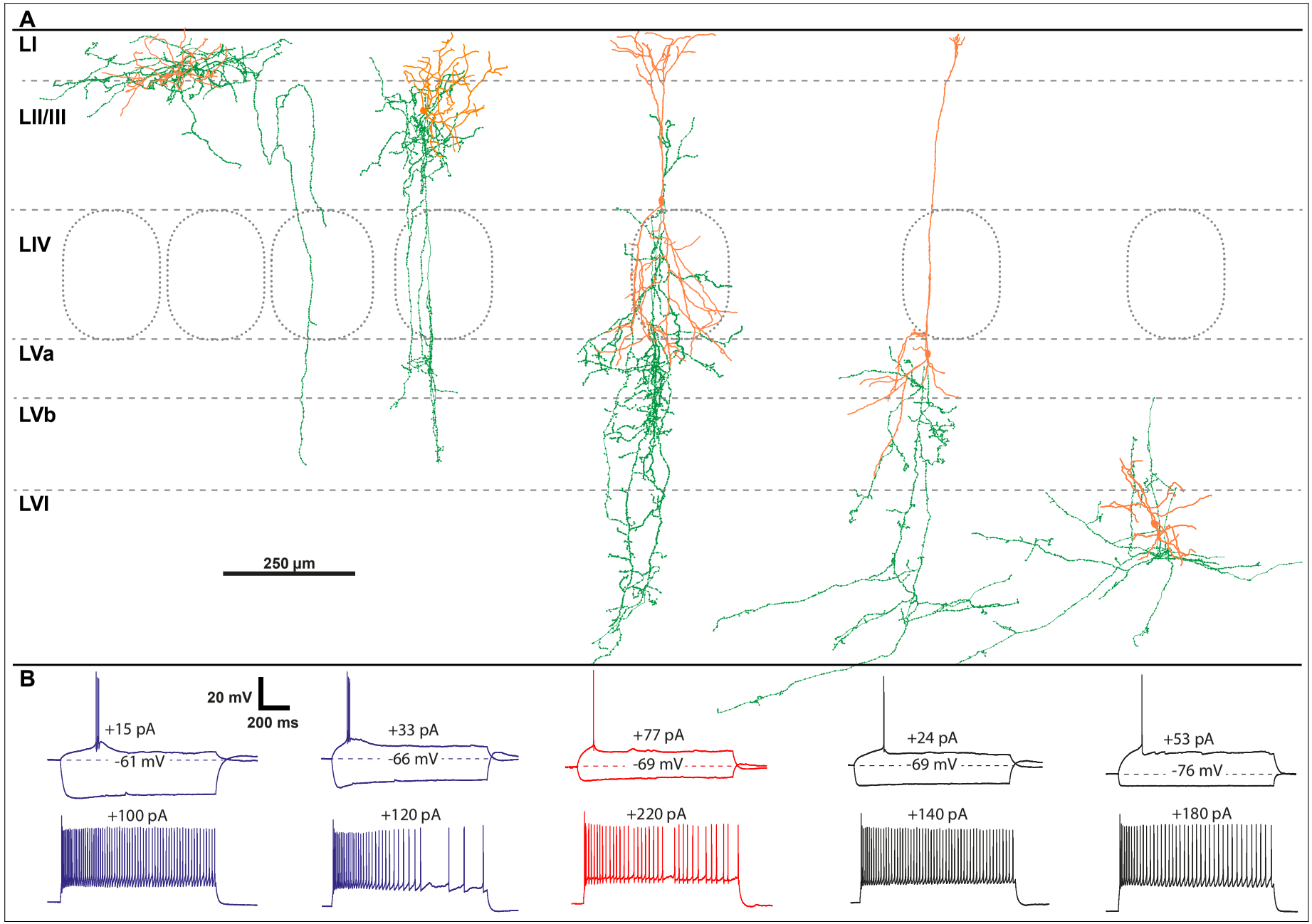

Figure 3.5. Examples of VIP cell morphology and corresponding intrinsic properties (legend continued on next page)

Figure 3.5. Examples of VIP cell morphology and corresponding intrinsic properties. A Reconstructed cells from various layers. Cells are characterized by a descending axon, usually extending into several of the remaining layers towards the white matter. From deep LII/III until LVa (see cell 3 and 4) somatodendritic configurations are a blend of bipolar and bitufted and show prominent vertically extended dendritic arbors. The more the soma is located at the poles of the column, the smaller the dendritic spanning field (see cell 1 and 5). With the exception of deep infragranular cells, VIP cells have at least one dendrite targeting LI, where it shows considerable branching. **B** Corresponding firing patterns of cells, introduced in A, in the same color code used in 3.4; Hyperpolarizing current step in all cells is –100 pA. Note that cells showing the BS and AD_{high} firing pattern are found in the upper half of the cortical column.

VIP cell morphology in general is characterized by a vertical orientation and a descending axon with an initial segment, which occasionally originates from a proximal dendrite instead of the soma. They have very rarely spines and if so these are confined to a specific segment. The depth of the soma within the cortical column is a good predictor of the extent of the dendrites. Most cells (from LII/III to LVa) have dendritic trees that are vertically oriented. The more ventral the higher the vertical expansion of their dendrites, which can include several layers. They reliably reach into LI, where they form short tufts or arborizations similar to apical pyramidal dendrites. Somatodendritic configurations are mostly bitufted or bipolar. VIP cell morphology deviates at the poles of the cortical column: LI and some upper LII cells are spread horizontally, whereas cells in infragranular layers (predomiantly LVb and LVI) are not eager to reach the dorsal parts of the cortex, while sometimes still retaining a vertical appearance with shorter and denser branching. Other cells, show a multipolar configuration. In the majority of VIP cells, especially in upper layers, the axon extends almost throughout the whole column. Generally, VIP cells have two different target domains, in which they branch frequently: For one, in proximity of the soma, in case they are located in LII/III. In addition, their descending axon branches in LV (mostly with a focus on LVa). Granular and infragranular cells also concentrate their axon there. Interestingly, most cells keep extending their axon deeper and occasionally reaching into the white matter. Infragranular cells with less vertical orientation also project more horizontally.

Despite having a diverse range of features, subdivision of VIP cells do not show cohesive sets of traits, that might hint at possible subcategories. In terms of both electrophysiology and morphology properties vary in a continuous manner. As mentioned before, many cells show a firing pattern that is a mix of the archetypes described previously (see the panel in 3.5). Similarly, distinguishing between VIP cell morphologies is challenging: Dendritic length and coverage changes gradually with soma location on the vertical axis until passing the LVa border. Except the uneven distribution of BS and AD_{high} cells, there is no indication that firing patterns and anatomical features relate to another.

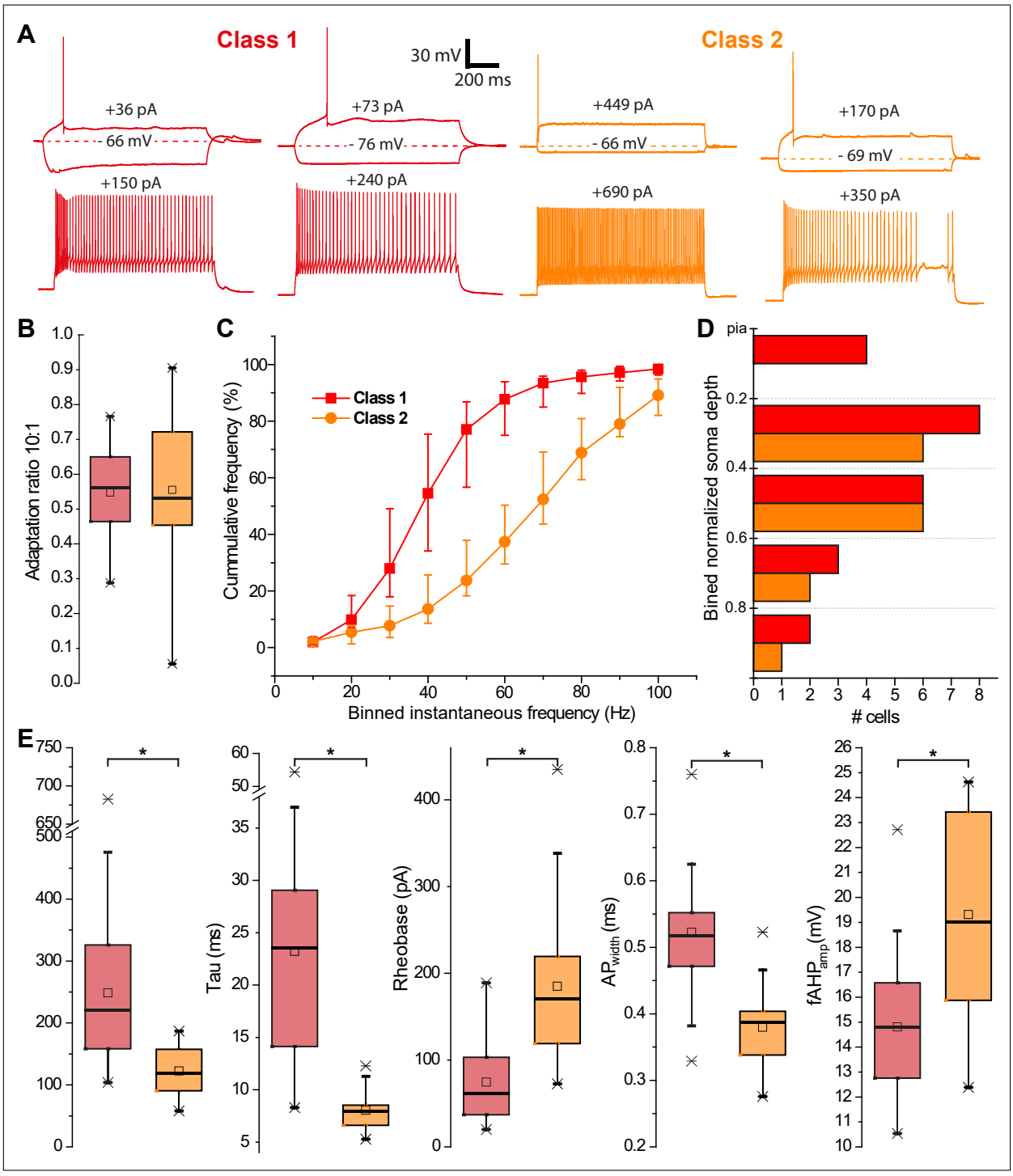

Figure 3.6. SST cell firing patterns recorded with K^+-based intracellular solution can by divided into two distinct classes

(legend continued on next page)

Figure 3.6. SST cell firing patterns recorded with K^+-based intracellular solution can by divided into two distinct classes. **A** Representative examples of different firing patterns of SST cells: first two cells in red are in Class 1, one being a LTS cell, the second a CA. The other two cells in orange are associated with Class 2. The first one shows the stereotypical FS phenotype, whereas the other is a stuttering quasi-FS. **B** Firing pattern adaptation of both classes is on average similar, but Class 2 shows a higher variance. **C** Dynamic frequency range of the two classes visualized by their cumulative instantaneous frequency. Symbols indicate the median the error bars mark the IQR. **D** Distribution cells according to normalized distance to pia and subclass: Class 1 is more prevalent in the upper half of supragranular layers. Class 2 is most frequent around the granular layer. **E** Intrinsic subthreshold properties and spike waveform between SST classes are significantly different: R_{in}, τ, rheobase, $width_{AP}$, all $P \leq 0.001$, absolute amplitude of fAHP, $P = 0.003$.

SST-cre positive cells

Patched SST cells also show considerable variability in intrinsic electrophysiological features and morphology. However, in both domains coherent characteristics emerge, which give rise to more distinct subpopulations. Describing the population as a whole would be an illusive representation for this reason. Two classes of cells can be distinguished (see 3.6): Class I, which makes up the majority of the sample (62.5%), includes cells with firing patterns that can be described as LTS or CA (illustrated in the first two examples of subfigure A). The LTS cells are exclusively encountered in the SST population. They are similar to CAs in terms of overall adaptation, but with three additional features: First, as their name suggests their rheobase is substantially lower (with a median half of CAs); second, their adaptation is less continuous, meaning ISIs increase abruptly after the first 100 ms, but less so thereafter. Third, spikes that occur in the aforementioned initial segment shorten substantially under strong stimulation similar to bursts. In the literature LTS cells are also characterized by spiking after the rebound of a hyperpolarizing current step: a feature missing in this study. The other group of cells have electrophysiological features, which either approximate FS cells or are indistinguishable from them. In terms of AHP and width, two quintessential properties of the FS phenotype, they show a higher amplitude and shorter duration (see last two examples of firing patterns in subfigure A). Stimulation above rheobase leads to clusters of spikes at seemingly random intervals. At moderate current injections, these

breaks decrease in frequency leading to the impression of stutters in otherwise continuous firing. Differences between FS and quasi-FS are not as clear-cut as suggested in previous publications (Ma et al., 2006; Xu et al., 2013). However, Class II show a wide range of adaptation (IQR:0.25 vs Class I IQR: 0.16), which suggest that there is further diversity. The dynamic frequency range of the classes is very distinct, with Class II cells reaching very high and sustained frequencies (see subfigure C). Class I cells are more frequent in every layer except LIV, where only 25% of the SST cells can be attributed to them (see subfigure 3.6 D). Class II are most numerous there, but can be found in every layer except LI. That being said, most of them cluster in the granular layer and its vicinity. Unlike in VIP cells, firing pattern clearly relate to electrophysiological properties (see subfigure E for some examples): Class I cells have a higher time constant (24.0 vs 7.0 ms), a lower rheobase (medians: 60 vs 180 pA) and high input resistance compared to the other class (medians: 200 vs 100 MΩ). In addition, their spikes at threshold stimulation have a lower width (medians: 0.50 vs 0.39 ms), greater width and a smaller or no AHPs (medians: 14.9 vs 19.1 mV). As in AP waveform parameters, Class II cells again show properties that are associated with FS like a low input resistance, short time constants, high rheobase.

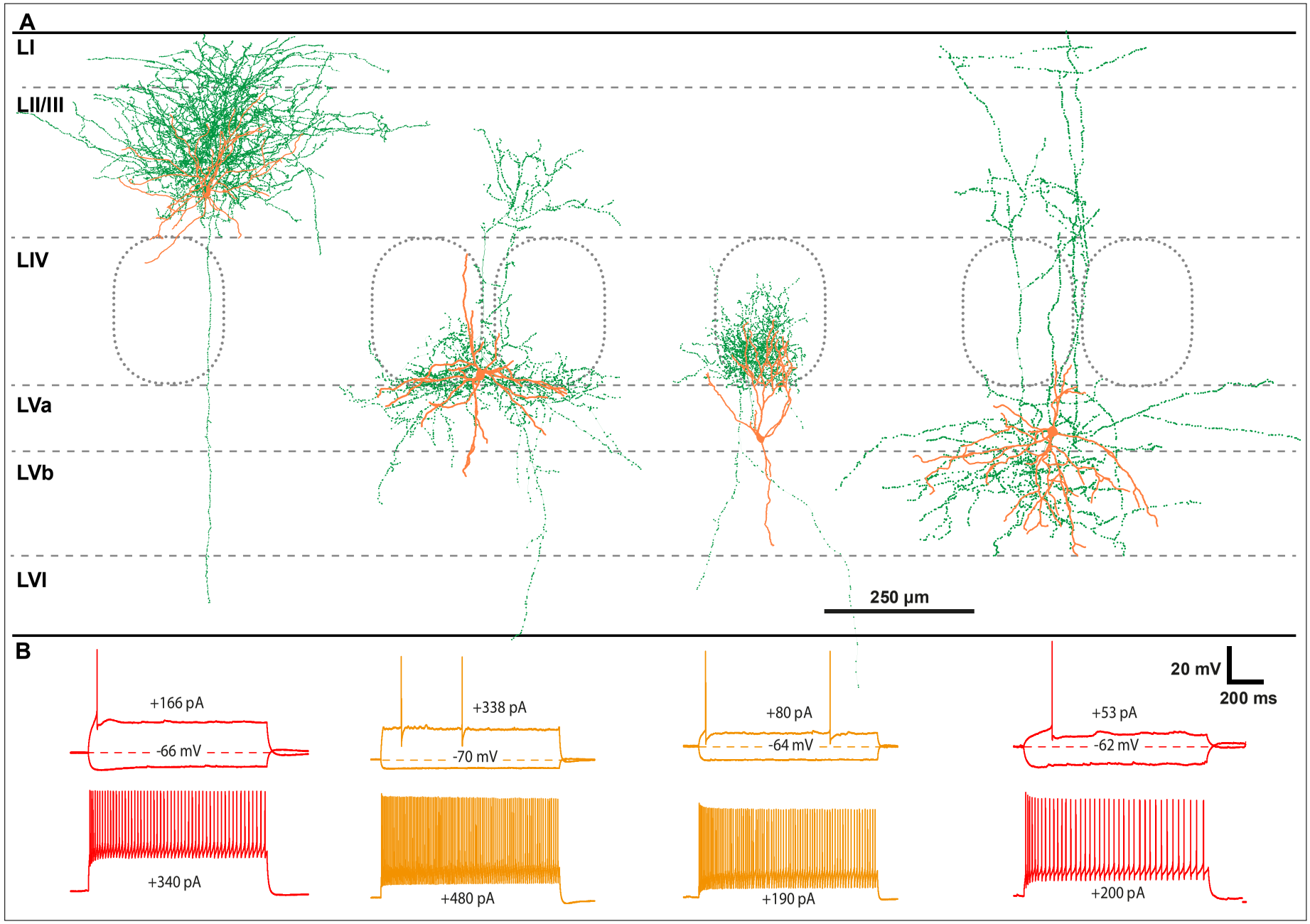

Figure 3.7. Examples of SST cell morphology and corresponding intrinsic properties
(legend continued on next page)

Figure 3.7. Examples of SST cell morphology and corresponding intrinsic properties. A Four examples of SST cell morphology: generally, SST cells are characterized by a multipolar somatodendritic configuration and high axonal density. The first and last cell are MCs characterized by substantial axon branching in L1. The axon of the L5 MC is cut several times, hence its projections in L1 are incomplete. The third cell from the left has the X94 morphology (see (Ma et al., 2006; Naka et al., 2019)), whereas the second has features reminiscent of a basket cell. **B** Corresponding firing patterns of cells, introduced in A, in the same color code for subclass used in 3.6; Hyperpolarizing current step in all cells is −100 pA. Morphology and firing pattern show a high correspondence: MCs are overwhelmingly associated with Class I, whereas X94 and other non-MC cells are exclusively Class II.

SST cell morphologies also provide evidence for further possible subdivisions. Generally, their somatodendritic configuration is multipolar and the extent of dendritic trees does not show a preference for either the horizontal or vertical axis. Generally, they carry more spines than VIP cells, but much less so than excitatory cells. They have an ascending axon with a substantial total length comparable to basket cells. Axon density is high at certain target regions, depending on cell identity. Although showing a bigger horizontal spread than VIP cells, the axon rarely extend over two barrels. Vertically, areas of dense innervation are usually confined to one layer. However, some cells which extend their axon into LI also show dense innervation of LII/III.

Similar to the electrophysiological data, distinct types of morphology with coherent features emerge. This manifests most prominently in different targets of their axonal projections. One type of granular and infragranular cells shows a clear preference for L4, where it branches extensively, but with a clear preference to one barrel. These cells are very distinct and have been called X94 cells, according to the mouse line they were first found in Ma et al. (2006). Another morphology type has an axon reaching LI with considerable branching in supragranular layers. Sometimes with strong horizontal T-shaped bifurcations with emphasis on LI, sometimes with projections with a less vertical orientation that fan out and are denser in upper LII/III. These cells are commonly referred to as MCs (see 1.1). MCs of deeper layers usually have an additional innervation area, mostly close to soma. That being said, supragranular layers also contain a considerable share of their axon. Besides the X94 cells, there are definitely types of other not-MC cells, but their rare occurrence makes systematic description difficult. Compared with other types described in this paragraph, their somatodendritic configu-

ration does not stand out. Their axonal branching is most prominent in vicinity to the soma. In addition, LI SST cells show also a strong horizontal orientation in their dendritic tree, which raises the question if they should be considered MCs or treated as a group of their own. Usually they are considered to be a group by themselves (Schuman et al., 2019), but due to their small numbers and high similarities to MCs in axonal branching and intrinsic properties they are included into Class I.

Parallels between morphology and electrophysiological features give further evidence of consistent subgroups. 7 out of the 8 identified MCs recorded with K^+-based intracellular solution are categorized as Class I, whereas all non-MCs are in Class II (7 out of 7). Many SST cells in this study could not be identified conclusively. The ascending axon of infragranular MCs is often cut, which impedes a judgement.

3.2 Specificity of stereotactic injections

Optogenetic mapping of neuronal circuitry demands a specific transduction of the afferent fibers, i.e. in this study the respective thalamic nucleus. Representative examples of injections are given in 3.9 and 3.11. The profile of YFP-ChR2 expressing fibers within barrel cortex was used as method of choice to control for specificity (as seen in 3.8). Evaluating expression in the thalamus was not practical for several reasons: first, YFP is exclusively expressed in the cell membrane. Consequently, differentiating between areas with transduced somata and fluorescence solely due to passing projections or other neurites is difficult particularly at magnifications of 20x or lower. Hence, judging the specificity simply based on the fluorescence signal in the thalamus is not advisable. Slézia et al. (2011), for example, report of thalamic relay cells in the border region of VPM, which extend their dendrites into POm. Second, identifying the exact site and extent of the injection for each hemisphere would entail an enormous amount of additional workload in terms of histological processing and imaging. Third, distinguishing the exact anatomical borders between the two thalamic nuclei requires either tracing or additional immunostaining, as for example done in Urbain et al. (2015).

Ultimately, the distinct patterns of cortical innervation by VPM and POm (see subsection 1.1.3 of the introduction) provide a suitable visual readout of their origin of thalamocortical afferents. The fiber distribution is assessed by the vertical YFP expression profile as shown in 3.8. Deviations from the expected pattern led to exclusion for further analysis. Every slice after fixation and staining was evaluated by considering the area defined by the length of the cortical column and a horizontal axis of 200 microns centered on the cell body of the patched cell. In rare cases YFP-expressing cortical cells were found along the axis, on which the injection pipette was retrieved (see for example transduction in the HC in 3.11). Experiments using slices from this hemisphere are also excluded. Retrograde uptake by axonal projections of cortical cells, which would lead to YFP-expressing cells in LVI of barrel cortex, was extensively examined: slices with a 40x acquisitions, used to capture the morphology of the recorded cell, were scanned in the YFP channel and no slice indicated transduced cells.

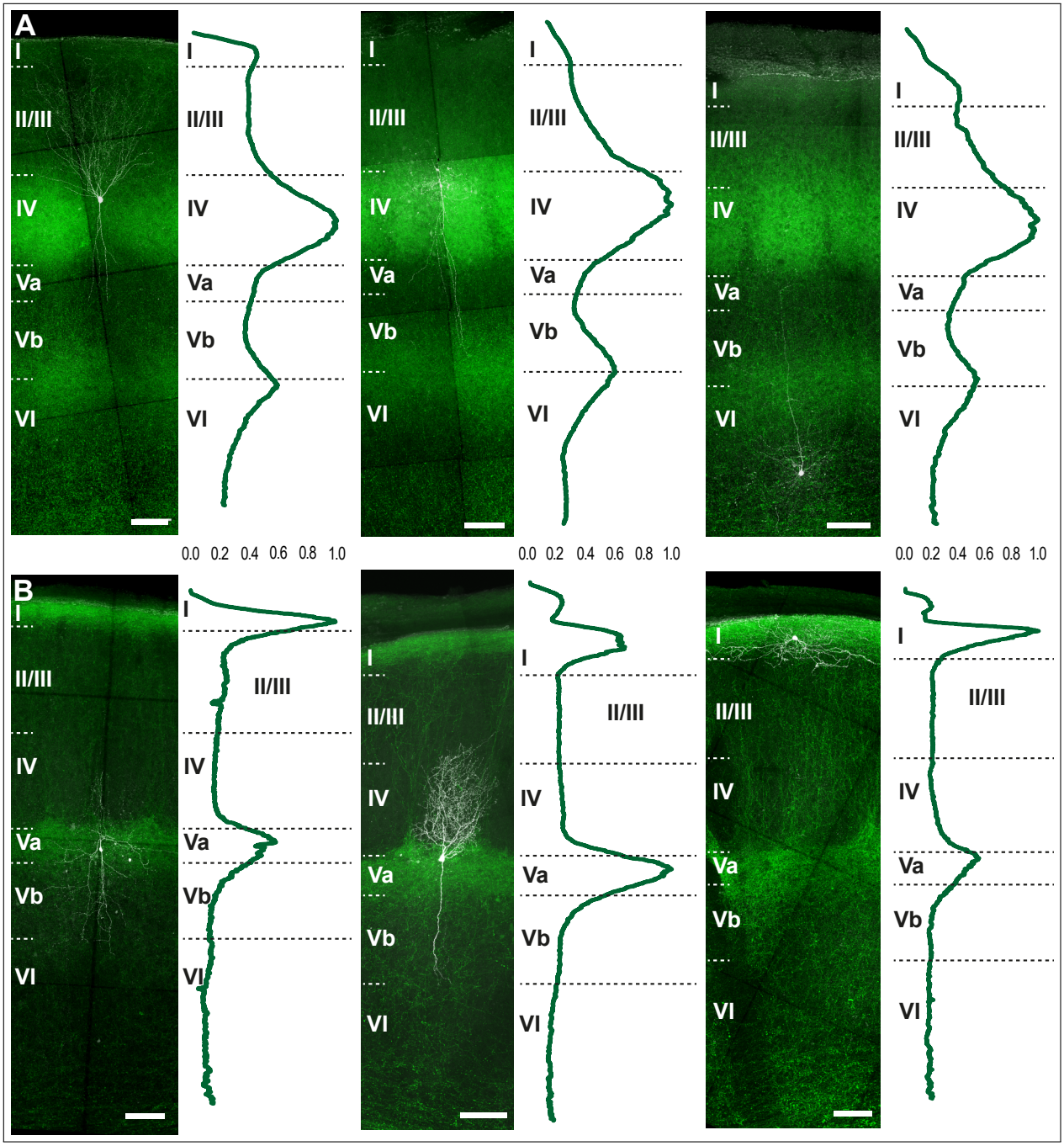

Figure 3.8. Evaluating specificity of injection via thalamocortical projection pattern
A and **B** show maximum intensity projections of representative examples of patched cells in grayscale and the underlying pattern of transduced TCAs revealed by YFP expression in green, for VPM and POm, respectively. Images are accompanied by the normalized vertical plot profile, obtained from sum z-projections. These plots were used to evaluate specificity of the injection. Due to their considerable thickness, some slices show a changing location of the pial surface; leading to a smearing of the signal there (see, for example, dual peaks in LI of last two POm injections). Scale bar: 100 µm.

3.3 Distribution patterns of thalamocortical innervation

As described previously in 2.2.3, slices were treated with TTX and 4-AP to ensure that optical stimulation leads only to direct monosynaptic EPSPs (see also subfigure C of 3.9). Under these conditions, a overwhelming majority of VIP and SST cells show postsynaptic responses given sufficient stimulation (see 3.10). Generally, no layer was devoid of input for either nucleus or cell type. In VPM injections, 53 out of 56 VIP cells (94.6%) are responsive to optical stimulation. The unresponsive cells are located at the poles of the cortical column. LI shows the highest incidence of cells lacking direct innervation. However, results should be interpreted with caution due to small sample size (n=2) . SST cells show a similarly frequent innervation with 52 out of 54 (96.3%) responding cells. The two unresponsive cells are located in LVb and LVI. When pooling both groups, 4 out of 5 cells showing no innervation are located in infragranular layers. However, an analysis according to distance to the pial surface does not show that these cells cluster at a particular depth.

Cells recorded when stimulating POm fibers were predominantly done with Cs^{+}-based solution (see 3.11 subfigure B). Since the firing pattern under these conditions cannot be associated to a certain cell type, correct targeting of fluorescent cells is an important visual control (see subfigure C) and was additionally confirmed by co-localization of tdTomato and Alexa633. On very rare occasion (once in the SST cre-line), morphology of tdTomato expressing cells strongly suggested an excitatory cell, which was excluded from the analysis. 3.12 shows the incidence of paralemniscal innervation. From all recordings 51 out 54 (94.4%) VIP cells show optically evoked EPSPs. The relative input frequency for SST cells is slightly lower, with 36 out of 41 (87.8%). Unresponsive VIP cells are found in LIV and LVb. However, both layers harbor a majority of cells with direct input. Unresponsive SST cells are found in the same layers with the addition of LII/III.

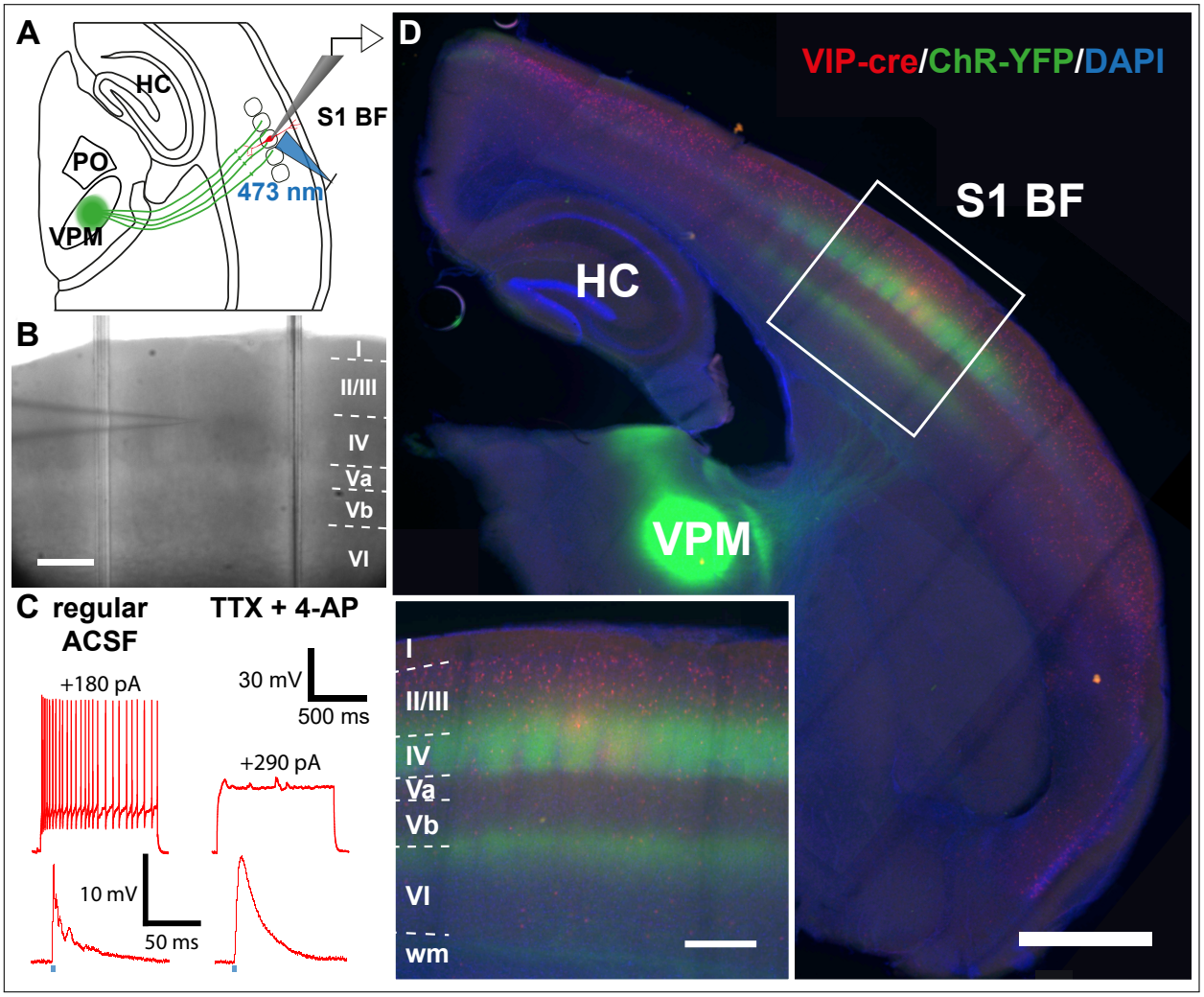

Figure 3.9. Example of VPM injection and experimental procedure
A Schematic illustrating the experimental approach: While recording from a red fluorescent putative postsynaptic cell (here: a VIP cell), ChR2-YFP expressing fibers are stimulated locally with blue laser light. **B** Infrared image of the barrel field of an acute slice. The pipette indicates the location of the recorded cell, which is upper LIV. Scale bar: 300 µm. **C** After characterization of intrinsic properties, TTX and 4-AP are washed in to abolish AP generation. Left traces show a spike train during current injection and optically evoked postsynaptic potentials before the wash in. After the bath application of aforementioned drugs, current injections does not lead to spiking and postsynaptic responses become monocomponent. **D** Example of a fixed slice after completion of experiments. Insert shows endogenous fluorescence of ChR2-YFP and tdTomato driven by VIP-cre in the barrel field. Injection into VPm shows the typical lemniscal termination pattern with strong signal at L4 and a band between L5B and L6. Scale bar of overview: 1 mm; scale bar of insert: 250 µm.

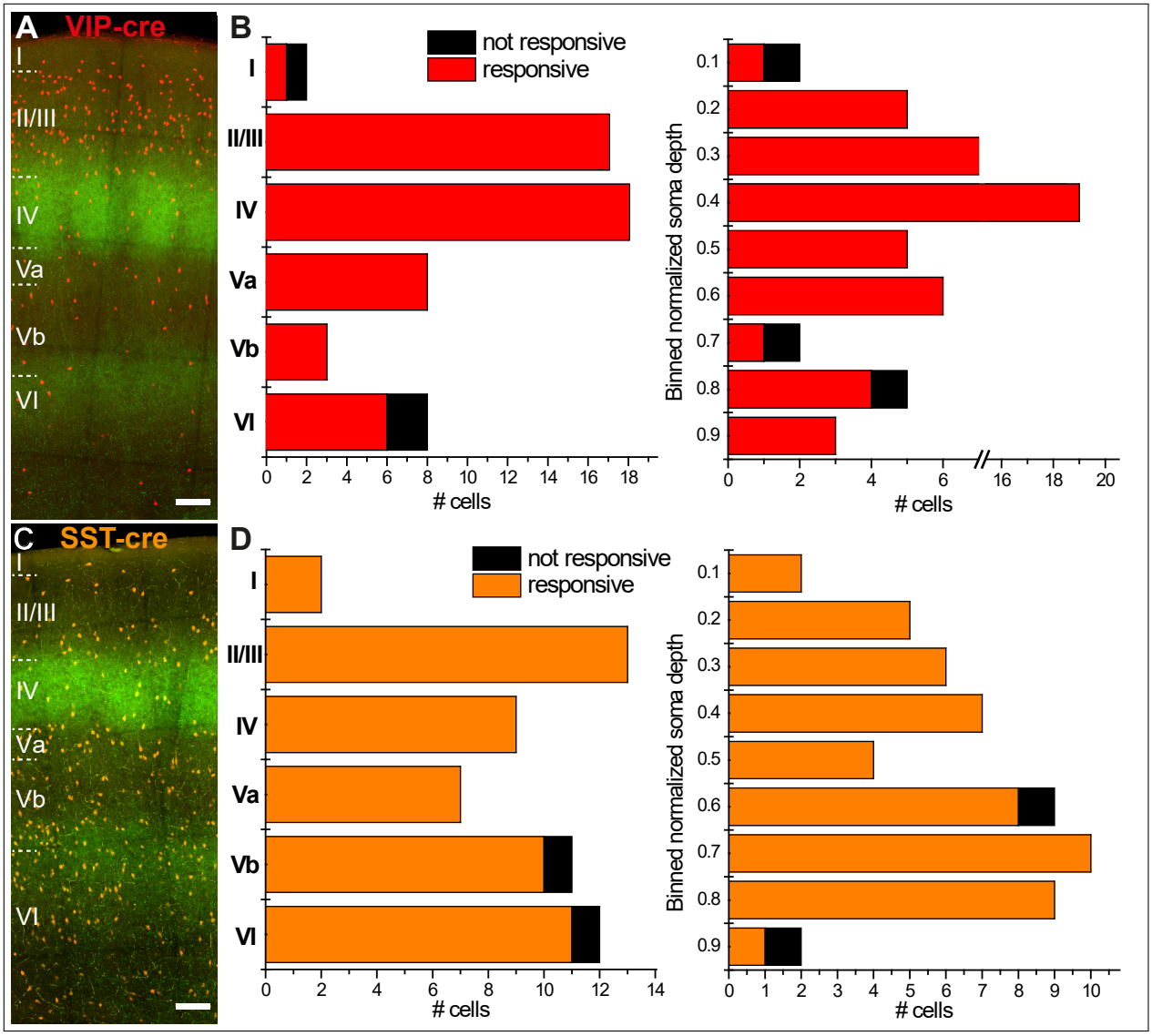

Figure 3.10. Incidence of VIP and SST cells responsive to optical stimulation of VPM fibers

A and **C** Maximum intensity projection of the transduced fibers revealing lemniscal projection resulting from VPM injections. Cre-dependent red fluorescence illustrates the distribution of VIP and, respectively SST cell populations; scale bar, 100 µm. **B** Frequency of responsive and unresponsive VIP cells according to soma location. The first bar plot shows the distribution according to layer and the second one according to normalized soma depth. 53 out of 56 cells are responsive to optical stimulation under TTX and 4-AP and were found in LI and LVI. **D** Input frequency onto SST cells illustrated in the same manner as B. 52 out of 54 cells show responses. Cells without VPM input were found in infragranular layers.

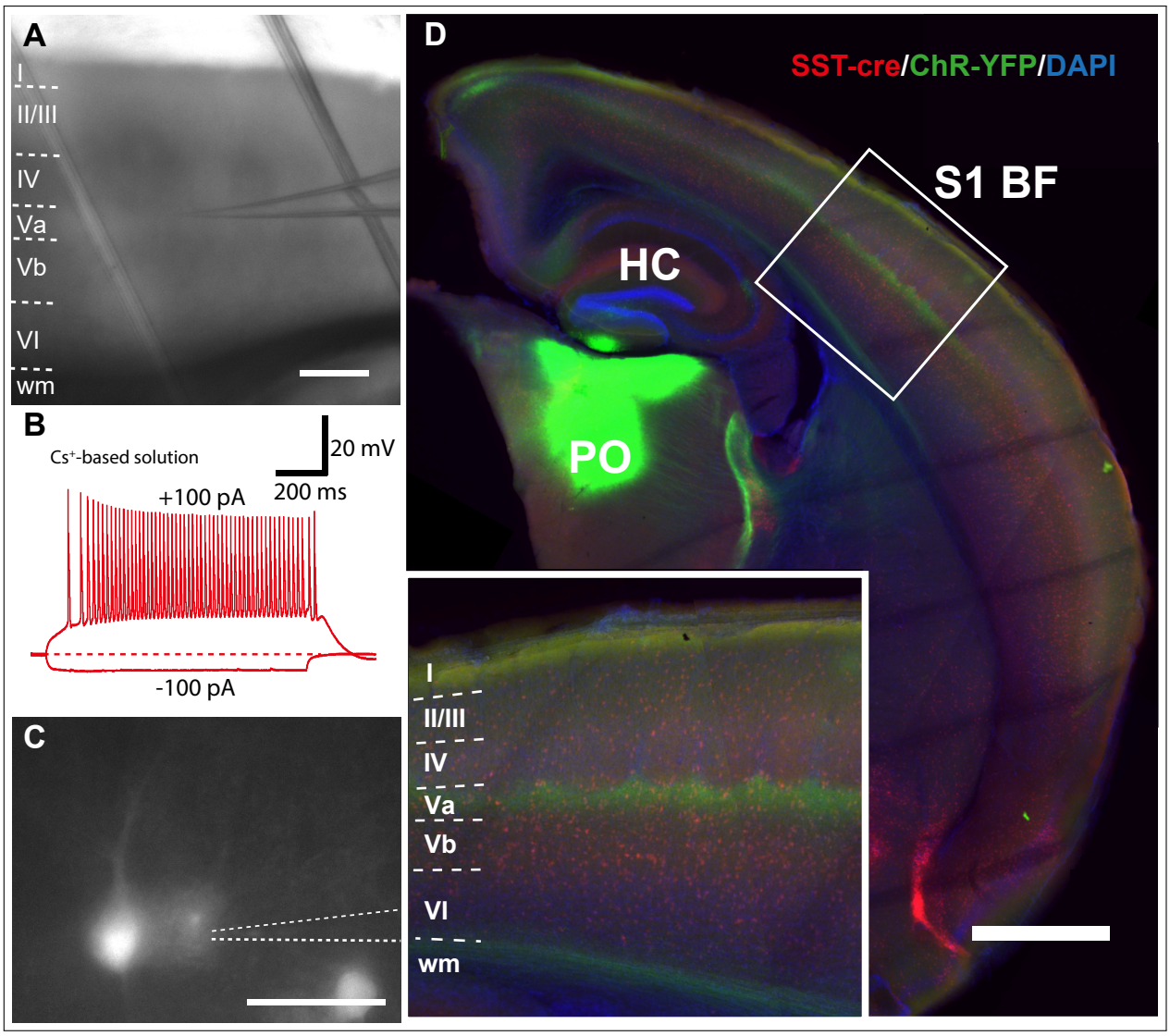

Figure 3.11. Example of POm injection and experimental conditions
A Infrared image of the barrel field of an acute slice. The pipette indicates the location of the recorded cell, located in LVa. Scale bar: 300 µm.
B Cells recorded with Cs^{+}-based solution show different spike wave form and firing patterns, impairing identification by intrinsic electrophysiological parameters **C** Visual confirmation of accurate targeting of fluorescent cells. This is particularly important when the intrinsic electropysiological properties cannot be used for confirmation of cell identity; scale bar: 50 µm. **D** Example of a slice after experiments showing endogenous fluorescence of ChR2-YFP. Injection into POm shows the typical paralemniscal termination pattern with strong signal in LI and LVa as seen in the insert; scale bar of overview: 1 mm; scale bar of insert: 250 µm.

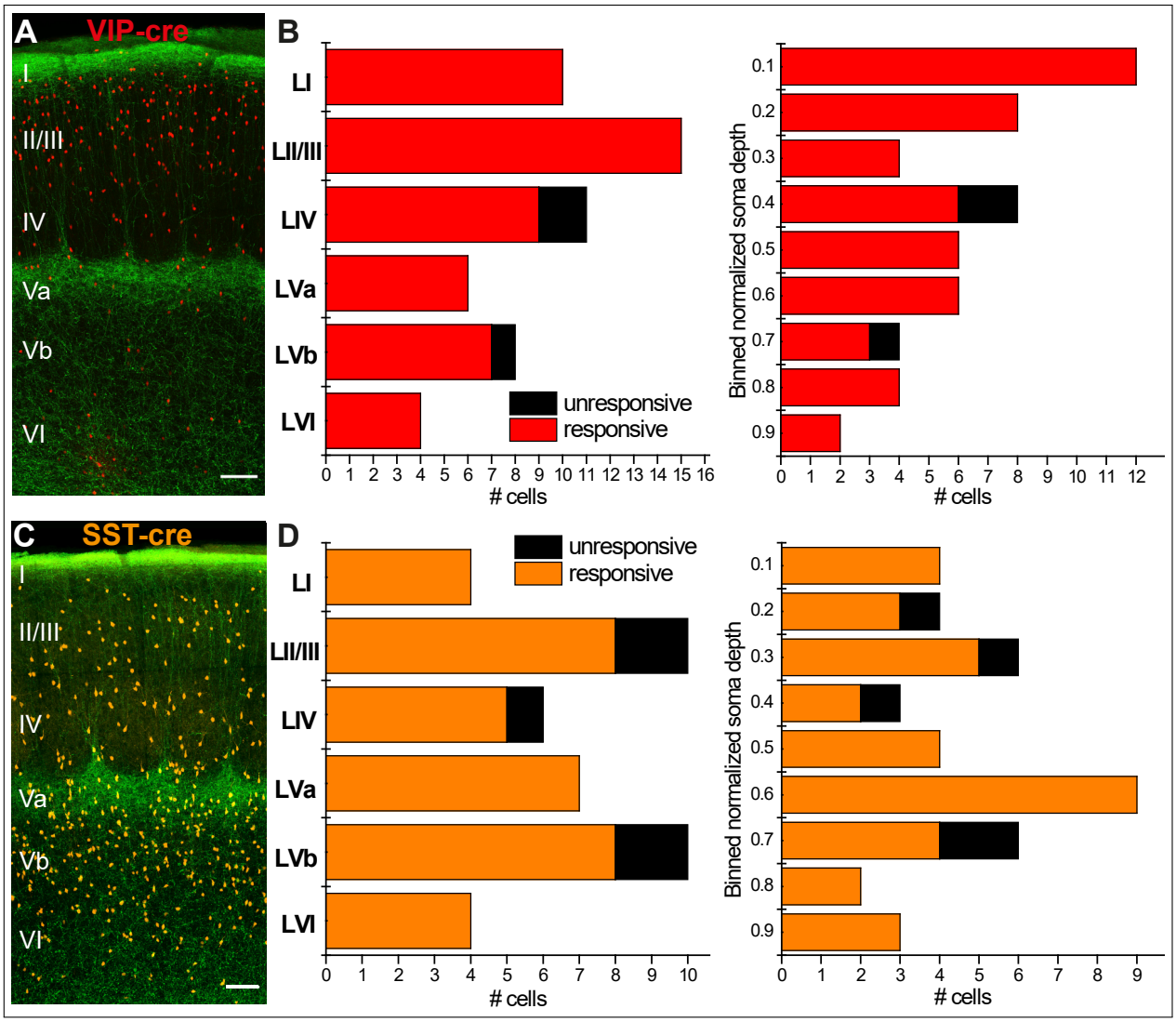

Figure 3.12. Incidence of VIP and SST cells responsive to optical stimulation of POm fibers

A and **C** Maximum intensity projection of the transduced fibers revealing paralemniscal projection resulting from POm injections. Cre-dependent red fluorescence illustrates the distribution of VIP and, respectively SST cell populations. Scale bar: 100 µm. **C** 3 out of 54 cells are unresponsive to optical stimulation under TTX and 4-AP and found in LVI and LVb . **D** Distribution of responsive SST cells illustrated in the same manner. 5 out of 41 cells (12.2 %) are unresponsive and found in LII/III, LIV and LVb.

3.4 Synaptic properties of direct thalamocortical innervation

After establishing that the respective cell indeed receives direct thalamic input, properties of the synaptic input are assessed. It has to be stressed that the quantified responses are under the same pharmacological conditions introduced previously. Hence, the responses might not have the same properties as expected from regular synaptic release. In addition, responses described upon VPM stimulation (as shown in 3.13) were recorded with K^+-based solution, which was done for proper characterization of biophysical properties. Responses of POm stimulation, however, were recorded primarily with Cs^+-based solution. In order to account for variability in expression levels of putative presynaptic fibers, optical EPSPs were compared at threshold stimulation levels. As can be appreciated in subfigure B of 3.13 and 3.14 the interquartile range (IQR) of laser intensities needed to evoke reliable responses varies about an order of magnitude.

3.4.1 Responses upon optical VPM-fiber stimulation

As shown in subfigure A 3.13 optically evoked responses, were predominantly monocomponent, suggesting either release from one single source or multiple highly synchronous ones. Synaptic latencies ranged from 2.97 to 6.56 ms and decreased with higher stimulus intensity. Distribution of latencies was similar between VIP and SST cells with an overall median of 3.73 ms. In terms of input strength there is a considerable difference: responses in VIP cells have a much higher EPSP integral (medians: 0.050 vs 0.164 mV*s; $P \leq 0.001$) and amplitude (medians 1.849 vs 0.963 mV; $P \leq 0.001$) than compared to their SST counterparts. However, rising times of responses, which are also influenced by overall size of the response, are not significantly different. Given the stark difference in EPSP integral between the populations, the expectation would be that SST cells have significantly lower rising times. Hence, evoked responses in SST cells are not scaled down versions of VIP cells, but also show a different kinetic properties with less steep rising phases (as seen in the raw traces).

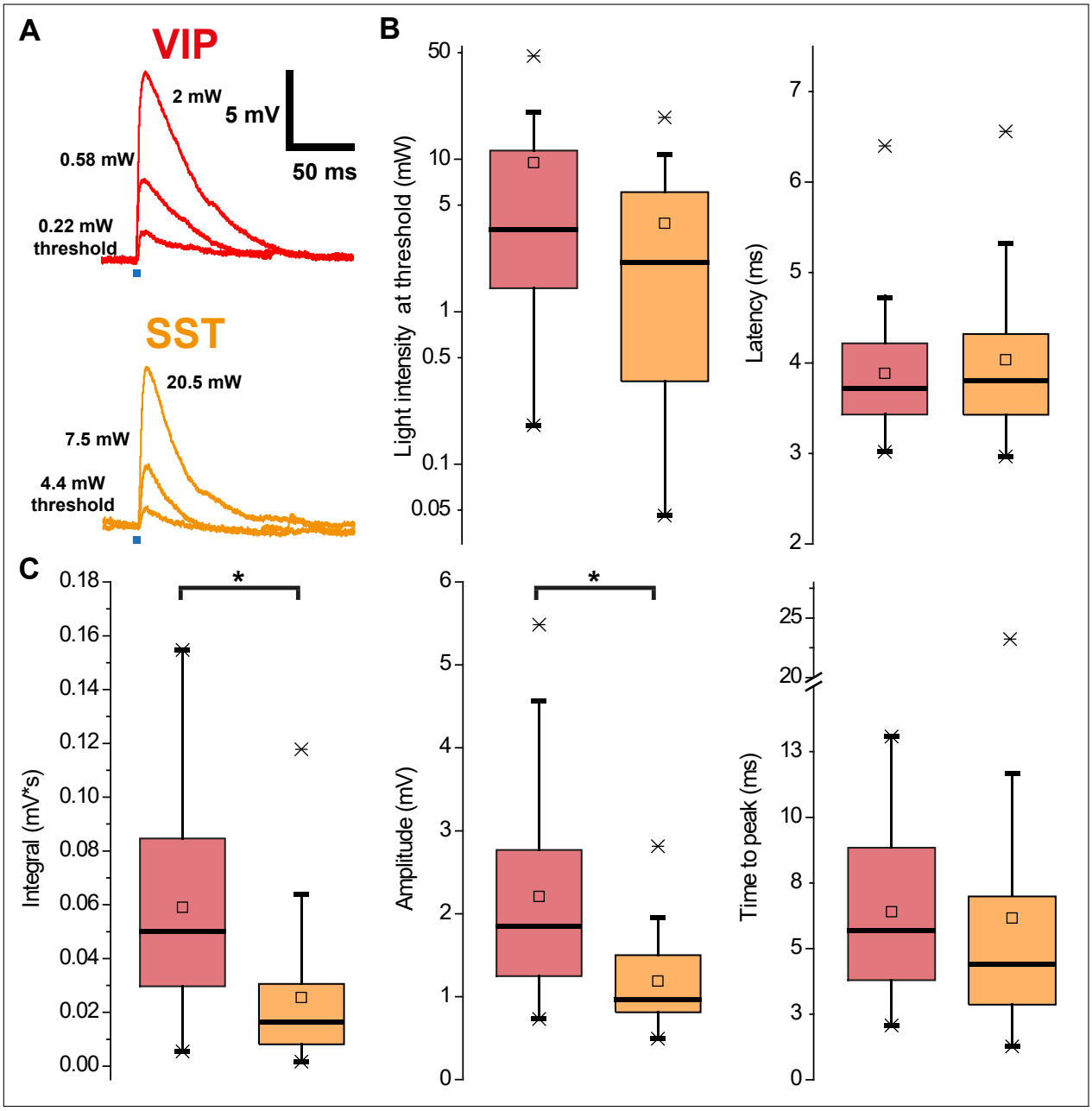

Figure 3.13. Properties of threshold responses upon optical stimulation of lemniscal fibers

A Examples of optically evoked responses with increasing laser stimulation shown for a VIP and a SST cell. Bold font indicates intensity used at first response. The blue marks delineate the onset of 1 ms stimulus. Duration is not to scale. Note that responses can be overwhelmingly characterized by mono-component function suggesting a singular synaptic event. **B** Stimulation intensity and EPSP latency between SST and VIP cells are similar. The little square within the boxplot indicates the average. **C** Inputs to VIP cells are significantly stronger in both EPSP integral (medians: 0.050 vs 0.164 mV*s) and amplitude (medians 1.849 vs 0.963 mV); in both cases $P \leq 0.001$.

3.4.2 Responses upon optical POm-fiber stimulation

Unlike in the previous figure, responses described in 3.14 are made with Cs^+-based solution. Hence, parameters described here cannot be compared with the previous subsection. Under these conditions, higher stimulation intensity of POm fibers is needed to evoke threshold responses in SST cells (median: 0.23 vs 0.44 mW; P = 0.011). VIP cells have considerable longer latencies (median: 6.6 vs 5.5 ms; P = 0.030). In addition, they show a much higher variability in reponse times (range: 7.1 vs 5.46 ms; IQR: 3.05 vs 1.89 ms). EPSPs of SST cells have considerable smaller amplitudes (median: 2.87 vs 1.65 mV; P = 0.003), whereas overall input strength quantified by integral is comparable (P = 0.357). Consequentially, SST cells show longer rising times (median: 4.8 vs 8.0 ms; P = 0.015), which makes up for smaller amplitudes.

3.4.3 Comparison of optical stimulation of VPM vs POm fibers

A general comparison between responses evoked by VPM vs POm fibers is difficult, since not all cells were recorded with the same intracellular solution. However, the sample of SST cells recorded with Cs^+-based solution was sufficient to compare the optical stimulation of fiber populations (as seen in 3.15). Threshold responses of POm stimulation have a significant longer latency (median: 4.5 vs 5.5 ms, P = 0.002, subfigure C). The integral of EPSPs evoked by VPM fibers are a little higher (see 3.15 subfigure D), but this tendency is not significant (median: 0.0828 vs 0.0360 mV*s; P = 0.095). Amplitudes, on the other hand, are substantially higher in VPM stimulation (mean: 3.03 vs 2.05 mV; t-test, P = 0.014), whereas rising times of EPSP are comparable.

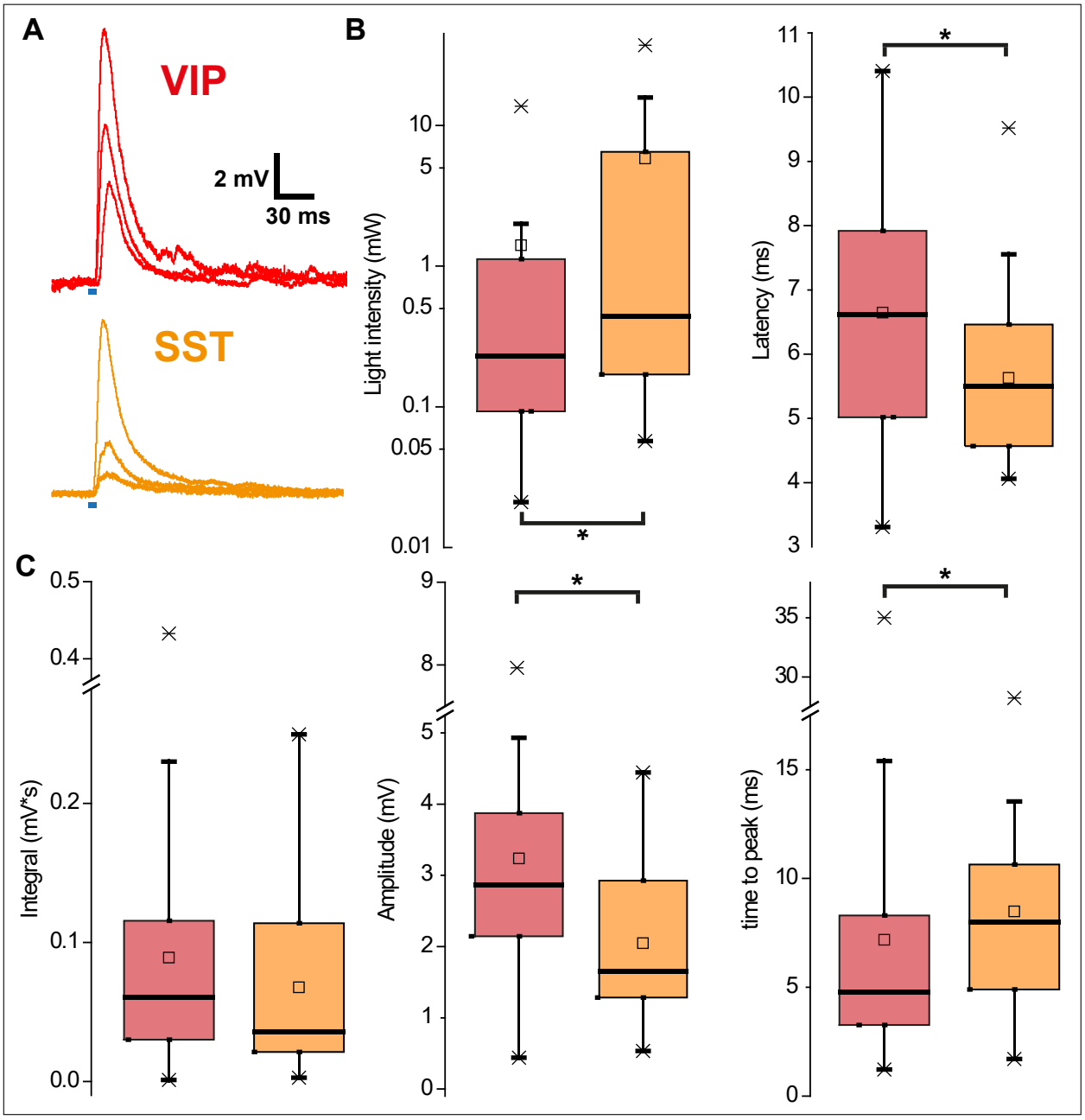

Figure 3.14. Properties of threshold responses upon optical stimulation of paralemniscal fibers

A Examples of optically evoked responses with increasing laser stimulation shown for a VIP and a SST cell. **B** Laser intensity necessary to evoke responses in SST cells is significantly higher (median: 0.23 vs 0.44 mW; P = 0.011), whereas latencies in VIP cells are higher and more variable (median: 6.6 vs 5.5 ms; P = 0.030). **C** Overall input strength quantified by EPSP integral is not significantly different, P = 0.357). However, VIP cells have responses with higher amplitudes (median: 2.87 vs 1.65 mV; P = 0.003), whereas SST cells have a longer rise time (median: 4.8 vs 8.0 ms; P = 0.015).

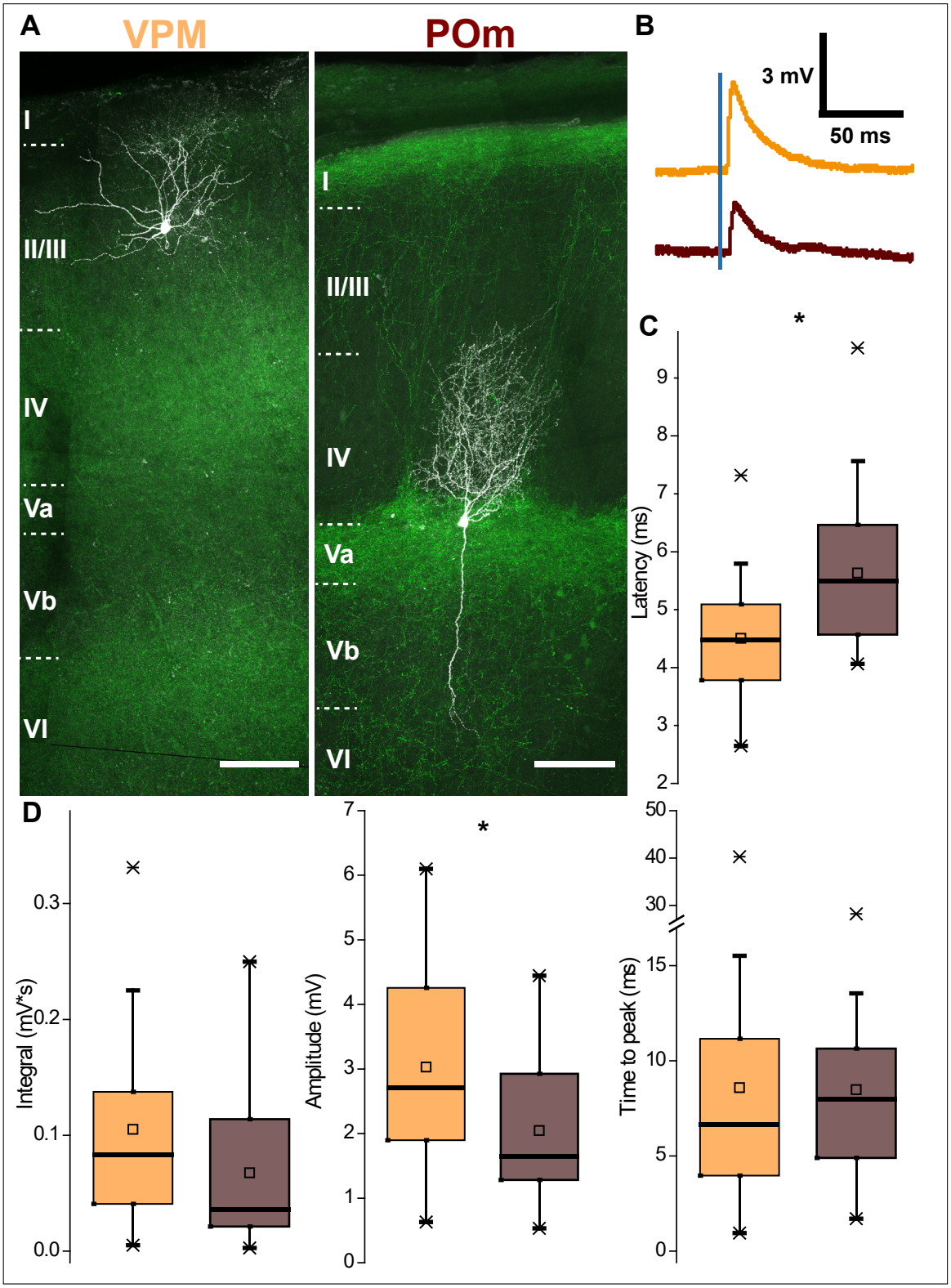

Figure 3.15. Differences between VPM and POm stimulation in SST cells recorded with Cs^{+}-based intracellular solution
(legend continued on next page)

Figure 3.15. Differences between VPM and POm stimulation in SST cells recorded with Cs^+-based intracellular solution. **A** Examples of two different biocytin-filled SST cells with transduced fibers of the respective nucleus in green as seen in 3.8. Scale bar: 100 µm. **B** Example of threshold responses according the respective fiber populations; VPM in orange, POm in brown. **C** Evoked responses by POm stimulation have a longer latency (median: 4.5 vs 5.5 ms, P = 0.002). **D** Integrals of EPSPs of POm stimulation have a non-significant tendency to be smaller (median: 0.0828 vs 0.0360; P = 0.095), whereas peak amplitudes are clearly lower (mean: 3.03 vs 2.05 mV; t-test, P = 0.014).

3.5 Thalamocortical innervation and cellular diversity

A proper characterization of AP wave form and firing pattern of cells could only be obtained in recordings with K^+-based intracellular solution, which were predominantly used for VPM stimulation. In case of VIP cells there was no apparent relationship between firing pattern and the properties of responses under TTX and 4-AP (data not shown). In addition, cells that are unresponsive under these conditions (see 3.10) are too infrequent to relate them to in-group diversity. Since mostly done with Cs^+-based solution, POm input could not be related to different firing pattern of the VIP cells.

3.5.1 SST subtypes

From the investigated populations, SST cells show apparent subtypes. Some SST cells show a FS phenotype, which is associated with strong thalamic innervation and feed-forward inhibition. Consequentially, the question arises if SST subtypes show differences in synaptic responses. In order to include both VPM and POm injections into the analysis, subtypes were identified by morphology and characterization of biophysical properties with Cs^+-based solution. Since SST subpopulations show robust and distinguishable morphological traits, it was possible to associate them with basic subthreshold parameters. Cells, identified as either MCs or nMCs (as seen in subfigure A of 3.16), show strong differences in R_{in} and time constant τ (see subfigure B). These parameters are used to classify SST cells, which could not be identified before, due to incompleteness of the axonal tree or insufficient staining. Cells with R_{in} and time constant τ higher than the first quartile of identified MCs (200.6 MΩ and 23.9 ms) are

assigned to this group, whereas recordings are deemed to be from nMCs if they were below the third quartile of identified cells (185.7 MΩ and 16.5 ms). As a result of this approach, 3 of 58 cells are not assigned to either category. Since L1 SST cells show very similar properties to MC cells in both electrophysiology and morphology, they are included in the following analysis (see subfigure C).

Rising times of threshold responses from both kinds of injections are similar (see 3.15 subfigure D) and were consequently pooled. However, nMCs show significantly shorter rising times (median: 4.70 vs 8.36 ms, P = 0.019). In addition, type of stimulated fiber and cell identity show a significant interaction effect onto response amplitudes (subfigure E, 2-way-ANOVA, P = 0.01): responses of nMC, when stimulating VPM projections, are considerably higher (medians: 4.18 vs 2.58 mV), whereas they are comparable in the POm condition and even have the tendency to be smaller (median: 1.46 vs 1.97 mV). This finding indicates that, lemniscal innervation of nMCs is by far the most prominent in comparison with other combinations of thalamocortical input and SST subclasses.

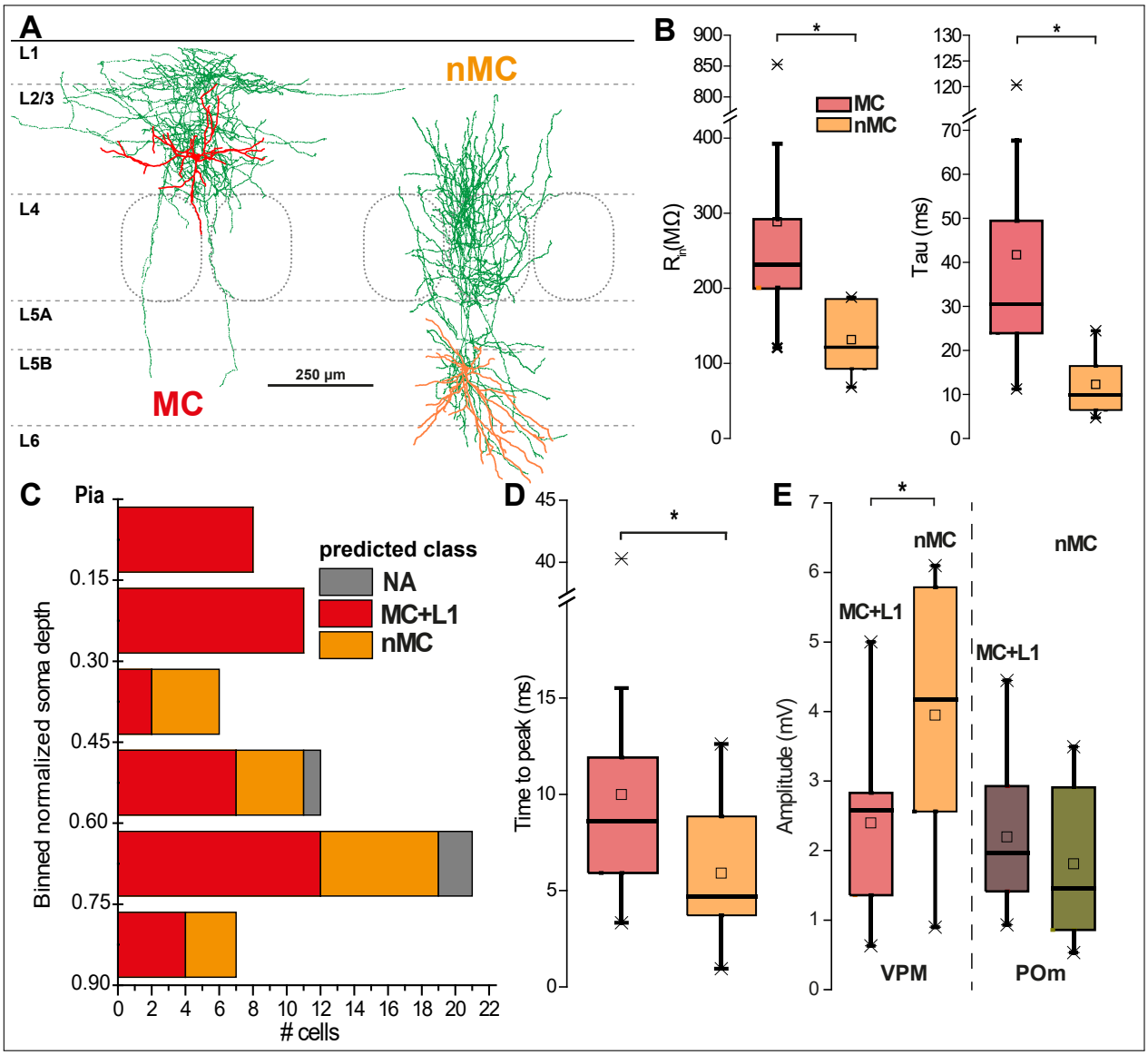

Figure 3.16. Properties of thalamocortical responses of morphological distinct SST cells
A Examples of reconstructions of different SST subtypes. MCs are characterized by an axonal plexus in LI as shown on the left, whereas non-MCs show often axonal branching in LIV. **B** Recordings made with Cs^{+}-based solution show clear-cut differences between morphological identified cells. **C** Distribution of assumed SST subtypes. Intrinsic properties of 3 cells are too ambiguous to assign them to either subtype. **D** Responses of non-MCs have a significantly shorter rise time. Data is pooled from the two nuclei, since they are similar (see 3.15); median: 8.36 vs 4.70 P = 0.019. **E** Amplitudes of responses shows a significant interaction effect between cell type and nucleus due to VPM stimulation of non-MCs; 2-way-ANOVA, P = 0.01.

Disscusion

4.1 Summary of results and interpretation

Most features of intrinsic properties and morphology of VIP and SST cells (as described in 3.1) are in line with previous reports: VIP cells show either one of three prototypical firing patterns or a blend of two them. However these phenotypes do not associate with other biophysical (i.e. in the domains of spike waveform or subthreshold parameters) or morphological features, which indicates there are no apparent subpopulations with cohesive features (see 3.5, [Prönneke et al., 2015; Prönneke, 2016]). That being said, BS and highly adapting cells are found exclusively in the upper half of the cortical column (as seen in subfigure D 3.4), which is the only indication of potential further differentiation.

In contrast, SST cells can be further differentiated into distinct groups with different firing patterns strongly associated with certain morphological types (see 3.6 and 3.7): In addition to the early described MC, there is a second group of SST cells with a quasi-FS phenotype and a non-MC morphology. This later category of cell is predominantly, but not exclusivly, found in L4 and L5 (see 3.6D). Several studies have described a similar population in murine primary vibrissal somatosensory cortex (Ma et al., 2006; Xu et al., 2013; Naka et al., 2019). Notably, this sample lacked some previously described hallmarks, which are BS-SST cells and rebound spiking, the signature characteristic of LTS cells (Kawaguchi and Kubota, 1993). However, these deviations can be attributed to differences in experimental conditions in particular animal age and composition of solutions used (see e.g. Tripathy et al. (2015); Tebaykin et al. (2018) and can be seen in other studies as well (Jiang et al., 2015).

Both VIP and SST cells are frequently and directly innervated by VPM and POm (see

figure 3.10 and 3.12). Interestingly, most of recorded L1 cells, which are not suspected to have far reaching descending dendrites (see, for example, Lee et al. [2015]; Schuman et al. [2019]), also receive VPM input. Consequently, even though lemnsical fibers are very sparse in the upper half of supragranular layers, they have to innervate GABAergic cells there. Indeed, fibers from the ventrobasal complex of thalamus in L1 have been reported before (Bernardo and Woolsey, 1987; Lu and Lin, 1993) and in-vivo responses of sensory stimulation in barrel cortex also suggest that L1 cells and apical pyramidal tufts are innervated by specific thalamic projections (Zhu and Connors, 1999).

There are some notable differences in the functional properties of optical fiber stimulation: EPSP amplitude at threshold stimulation is higher in VIP cells for both VPM and POm input (see figure 3.13 and 3.14). Moreover, overall synaptic input strength of the lemniscal pathway -quantified by the EPSP integral- is substantially stronger in VIP cells (see figure 3.13). Consequently, the thalamocortical innervation to VIP cells is of considerable size and efficacy, which is in line with previous sporadic evidence (Staiger et al., 1996b; Wall et al., 2016; Williams and Holtmaat, 2018).

Postsynaptic input amplitudes onto SST cells are particularly small for POm fiber stimulation (see figure 3.15). These results will be discussed in a separate section.

Thalamocortical innervation, assessed by input incidence and threshold responses, does not interact with the diversity within the VIP population. SST subtypes, on the other hand, show some effects in regard to thalamocortical input. Evoked threshold responses in cells associated to nMC morphology have generally shorter rising times. In addition, considering VPM stimulation and Cs^{+} solution, they have substantially higher amplitudes (see 3.16). Taken together, these differences in synaptic properties suggest that thalamocortical innervation of nMC -in concert with their intrinsic properties- is also more like those for PV cells.

4.2 Methodological considerations

The sample presented here does not differentiate between quasi-FS and proper FS (meaning PV expressing) cells. However, sufficiently preserved intracellular labeling suggests that the non-MCs category also includes morphologies that have not been described in the X94 line (see the different class II cells of 3.7 and Ma et al. [2006] and Xu et al. [2013]). These observations suggest that some non-MCs cells could express the marker PV. Indeed, there are several publications in line with this assumption. Hu et al. (2013), for example, report that 6-10 % of the cells labeled by the SST-cre line belong to this population. The question arises if these cells are mislabeled due to off-target expression of cre or if they present the end of the spectrum of intrinsic electrophysiological properties of SST cells. Lee et al. (2010) report an overlap of PV and SST cells on the level of transcription, which they attribute to PV cells containing SST-ribonucleic acid (RNA). Consequently, off-target expression in at least some of the FS cells seems to be a likely explanation. Furthermore, PV cells are also labeled in a Htr3a cre line (see Allen Brain Atlas Cell Type Database; Gouwens et al. [2019]), which is supposed to target a non-overlapping population. PV cells in particular seem to show transient RNA of other lineages or might be the default fate of several interneuron populations that has to be repressed with some diligence to maintain another lineage (see for example Malik et al. [2019]). However, the identity of FS-SST cells has not been directly addressed with methods such as lineage tracing and dual recombination (Lim et al., 2018; Madisen et al., 2015) and is not conclusively resolved. Judging from the relative frequency of the typical X94 cell, these cells can only be a small minority of the non-MCs and SST-Class 2 category. The effect of the inclusion of these cells is unclear, since unambiguous distinction from quasi-FS is rarely possible. Interestingly, the distribution of amplitudes of thalamocortical responses does not suggest that these cells have a stronger input than VIP cells. PV-FS neurons, on the other hand, are known to receive a robust thalamic drive, with even stronger responses than excitatory cells (Ji et al., 2015). However, even considering only the upper range of response amplitudes to SST cells, input to VIP cells was substantially higher upon VPM stimulation (see 3.13). In addition, cells with a marked FS phenotype, identified with K^+-based

solution, do not appear as outliers within the distribution of cells labeled with SST-cre. Consequently, no attempt was made to exclude cells that potentially might not belong to the SST population.

In the recent years, optogenetics became a wide-spread method for investigating neuronal circuitry. Even though having many advantages, this approach comes at the price of introducing several unknowns into the stimulation, which make quantitative interpretations at times difficult. There are several confounding factors that have to be mentioned: for one, ChR2 expression density likely varies not only between different injections, but also from cell to cell. Unfortunately, this factor is hard to ascertain and is rarely reported. Consequently, very similar stimulation strengths can yield very different responses, even when the underlying connectivity is the same. In order to control for such an effect, many studies use a second cell as a mean to normalize response sizes from slice to slice (see for example Pfeffer et al. [2013]; Ji et al. [2015]; Audette et al. [2017]). The ideal reference cell should have very consistent input from the presynaptic population, but synaptic connectivity onto every type of neocortical neuron is inherently variable. An additionally recorded cell only yields benefits to the extent, in which its input strength varies less than the connection of interest. Since it is uncertain if such a condition is met, in particular in case of POm stimulation, this approach was not chosen in this work. Another possibility is to normalize recorded response amplitudes by the average of several reference cells in the same layer and slice (as for example done for excitatory inputs in Ji et al. [2015]). This approach has far more validity, however, it is incompatible with a thorough morphological characterization, which is essential for understanding interneuron diversity. That being said, to ensure that insufficient expression levels can be excluded as reason for the lack of direct responses, recordings from cells with expected higher input strength were used as positive controls: like LIV spiny stellate cells, in case of stimulation of VPM fibers or LVa PCs in case of POm. A second important aspect, which has to be mentioned, is the effective illumination of the optical stimulation. Most studies report the used intensities as measured directly from the light source. The effective stimulation strength, however, is also determined by various other factors such as the coupling efficiency and the illuminated area. Hence, comparisons

between different studies have to be done with caution and mindful of the particularities. Laser stimulation as used in this study provides a high power light beam that can be easily coupled and provides a comparatively small field of illumination. However, intensities in this work are comparable to Petreanu et al. (2009), in which stimulation of up to 1.2 mW with a much smaller beam diameter of 6–16 µm was used. To sum up, the stimulation used in this work is estimated to be on the upper end of the spectrum when compared to similar experiments, yet appropriate to the experimental impediments.

Interpreting synaptic properties of input in the used condition has to be done with caution. The influence of TTX and 4-AP make stimulated vesicle release and recording condition rather artificial. The unusual long synaptic latencies, which are known to be much shorter in paired recordings, are a good indication of this fact. Hu and Agmon (2016) achieved in-vitro paired recordings between neurons of various types (including one SST cell) in the primary somatosensory cortex and projection cells of the respective thalamic relay nucleus. Latencys of unitary EPSPs ranged from 1.22 to 2.62 ms. It is unclear how much the axonal conduction contributes to these values, but it is reasonable to assume that selective stimulation of fiber terminals as done in this study would lead to even shorter time spans. So why are the latencies reported in this work a multiple of those values? Two factors are the likely contributors of this lengthening. First, presynaptic ChR2 stimulation is known to be temporally less precise, which is potentiated in a threshold response paradigm. Cruikshank et al. (2010), for example, using a minimal optogenetic stimulation reported latencies of up to 5.35 ms in regular ACSF. Second, the abolishment of neuronal spiking and the partial blockade of repolarizing K^+ leads to unknown biophysical conditions in both pre- and postsynaptic cell membranes. This has not only likely effects on charging and conduction velocity, but also changes the recruitment of presynaptic Ca^{2+} channels from all-or-none to dose-dependent mediated by optically-evoked depolarization. A helpful reference for understanding presynaptic Ca^{2+} dynamics and their transposition into vesicle release are works like Schneggenburger and Neher (2000) in the calyx of held, because they can be carried out with more graded manipulations in the absence of APs, similar to the experimental conditions in this work. Their data obtained by presynaptic Ca^{2+} uncaging

paired with postsynaptic recordings show latencies in responses up to 10 ms when flashes elevated internal Ca^{2+} concentrations below 5 µM; assuming that recruitment and dynamics of ChR2 might add an additional delay of up to several milliseconds between stimulation and measured responses, and we reach the upper range of reported latencies of this work. Indeed, the bath application of TTX and 4-AP have previously been reported to delay synaptic responses and are in line with previous studies. Petreanu et al. (2009), for example, report of latencies upon perisomatic stimulation ranging from 6 - 18 ms. Interestingly, onsets of responses of POm stimulation are more delayed compared to VPM, at least in SST cells patched with Cs^{+}-based solution. There are two plausible explanation for this effect. For one, distinct spatial properties like a bigger axonal diameter and/or a different ion channel composition of the presynaptic cell membrane could lead to different biophysical properties. These in turn could cause differences like slower electrotonic spread or recruitment of Ca^{2+} channels by giving POm terminals a higher time constant. Another possible explanation would be that the sites of synaptic release are located at more distal dendrites and are actually outside the field of stimulation. The initial depolarization and the site of the synapse would then be at different locations, connected by transduced fibers passing through the field of illumination. Either passive propagation or some sort of suprathreshold event like Ca^{2+} spikes would take up additional time to reach a distal synapse. VIP cells in the granular layer and its vicinity, for example, are characterized by their vertically elongated dendrites that reach LI. The high variability of latencies to optical stimulation of POm fibers (shown in subfigure 3.14) could be caused by an overlap of dense termination and distal dendritic branching. In addition, VIP cells show significantly later response onsets than SST cells. As described earlier in this paragraph, the latency is predominantly determined by the presynaptic compartment. The stimulation of passing projections is a more reasonable explanation than VIP and SST cells being innervated by different populations of POm fibers.

Last but not least, there are some naturally occurring synaptic properties, which cannot be assessed with this methodology. The true reliability of the synaptic release cannot be determined, since the stimulation is set to trigger Ca^{2+} channels directly.

However, this factor might be highly relevant to understand thalamocortical input. In case of the one paired recording with the postsynaptic SST cell, Hu and Agmon (2016), for example, report a failure rate of 17%, whereas any other cell shows no failures at all. Are data presented here therefore biased in favor of SST cells? The opposite might be the case: input strength assessed here is based on single flash stimulation and does not account for short term dynamics of the synapse. In the aforementioned study, facilitation and summation of EPSPs caused by presynaptic bursts strongly increased spiking probability of the SST cell, which was targeted via the X94 line. This effect is very likely to be stronger in MCs, which have a much higher time constant. These phenomenons are not investigated here, because the pharmacological treatment and the kinetics of the used ChR2 variant make high frequency stimulation nonsensical.

4.2.1 Possible POm innervation of SST cells

This work is in conflict with previous published research in respect of the POm innervation to SST cells (Audette et al., 2017; Williams and Holtmaat, 2018). How can this disparity be explained? There are two straightforward explanations, which are going to be discussed in detail.

First, could the results reported here be due to an unspecific stimulation? ChR2 expression outside of the PO is controlled by assessing the projection pattern of transduced fibers. In addition, slices used in experiments were checked for transduction of cortical cells by retrograde spread or backspill along the retracted pipette. Assessing the specificity of injection directly in the thalamus turned out to be not practical, so sparse contamination by other thalamic nuclei other than the VPM cannot be excluded definitively. However, SST-specific rabies tracing does not suggest that such connectivity exists (Wall et al., 2016). The other possible source of unspecific responses is a stimulation of PO fibers leading to suprathreshold events in excitatory cells in cortex. The application of TTX and 4-AP is used to ensure direct monosynaptic stimulation. Since its first use by Petreanu et al. (2009), this assumption has not been called into question. The most elegant negative control would be to record from a cell type which is encompassed by transduced fiber terminals, but is known to lack their innervation. Unfortunately, there is no known type of neocortical neuron, suitable to demonstrate

the assumed specificity of the used optical stimulation; at least to the knowledge of the author. In the aforementioned study applying TTX alone led to elimination of ”98 $\pm$ 1.9% of the excitatory postsynaptic currents evoked in the absence of drugs”, while using a comparable irradiance. There are many indicators that the stimulation used in this study is passing only one synapse. First, after the bath application responses are usually monocomponent with occasional multiple peaks at higher stimulation intensity. Second, measured postsynaptic responses are highly reliable and scale with stimulus intensity, which are features in conflict with release caused by some sort of all-or-none suprathreshold response. Third, even though fast spiking PV cells are known to receive strong thalamic input, recorded responses did not show signs of disynaptic inhibiton, even when assessed in VC at different holding potentials.

Another explanation for the stated discrepancy in the findings is that experimental conditions in the other studies were insufficient to detect smaller or more distal inputs. Indeed, there are several factors that suggest this. Audette et al. (2017) used K^+-based intracellular solution, which makes it harder to detect distal inputs. Comparing intensity of stimulation, on the other hand, is not straightforward. Unlike this study, they used a 5 ms long light pulse. It is unclear how pulse width influences recruitment of fibers in this particular case. A computational study by Foutz et al. (2012), using wild-type ChR2, suggests a difference of about two orders of magnitude when considering the AP threshold irradiance. Hence it is reasonable to assume, that this factor is probably the most influential. The light stimulation was administered via a light-emitting diode (LED) under otherwise similar conditions and had a irradiance of 2.13 mW over an circular area of about 1 mm, which is in the vicinity of parameters in this study. In addition, it has to be mentioned that Audette et al. (2017) excluded SST cells with an FS phenotype. It is unclear if this applied to all non-MCs or just a subpopulation of them and is not done in this study. Optogenetic stimulation of a putative POm-SST synapses in Williams and Holtmaat (2018) paints a similar picture. First of all, the data set is comprised of only 3 LII/III SST cells, which were also recorded with K^+-based intracellular solution. Second, stimulation pre bath application evoked only small post-synaptic potentials of an average of 1.21 mV before wash in, hinting at very low intensity

stimulation. However, the same experimental procedure in VIP cells shows a reduction, but not an abolishment of responses. In summary, differences in observations in the described studies and this work are likely due to the use of different intracellular solutions. A comparison of responses evoked by VPM versus POm fiber stimulation suggests that synapses of the latter nucleus target more distal dendrites of SST cells. Latencies of responses show a considerable increase, whereas rising time and integral stay comparable (see figure 3.15). EPSPs originated from more distal dendrites have a ”smeared” appearance when recorded at the soma, which is due to dendritic attenuation. This phenomenon has a strong effect on peak amplitudes, but less so on the integral (Williams and Mitchell, 2008).

4.3 Integration into current literature

The data presented in this work firmly establishes the thalamocortical innervation of VIP cells by the two main afferent nuclei VPM and POm. Although anatomical evidence has long suggested a direct drive by sensory inputs (Staiger et al., 1996b), it is an often overlooked fact in the current understanding of VIP cell function. Research of recent years has placed them as an integrator of top-down input from other cortical areas and neuromodulatory sources (see [Wang and Yang, 2018] for a recent review). Thalamocortical innervation is yet another source of long range input and has likely a similar influence on VIP cell activity as previously described afferents. Hence, also direct influence of immediate sensory information from the periphery has to be considered in understanding VIP function. This more general capacity to be driven by various sources outside the local network, makes them central hubs of information processing. The question of how these diverse inputs are translated into VIP activity arises. Future research is needed to illuminate how all these various sources are integrated along their extensive vertical dendrites and determine VIP firing. It is noteworthy, that the input-output function of individual cells is highly dependent on different contexts like the cortical state or the presence of neuromodulation (Prönneke et al., 2019). The data presented here casts doubt on the usefulness of current approaches to further differentiate VIP cells. Recent publications by He et al. (2016) and Paul et al. (2017)

suggest that VIP cells can be further divided by the secondary markers CR and CCK. However, differences in their properties do not appear to be very salient and there is even a non-negligible overlap between the groups. Similarly, thalamocortical circuitry does not provide further insight in VIP cell variability. Consequently, the underlying variables suitable to explain the spectrum of intrinsic properties of VIP cells are yet to be determined. It seems reasonable to assume, that traits of VIP cells, which manifest on a continuous spectrum, are rather driven by gradual environmental factors than cell lineage or hard-wired genetic programming. Mardinly et al. (2016), for example, have shown that the transcription of VIP cells is particularly susceptible to changes due to sensory experience.

In addition, the findings of this work provide an explanation of the present ambiguity in the literature on thalamocortical innervation of SST cells. Inputs onto SST cells have comparatively low amplitudes which make their detection more difficult. Nevertheless, their slower kinetics promotes the summation of responses, which can lead to considerable thalamocortical recruitment of SST cells as seen in Tan et al. (2008). Furthermore, it is reasonable to assume that thalamocortical synapses onto SST cells are facilitating as it is known for intracortical excitatory input. Hence, given sustained down-stream activity, SST cells can be possible mediator of feed-forward inhibition in the upper dynamic range of incoming activity. This mechanism would be complementary to inhibition mediated by PV cells, which is known to be temporally precise, but strongly depressing. Consequently, the clear-cut functional separation, that has been assumed between SST and PV (as, for example, described in Tremblay et al. [2016]), is more fluid than previously thought. Recent work by Scala et al. (2019) hints at why this issue has been neglected so far: SST subpopulations seem to have traits that are particular to the respective modality of the cortical region. The nMC morphology seems to be unique to primary somatosensory cortex, since they cannot be found in L4 of its equivalent of the visual system. SST cells of a similar transcriptional cell cluster also exists there, but their biophysical profile is intermediate between ”classic” MCs and nMC, providing further evidence for a phenotype sliding on a spectrum (also see Malik et al. [2019]).

Surprisingly, the presence of direct thalamocortical innervation by both nuclei is independent of soma location and comparable between the two interneuron populations. This finding has an important possible functional implication: information is processed more in parallel than previously suggested by the canonical microcircuit paradigm. Studies on primary visual and auditory cortex paint a similar picture. Ji et al. (2015) report L1 cells to be strongly innervated by the respective specific thalamic nucleus. In addition, they also report SST and VIP cells having similar patterns of input incidence. However, these cells were predominantly found in L4. Considering the different approach in optical stimulation, these cells could be the tip of the iceberg. It seems reasonable to assume that thalamocortical circuits of primary sensory cortices follow a common blue print with only minor deviations. Input by POm shows the same parallel quality. Information conveyed by this nucleus is probably less sensory driven and determined by factors like arousal state, which makes its impact in-vivo hard to estimate. However, the data presented here indicates that it is a potent driver of VIP cells. Along the line of these findings, Williams and Holtmaat (2018) revealed that this connection could be an important player in regulating synaptic plasticity when paired with lemniscal activity. As seen in the case of VPM innervation, influence on SST cells is comparatively weak. However, it is reasonable to assume that POm-SST synapses are acting in a similar manner as described for the lemniscal pathway in the previous paragraph. Given inhibitory input by VIP cells, it remains to be seen how POm activity affects SST cells and under which conditions.

Other non-PV interneurons, not targeted in this study, are also known to receive thalamic input (Chittajallu et al., 2013) and there is no type of neuron in barrel cortex that has not the potential to receive direct thalamocortical input. Ultimately, the question arises if long range input has a cell type specific quality at all? Effects seen in cre-dependent rabies tracing (like Wall et al. [2016]) barely show categorical differences and are usually modest in size, when compared to variability of the tracing. The alternative view, also known as Peter's rule, states that connectivity is primarily determined by an overlap of axon and dendrite. Indeed, differences in distribution of cell popula-

tions and their dendritic profile can account for most if not all differences in connectivity incidence. To the knowledge of the author, there is no apparent example of such a deviance, neither is it suggested by this work. In conclusion, after extensive search for a presynaptic fiber population as a possible negative control and lack of any evidence of the contrary, one has to assume that long-range connectivity into and possibly within the neocortex is guided by one principle: opportunism.

Bibliography

Adelman, W. J. Voltage clamp studies on the effect of internal cesium ion on sodium and potassium currents in the squid giant axon. *The Journal of General Physiology*, 50(2):279–93 (1966).

Agmon, A. and Connors, B. W. Thalamocortical responses of mouse somatosensory (barrel) cortex in vitro. *Neuroscience*, 41(2-3):365–79 (1991).

Agmon, A. and Connors, B. W. Correlation between intrinsic firing patterns and thalamocortical synaptic responses of neurons in mouse barrel cortex. *The Journal of Neuroscience*, 12(1):319–29 (1992).

Ahissar, E., Sosnik, R., and Haidarliu, S. Transformation from temporal to rate coding in a somatosensory thalamocortical pathway. *Nature*, 406(6793):302–06 (2000).

Andersen, P., Eccles, J. C., and Løyning, Y. Pathway of postsynaptic inhibtion in the hippocampus. *Journal of Neurophysiology*, 27(4):608–19 (1964).

Armstrong-James, M., Fox, K., and Das-Gupta, A. Flow of excitation within rat barrel cortex on striking a single vibrissa. *Journal of Neurophysiology*, 68(4):1345–58 (1992).

Ascoli, G., Alonso-Nanclares, L., Anderson, S. a., et al. Petilla terminology: nomenclature of features of GABAergic interneurons of the cerebral cortex. *Nature Reviews. Neuroscience*, 9(7):557–68 (2008).

Atallah, B. V., Bruns, W., Carandini, M., and Scanziani, M. Parvalbumin-expressing interneurons linearly transform cortical responses to visual stimuli. *Neuron*, 73(1):159–70 (2012).

Audette, N. J., Urban-Ciecko, J., Matsushita, M., and Barth, A. L. POm Thalamocortical Input Drives Layer-Specific Microcircuits in Somatosensory Cortex. *Cerebral Cortex*, 28(4):1312–28 (2017).

Bacci, A., Huguenard, J. R., and Prince, D. A. Functional autaptic neurotransmission in fast-spiking interneurons: A novel form of feedback inhibition in the neocortex. *Journal of Neuroscience*, 23(3):859–66 (2003).

Barry, P. H. JPCalc, a software package for calculating liquid junction potential corrections in patch-clamp, intracellular, epithelial and bilayer measurements and for correcting junction potential measurements. *Journal of Neuroscience Methods*, 51(1):107–16 (1994).

Beierlein, M., Gibson, J. R., and Connors, B. W. Two dynamically distinct inhibitory networks in layer 4 of the neocortex. *Journal of Neurophysiology*, 90(5):2987–3000 (2003).

Belford, G. R. and Killackey, H. P. Vibrissae representation in subcortical trigeminal centers of the neonatal rat. *The Journal of Comparative Neurology*, 183(2):305–21 (1979).

Berger, T. K., Perin, R., Silberberg, G., and Markram, H. Frequency-dependent disynaptic inhibition in the pyramidal network: a ubiquitous pathway in the developing rat neocortex. *The Journal of Physiology*, 587(22):5411–25 (2009).

Bernardo, K. L. and Woolsey, T. A. Axonal trajectories between mouse somatosensory thalamus and cortex. *The Journal of Comparative Neurology*, 258(4):542–64 (1987).

Bock, D. D., Lee, W.-C. A., Kerlin, A. M., Andermann, M. L., Hood, G., Wetzel, A. W., Yurgenson, S., Soucy, E. R., Kim, H. S., and Reid, R. C. Network anatomy and in vivo physiology of visual cortical neurons. *Nature*, 471(7337):177–82 (2011).

Brecht, M. and Sakmann, B. Dynamic representation of whisker deflection by synaptic potentials in spiny stellate and pyramidal cells in the barrels and septa of layer 4 rat somatosensory cortex. *The Journal of Physiology*, 543(1):49–70 (2002).

Brecht, M., Roth, A., and Sakmann, B. Dynamic receptive fields of reconstructed pyramidal cells in layers 3 and 2 of rat somatosensory barrel cortex. *The Journal of Physiology*, 553(Pt 1):243–65 (2003).

Brock, L. G., Coombs, J. S., and Eccles, J. C. The recording of potentials from motoneurones with an intracellular electrode. *The Journal of Physiology*, 117(4):431–60 (1952).

Brodmann, K. *Vergleichende Lokalisationslehre der Grosshirnrinde*. Verlag von Johann Ambrosius Barth, Leipzig, Germany (1909).

Bruno, R. M. and Sakmann, B. Cortex is driven by weak but synchronously active thalamocortical synapses. *Science*, 312(5780):1622–27 (2006).

Bruno, R. M. and Simons, D. J. Feedforward mechanisms of excitatory and inhibitory cortical receptive fields. *The Journal of Neuroscience*, 22(24):10966–75 (2002).

Buhl, E. H., Han, Z. S., Lorinczi, Z., Stezhka, V. V., Karnup, S. V., and Somogyi, P. Physiological properties of anatomically identified axo-axonic cells in the rat hippocampus. *Journal of Neurophysiology*, 71(4):1289–307 (1994).

Bureau, I., von Saint Paul, F., and Svoboda, K. Interdigitated paralemniscal and lemniscal pathways in the mouse barrel cortex. *PLoS Biology*, 4(12):e382 (2006).

Caputi, A., Rozov, A., Blatow, M., and Monyer, H. Two calretinin-positive gabaergic cell types in layer 2/3 of the mouse neocortex provide different forms of inhibition. *Cerebral Cortex*, 19(6):1345–59 (2009).

Cauli, B., Audinat, E., Lambolez, B., Angulo, M. C., Ropert, N., Tsuzuki, K., Hestrin, S., and Rossier, J. Molecular and physiological diversity of cortical nonpyramidal cells. *The Journal of Neuroscience*, 17(10):3894–906 (1997).

Cauli, B., Porter, J. T., Tsuzuki, K., Lambolez, B., Rossier, J., Quenet, B., and Audinat, E. Classification of fusiform neocortical interneurons based on unsupervised clustering. *Proceedings of the National Academy of Sciences of the United States of America*, 97(11):6144–49 (2000).

Celio, M. Parvalbumin in most gamma-aminobutyric acid-containing neurons of the rat cerebral cortex. *Science*, 231(4741):995–97 (1986).

Celio, M. Calbindin D-28k and parvalbumin in the rat nervous system. *Neuroscience*, 35(2):375–475 (1990).

Cetin, A., Komai, S., Eliava, M., Seeburg, P. H., and Osten, P. Stereotaxic gene delivery in the rodent brain. *Nature Protocols*, 1(6):3166–73 (2006).

Chattopadhyaya, B., Di Cristo, G., Higashiyama, H., Knott, G. W., Kuhlman, S. J., Welker, E., and Huang, Z. J. Experience and activity-dependent maturation of perisomatic GABAergic innervation in primary visual cortex during a postnatal critical period. *The Journal of Neuroscience*, 24(43):9598–611 (2004).

Chiaia, N. L., Rhoades, R. W., Fish, S. E., and Killackey, H. P. Thalamic processing of vibrissal information in the rat: II. Morphological and functional properties of medial ventral posterior nucleus and posterior nucleus neurons. *The Journal of Comparative Neurology*, 314(2):217–36 (1991).

Chittajallu, R., Pelkey, K. a., and McBain, C. J. Neurogliaform cells dynamically regulate somatosensory integration via synapse-specific modulation. *Nature Neuroscience*, 16(1):13–15 (2013).

Chu, Z., Galarreta, M., and Hestrin, S. Synaptic interactions of late-spiking neocortical neurons in layer 1. *The Journal of Neuroscience*, 23(1):96–102 (2003).

Colonnier, M. L. Experimental degeneration in the cerebral cortex. *Journal of anatomy*, 98:47–53 (1964).

Colonnier, M. L. The structural design of the neocortex. In *Brain and Conscious Experience*, pages 1–23. Springer, Berlin (1965).

Condé, F., Lund, J. S., Jacobowitz, D. M., Baimbridge, K. G., and Lewis, D. A. Local circuit neurons immunoreactive for calretinin, calbindin D-28k or parvalbumin in monkey prefronatal cortex: Distribution and morphology. *Journal of Comparative Neurology*, 341(1):95–116 (1994).

Connor, J. R. and Peters, A. Vasoactive intestinal polypeptide-immunoreactive neurons in rat visual cortex. *Neuroscience*, 12(4):1027–44 (1984).

Connors, B. W., Gutnick, M. J., and Prince, D. A. Electrophysiological properties of neocortical neurons in vitro. *Journal of Neurophysiology*, 48(6):1302–20 (1982).

Constantinople, C. M. and Bruno, R. M. Deep cortical layers are activated directly by thalamus. *Science*, 340(6140):1591–94 (2013).

Coombs, J. S., Eccles, J. C., and Fatt, P. The electrical properties of the motoneurone membrane. *The Journal of Physiology*, 130(2):291–325 (1955).

Coons, A. H., Creech, H. J., and Jones, R. N. Immunological properties of an antibody containing a fluorescent group. *Experimental Biology and Medicine*, 47(2):200–02 (1941).

Creutzfeldt, O. D., Lux, H. D., and Nacimiento, A. C. Intrazelluläre Reizung corticaler Nervenzellen. *Pflügers Archiv*, 281(2):129–51 (1964).

Cruikshank, S. J., Lewis, T. J., and Connors, B. W. Synaptic basis for intense thalamocortical activation of feedforward inhibitory cells in neocortex. *Nature Neuroscience*, 10(4):462–68 (2007).

Cruikshank, S. J., Urabe, H., Nurmikko, A. V., and Connors, B. W. Pathway-specific feedforward circuits between thalamus and neocortex revealed by selective optical stimulation of axons. *Neuron*, 65(2):230–245 (2010).

Dávid, C., Schleicher, A., Zuschratter, W., and Staiger, J. F. The innervation of parvalbumin-containing interneurons by VIP-immunopositive interneurons in the primary somatosensory cortex of the adult rat. *The European Journal of Neuroscience*, 25(8):2329–40 (2007).

de Kock, C. P. J. and Sakmann, B. Spiking in primary somatosensory cortex during natural whisking in awake head-restrained rats is cell-type specific. *Proceedings of the National Academy of Sciences of the United States of America*, 106(38):16446–50 (2009).

DeFelipe, J., Hendry, S. H., and Jones, E. G. Visualization of chandelier cell axons by parvalbumin immunoreactivity in monkey cerebral cortex. *Proceedings of the National Academy of Sciences*, 86(6):2093–97 (1989).

DeFelipe, J., López-Cruz, P. L., Benavides-Piccione, R., et al. New insights into the classification and nomenclature of cortical GABAergic interneurons. *Nature Reviews. Neuroscience*, 14(3):202–16 (2013).

Diamond, M. E., Armstrong-James, M., Budway, M. J., and Ebner, F. F. Somatic sensory responses in the rostral sector of the posterior group (POm) and in the ventral posterior medial nucleus (VPM) of the rat thalamus: Dependence on the barrel field cortex. *The Journal of Comparative Neurology*, 319(1):66–84 (1992).

Dodt, H. U., Frick, A., Kampe, K., and Zieglgänsberger, W. NMDA and AMPA receptors on neocortical neurons are differentially distributed. *European Journal of Neuroscience*, 10(11):3351–57 (1998).

Donato, F., Rompani, S. B., and Caroni, P. Parvalbumin-expressing basket-cell network plasticity induced by experience regulates adult learning. *Nature*, 504(7479):272–76 (2013).

Douglas, R. J. and Martin, K. A. A functional microcircuit for cat visual cortex. *The Journal of Physiology*, 440(1):735–69 (1991).

Eckenstein, F. and Thoenen, H. Production of specific antisera and monoclonal antibodies to choline acetyltransferase: characterization and use for identification of cholinergic neurons. *The EMBO Journal*, 1(3):363–68 (1982).

Feldmeyer, D., Egger, V., Lübke, J., and Sakmann, B. Reliable synaptic connections between pairs of excitatory layer 4 neurones within a single 'barrel' of developing rat somatosensory cortex. *The Journal of Physiology*, 521(1):169–90 (1999).

Feldmeyer, D., Lübke, J., Silver, R. A., and Sakmann, B. Synaptic connections between layer 4 spiny neurone- layer 2/3 pyramidal cell pairs in juvenile rat barrel cortex: physiology and anatomy of interlaminar signalling within a cortical column. *The Journal of Physiology*, 538(3):803–22 (2002).

Férézou, I., Cauli, B., Hill, E. L., Rossier, J., Hamel, E., and Lambolez, B. 5-HT 3 receptors mediate serotonergic fast synaptic excitation of neocortical vasoactive intestinal peptide/cholecystokinin interneurons. *The Journal of Neuroscience*, 22(17):7389–97 (2002).

Fino, E. and Yuste, R. Dense inhibitory connectivity in neocortex. *Neuron*, 69(6):1188–203 (2011).

Foutz, T. J., Arlow, R. L., and McIntyre, C. C. Theoretical principles underlying optical stimulation of a channelrhodopsin-2 positive pyramidal neuron. *Journal of Neurophysiology*, 107(12):3235–45 (2012).

Franklin, K. and Paxinos, G. *The mouse brain in stereotaxic coordinates*. Academic Press, San Diego, 2nd edition (2001).

Fu, Y., Tucciarone, J. M., Espinosa, J. S., Sheng, N., Darcy, D. P., Nicoll, R. A., Huang, Z. J., and Stryker, M. P. A cortical circuit for gain control by behavioral state. *Cell*, 156(6):1139–52 (2014).

Fuxe, K., Hökfelt, T., Said, S., and Mutt, V. Vasoactive intestinal polypeptide and the nervous system: Immunohistochemical evidence for localization in central and peripheral neurons, particularly intracortical neurons of the cerebral cortex. *Neuroscience Letters*, 5(5):241–46 (1977).

Galarreta, M. and Hestrin, S. Frequency-dependent synaptic depression and the balance of excitation and inhibition in the neocortex. *Nature Neuroscience*, 1(7):587–94 (1998).

Garcia-Junco-Clemente, P., Ikrar, T., Tring, E., Xu, X., Ringach, D. L., and Trachtenberg, J. T. An inhibitory pull–push circuit in frontal cortex. *Nature Neuroscience*, 20(3):389–92 (2017).

Gentet, L. J., Kremer, Y., Taniguchi, H., Huang, Z. J., Staiger, J. F., and Petersen, C. C. H. Unique functional properties of somatostatin-expressing GABAergic neurons in mouse barrel cortex. *Nature Neuroscience*, 15(4):607–12 (2012).

Gibson, J. R., Beierlein, M., and Connors, B. W. Two networks of electrically coupled inhibitory neurons in neocortex. *Nature*, 402(6757):75–79 (1999).

Gonchar, Y. and Burkhalter, A. Three distinct families of GABAergic neurons in rat visual cortex. *Cerebral Cortex*, 7(4):347–58 (1997).

Gouwens, N. W., Sorensen, S. A., Berg, J., et al. Classification of electrophysiological and morphological neuron types in the mouse visual cortex. *Nature Neuroscience*, 22(7):1182–95 (2019).

Groh, A., Bokor, H., Mease, R., Plattner, V. M., Hangya, B., Stroh, A., Deschenes, M., and Acsády, L. Convergence of cortical and sensory driver inputs on single thalamocortical cells. *Cerebral Cortex*, 24(12):3167–79 (2013).

Gulyás, A. I., Hájos, N., and Freund, T. F. Interneurons Containing Calretinin Are Specialized to Control Other Interneurons in the Rat Hippocampus. *The Journal of Neuroscience*, 16(10):3397–411 (1996).

Gupta, A., Wang, Y., and Markram, H. Organizing Principles for a Diversity of GABAergic Interneurons and Synapses in the Neocortex. *Science*, 287(5451):273–78 (2000).

Gutnick, M. and Prince, D. Dye coupling and possible electrotonic coupling in the guinea pig neocortical slice. *Science*, 211(4477):67–70 (1981).

Haider, B., Häusser, M., and Carandini, M. Inhibition dominates sensory responses in the awake cortex. *Nature*, 493(7430):97–100 (2013).

Hamill, O. P., Marty, A., Neher, E., Sakmann, B., and Sigworth, F. J. Improved patch-clamp techniques for high-resolution current recording from cells and cell-free membrane patches. *Pflügers Archiv*, 391(2):85–100 (1981).

Hattox, A. M. and Nelson, S. B. Layer V neurons in mouse cortex projecting to different targets have distinct physiological properties. *Journal of Neurophysiology*, 98(6):3330–40 (2007).

He, M., Tucciarone, J., Lee, S., Nigro, M. J., Kim, Y., Levine, J. M., Kelly, S. M., Krugikov, I., Wu, P., Chen, Y., Gong, L., Hou, Y., Osten, P., Rudy, B., and Huang, Z. J. Strategies and tools for combinatorial targeting of GABAergic neurons in mouse cerebral cortex. *Neuron*, 91(6):1228–43 (2016).

Helmchen, F. and Denk, W. Deep tissue two-photon microscopy. *Nature Methods*, 2(12):932–40 (2005).

Hendrickson, A. E., Hunt, S. P., and Wu, J.-Y. Immunocytochemical localization of glutamic acid decarboxylase in monkey striate cortex. *Nature*, 292(5824):605–07 (1981).

Hendry, S., Jones, E., Emson, P., Lawson, D., Heizmann, C., and Streit, P. Two classes of cortical GABA neurons defined by differential calcium binding protein immunoreactivities. *Experimental Brain Research*, 76(2):467–72 (1989).

Hendry, S. H., Jones, E. G., DeFelipe, J., Schmechel, D., Brandon, C., and Emson, P. C. Neuropeptide-containing neurons of the cerebral cortex are also GABAergic. *Proceedings of the National Academy of Sciences*, 81(20):6526–30 (1984).

Herkenham, M. Laminar organization of thalamic projections to the rat neocortex. *Science*, 207(4430):532–35 (1980).

Hersch, S. M. and White, E. L. Thalamocortical synapses involving identified neurons in mouse primary somatosensory cortex: A terminal degeneration and golgi/EM study. *The Journal of Comparative Neurology*, 195(2):253–63 (1981).

Hestrin, S. and Armstrong, W. E. Morphology and physiology of cortical neurons in layer I. *The Journal of Neuroscience*, 16(17):5290–300 (1996).

Hippenmeyer, S., Vrieseling, E., Sigrist, M., Portmann, T., Laengle, C., Ladle, D. R., and Arber, S. A developmental switch in the response of DRG neurons to ETS transcription factor signaling. *PLoS Biology*, 3(5):e159 (2005).

Hofer, S. B., Ko, H., Pichler, B., Vogelstein, J., Ros, H., Zeng, H., Lein, E., Lesica, N. A., and Mrsic-Flogel, T. D. Differential connectivity and response dynamics of excitatory and inhibitory neurons in visual cortex. *Nature Neuroscience*, 14(8):1045–52 (2011).

Hoogland, P. V., Welker, E., and Van der Loos, H. Organization of the projections from barrel cortex to thalamus in mice studied with Phaseolus vulgaris-leucoagglutinin and HRP. *Experimental Brain Research*, 68(1):73–87 (1987).

Horikawa, K. and Armstrong, W. A versatile means of intracellular labeling: injection of biocytin and its detection with avidin conjugates. *Journal of Neuroscience Methods*, 25(1):1–11 (1988).

Hu, H. and Agmon, A. Differential excitation of distally versus proximally targeting cortical interneurons by unitary thalamocortical bursts. *Journal of Neuroscience*, 36(26):6906–16 (2016).

Hu, H., Cavendish, J. Z., and Agmon, A. Not all that glitters is gold : off-target recombination in the somatostatin – IRES-Cre mouse line labels a subset of fast-spiking interneurons. *Frontiers in Neural Circuits*, 7:195 (2013).

Hubel, D. H. and Wiesel, T. N. Receptive fields, binocular interaction and functional architecture in the cat's visual cortex. *The Journal of Physiology*, 160(1):106–54 (1962).

Hull, C., Isaacson, J. S., and Scanziani, M. Postsynaptic mechanisms govern the differential excitation of cortical neurons by thalamic inputs. *The Journal of Neuroscience*, 29(28):9127–36 (2009).

Inan, M., Blazquez-Llorca, L., Merchan-Perez, A., Anderson, S. A., DeFelipe, J., and Yuste, R. Dense and overlapping innervation of pyramidal neurons by chandelier cells. *Journal of Neuroscience*, 33(5):1907–14 (2013).

Jackson, J., Ayzenshtat, I., Karnani, M. M., and Yuste, R. VIP+ interneurons control neocortical activity across brain states. *Journal of Neurophysiology*, 115(6):3008–17 (2016).

Jacobowitz, D. M. and Winsky, L. Immunocytochemical localization of calretinin in the forebrain of the rat. *The Journal of Comparative Neurology*, 304(2):198–218 (1991).

Jensen, K. F. and Killackey, H. P. Terminal arbors of axons projecting to the somatosensory cortex of the adult rat. I. The normal morphology of specific thalamocortical afferents. *The Journal of Neuroscience*, 7(11):3529–43 (1987).

Ji, X.-Y., Zingg, B., Mesik, L., Xiao, Z., Zhang, L. I., and Tao, H. W. Thalamocortical innervation pattern in mouse auditory and visual cortex: laminar and cell-type specificity. *Cerebral Cortex*, 26(6):1–14 (2015).

Jiang, X., Shen, S., Cadwell, C. R., Berens, P., Sinz, F., Ecker, A. S., Patel, S., and Tolias, A. S. Principles of connectivity among morphologically defined cell types in adult neocortex. *Science*, 350(6264):aac9462, 1–9 (2015).

Jouhanneau, J.-S., Ferrarese, L., Estebanez, L., Audette, N. J., Brecht, M., Barth, A. L., and Poulet, J. F. Cortical fosGFP expression reveals broad receptive field excitatory neurons targeted by POm. *Neuron*, 84(5):1065–78 (2014).

Kapfer, C., Glickfeld, L. L., Atallah, B. V., and Scanziani, M. Supralinear increase of recurrent inhibition during sparse activity in the somatosensory cortex. *Nature Neuroscience*, 10(6):743–53 (2007).

Karagiannis, A., Gallopin, T., Dávid, C., Battaglia, D., Geoffroy, H., Rossier, J., Hillman, E. M. C., Staiger, J. F., and Cauli, B. Classification of NPY-expressing neocortical interneurons. *The Journal of Neuroscience*, 29(11):3642–59 (2009).

Kawaguchi, Y. Groupings of nonpyramidal and pyramidal cells with specific physiological and morphological characteristics in rat frontal cortex. *Journal of Neurophysiology*, 69(2):416–31 (1993).

Kawaguchi, Y. Physiological subgroups of nonpyramidal cells with specific morphological characteristics in layer II/III of rat frontal cortex. *The Journal of Neuroscience*, 15(4):2638–55 (1995).

Kawaguchi, Y. and Kubota, Y. Correlation of physiological subgroupings of nonpyramidal cells with parvalbumin- and calbindinD28k-immunoreactive neurons in layer V of rat frontal cortex. *Journal of Neurophysiology*, 70(1):387–96 (1993).

Kawaguchi, Y. and Kubota, Y. Physiological and morphological identification of somatostatin- or vasoactive intestinal polypeptide-containing cells among GABAergic cell subtypes in rat frontal cortex. *The Journal of Neuroscience*, 16(8):2701–15 (1996).

Kawaguchi, Y., Katsumaru, H., Kosaka, T., Heizmann, C. W., and Hama, K. Fast spiking cells in rat hippocampus (CA1 region) contain the calcium-binding protein parvalbumin. *Brain Research*, 416(2):369–74 (1987).

Keller, A. and White, E. L. Synaptic organization of GABAergic neurons in the mouse SmI cortex. *The Journal of Comparative Neurology*, 262(1):1–12 (1987).

Kerlin, A. M., Andermann, M. L., Berezovskii, V. K., and Reid, R. C. Broadly tuned response properties of diverse inhibitory neuron subtypes in mouse visual cortex. *Neuron*, 67(5):858–71 (2010).

Kerr, J. N. D., de Kock, C. P. J., Greenberg, D. S., Bruno, R. M., Sakmann, B., and Helmchen, F. Spatial organization of neuronal population responses in layer 2/3 of rat barrel cortex. *The Journal of Neuroscience*, 27(48):13316–28 (2007).

Khan, A. G., Poort, J., Chadwick, A., Blot, A., Sahani, M., Mrsic-Flogel, T. D., and Hofer, S. B. Distinct learning-induced changes in stimulus selectivity and interactions

of GABAergic interneuron classes in visual cortex. *Nature Neuroscience*, 21(6):851–59 (2018).

Killackey, H. P. Anatomical evidence for cortical subdivisions based on vertically discrete thalamic projections from the ventral posterior nucleus to cortical barrels in the rat. *Brain Research*, 51(C):326–31 (1973).

Kim, U. and Ebner, F. F. Barrels and septa: separate circuits in rat barrels field cortex. *The Journal of Comparative Neurology*, 408(4):489–505 (1999).

Koralek, K.-A., Jensen, K. F., and Killackey, H. P. Evidence for two complementary patterns of thalamic input to the rat somatosensory cortex. *Brain Research*, 463(2):346–51 (1988).

Kosaka, T., Heizmann, C. W., Tateishi, K., Hamaoka, Y., and Hama, K. An aspect of the organizational principle of the γ-aminobutyric acidergic system in the cerebral cortex. *Brain Research*, 409(2):403–08 (1987).

Krnjević, K. and Phillis, J. W. Iontophoretic studies of neurones in the mammalian cerebral cortex. *The Journal of Physiology*, 165(2):274–304 (1963).

Larsson, L. I., Fahrenkrug, J., Schaffalitzky De Muckadell, O., Sundler, F., Hakanson, R., and Rehfeld, J. R. Localization of vasoactive intestinal polypeptide (VIP) to central and peripheral neurons. *Proceedings of the National Academy of Sciences*, 73(9):3197–3200 (1976).

Lee, A. J., Wang, G., Jiang, X., Johnson, S. M., Hoang, E. T., Lanté, F., Stornetta, R. L., Beenhakker, M. P., Shen, Y., and Julius Zhu, J. Canonical Organization of Layer 1 Neuron-Led Cortical Inhibitory and Disinhibitory Interneuronal Circuits. *Cerebral Cortex*, 25(8):2114–26 (2015).

Lee, S., Hjerling-Leffler, J., Zagha, E., Fishell, G., and Rudy, B. The largest group of superficial neocortical GABAergic interneurons expresses ionotropic serotonin receptors. *The Journal of Neuroscience*, 30(50):16796–808 (2010).

Lee, S., Kruglikov, I., Huang, Z. J., Fishell, G., and Rudy, B. A disinhibitory circuit mediates motor integration in the somatosensory cortex. *Nature Neuroscience*, 16(11):1662–70 (2013).

Lee, S.-H., Kwan, A. C., and Dan, Y. Interneuron subtypes and orientation tuning. *Nature*, 508(7494):E1–2 (2014).

Li, C. L. and Jasper, H. Microelectrode studies of the electrical activity of the cerebral cortex in the cat. *The Journal of Physiology*, 121(1):117–40 (1953).

Li, L.-Y., Xiong, X. R., Ibrahim, L. A., Yuan, W., Tao, H. W., and Zhang, L. I. Differential receptive field properties of parvalbumin and somatostatin inhibitory neurons in mouse auditory cortex. *Cerebral Cortex*, 25(7):1782–91 (2015).

Li, P. and Huntsman, M. M. Two functional inhibitory circuits are comprised of a heterogeneous population of fast-spiking cortical interneurons. *Neuroscience*, 265:60–71 (2014).

Lim, L., Pakan, J. M., Selten, M. M., Marques-Smith, A., Llorca, A., Bae, S. E., Rochefort, N. L., and Marín, O. Optimization of interneuron function by direct coupling of cell migration and axonal targeting. *Nature Neuroscience*, 21(7):920–931 (2018).

Lin, J. Y., Lin, M. Z., Steinbach, P., and Tsien, R. Y. Characterization of engineered channelrhodopsin variants with improved properties and kinetics. *Biophysical Journal*, 96(5):1803–14 (2009).

Ling, G. and Gerard, R. W. The normal membrane potential of frog sartorius fibers. *Journal of Cellular and Comparative Physiology*, 34(3):383–396 (1949).

Lorente de Nó, R. Studies of the structure of the cerebral cortex. I. The area entorhinalis. *J. Psychol. Neurol.*, (45):381–438 (1933).

Lorente de Nó, R. Studies of the structure of the cerebral cortex. II. Continuation of the study of the ammonic system. *J. Psychol. Neurol.*, (46):113–77 (1934).

Lorente de Nó, R. *Physiology of the nervous system.* Oxford University Press, New York (1938).

Lu, S.-M. and Lin, R. C. Thalamic afferents of the rat barrel cortex: a light-and electron-microscopic study using phaseolus vulgaris leucoagglutinin as an anterograde tracer. *Somatosensory & Motor Research*, 10(1):1–16 (1993).

Lübke, J., Egger, V., Sakmann, B., and Feldmeyer, D. Columnar organization of dendrites and axons of single and synaptically coupled excitatory spiny neurons in layer 4 of the rat barrel cortex. *Journal of Neuroscience*, 20(14):5300–11 (2000).

Ma, W.-P., Liu, B.-h., Li, Y.-t., Huang, Z. J., Zhang, L. I., and Tao, H. W. Visual representations by cortical somatostatin inhibitory neurons–selective but with weak and delayed responses. *The Journal of Neuroscience*, 30(43):14371–79 (2010).

Ma, Y., Hu, H., Berrebi, A. S., Mathers, P. H., and Agmon, A. Distinct subtypes of somatostatin-containing neocortical interneurons revealed in transgenic mice. *The Journal of Neuroscience*, 26(19):5069–82 (2006).

Madisen, L., Zwingman, T. A., Sunkin, S. M., Oh, S. W., Zariwala, H. A., Gu, H., Ng, L. L., Palmiter, R. D., Hawrylycz, M. J., Jones, A. R., Lein, E. S., and Zeng, H. A robust and high-throughput Cre reporting and characterization system for the whole mouse brain. *Nature Neuroscience*, 13(1):133–40 (2010).

Madisen, L., Garner, A. R., Shimaoka, D., et al. Transgenic Mice for Intersectional Targeting of Neural Sensors and Effectors with High Specificity and Performance. *Neuron*, 85(5):942–58 (2015).

Malik, R., Pai, E. L.-L., Rubin, A. N., Stafford, A. M., Angara, K., Minasi, P., Rubenstein, J. L., Sohal, V. S., and Vogt, D. Tsc1 represses parvalbumin expression and fast-spiking properties in somatostatin lineage cortical interneurons. *Nature Communications*, 10(1):4994 (2019).

Mardinly, A. R., Spiegel, I., Patrizi, A., Centofante, E., Bazinet, J. E., Tzeng, C. P., Mandel-Brehm, C., Harmin, D. A., Adesnik, H., Fagiolini, M., and Greenberg, M. E. Sensory experience regulates cortical inhibition by inducing IGF1 in VIP neurons. *Nature*, 531(7594):371–375 (2016).

Margrie, T. W., Meyer, A. H., Caputi, A., Monyer, H., Hasan, M. T., Schaefer, A. T., Denk, W., and Brecht, M. Targeted whole-cell recordings in the mammalian brain in vivo. *Neuron*, 39(6):911–18 (2003).

Markram, H., Wang, Y., and Tsodyks, M. Differential signaling via the same axon of neocortical pyramidal neurons. *Proceedings of the National Academy of Sciences of the United States of America*, 95(9):5323–28 (1998).

Markram, H., Muller, E., Ramaswamy, S., et al. Reconstruction and simulation of neocortical microcircuitry. *Cell*, 163(2):456–92 (2015).

Marshall, W. H., Woolsey, C. N., and Bard, P. Observations on cortical somatic sensory mechanism of cat and monkey. *Journal of Neurophysiology*, 4(1):1–24 (1941).

Martinotti, C. Contributo allo studio della corteccia cerebrale, ed all'origine centrale dei nervi. *Ann. Freniatr. Sci. Affini.*, (1):14–381 (1889).

Marx, M., Günter, R. H., Hucko, W., Radnikow, G., and Feldmeyer, D. Improved biocytin labeling and neuronal 3D reconstruction. *Nature Protocols*, 7(2):394–407 (2012).

McCormick, D. A. and Huguenard, J. R. A model of the electrophysiological properties of thalamocortical relay neurons. *Journal of Neurophysiology*, 68(4):1384–1400 (1992).

McCormick, D. A., Connors, B. W., Lighthall, J. W., and Prince, D. A. Comparative electrophysiology of pyramidal and sparsely spiny stellate neurons of the neocortex. *Journal of Neurophysiology*, 54(4):782–806 (1985).

McKay, R. D. G. and Hockfield, S. J. Monoclonal antibodies distinguish antigenically discrete. *Neurobiology*, 79(November):6747–51 (1982).

Miyoshi, G., Hjerling-Leffler, J., Karayannis, T., Sousa, V. H., Butt, S. J. B., Battiste, J., Johnson, J. E., Machold, R. P., and Fishell, G. Genetic fate mapping reveals that the

caudal ganglionic eminence produces a large and diverse population of superficial cortical interneurons. *The Journal of Neuroscience*, 30(5):1582–94 (2010).

Morison, R. S. and Dempsey, E. W. A study of thalamo-cortical relations. *American Journal of Physiology*, 135(2):281–92 (1941).

Morrone, M. C., Burr, D. C., and Maffei, L. Functional implications of cross-orientation inhibition of cortical visual cells. I. Neurophysiological evidence. *Proceedings of the Royal Society of London. Series B. Biological Sciences*, 216(1204):335–54 (1982).

Mountcastle, V. B. Modality and topographic properties of single neurons of cat's somatic sensory cortex. *Journal of Neurophysiology*, 20(4):408–34 (1957).

Mountcastle, V. B., Talbot, W. H., Sakata, H., and Hyvärinen, J. Cortical neuronal mechanisms in flutter-vibration studied in unanesthetized monkeys. Neuronal periodicity and frequency discrimination. *Journal of Neurophysiology*, 32(3):452–84 (1969).

Muñoz, W., Tremblay, R., Levenstein, D., and Rudy, B. Layer-specific modulation of neocortical dendritic inhibition during active wakefulness. *Science*, 355(6328):954–59 (2017).

Murayama, M., Pérez-Garci, E., Nevian, T., Bock, T., Senn, W., and Larkum, M. E. Dendritic encoding of sensory stimuli controlled by deep cortical interneurons. *Nature*, 457(7233):1137–41 (2009).

Nagel, G., Szellas, T., Huhn, W., Kateriya, S., Adeishvili, N., Berthold, P., Ollig, D., Hegemann, P., and Bamberg, E. Channelrhodopsin-2, a directly light-gated cation-selective membrane channel. *Proceedings of the National Academy of Sciences*, 100(24):13940–45 (2003).

Naka, A., Veit, J., Shababo, B., Chance, R. K., Risso, D., Stafford, D., Snyder, B., Egladyous, A., Chu, D., Sridharan, S., Mossing, D. P., Paninski, L., Ngai, J., and Adesnik, H. Complementary networks of cortical somatostatin interneurons enforce layer specific control. *eLife*, 8:1–36 (2019).

Ogawa, T., Ito, S., and Kato, H. Membrane characteristics of visual cortical neurons in in vitro slices. *Brain Research*, 226(1-2):315–19 (1981).

Ohno, S., Kuramoto, E., Furuta, T., Hioki, H., Tanaka, Y. R., Fujiyama, F., Sonomura, T., Uemura, M., Sugiyama, K., and Kaneko, T. A morphological analysis of thalamocortical axon fibers of rat posterior thalamic nuclei: a single neuron tracing study with viral vectors. *Cerebral Cortex*, 22(12):2840–57 (2012).

Okun, M. and Lampl, I. Instantaneous correlation of excitation and inhibition during ongoing and sensory-evoked activities. *Nature Neuroscience*, 11(5):535–37 (2008).

O'Leary, J. L. Structure of the area striata of the cat. *The Journal of Comparative Neurology*, 75(1):131–64 (1941).

Oliva, A. A., Jiang, M., Lam, T., Smith, K. L., and Swann, J. W. Novel hippocampal interneuronal subtypes identified using transgenic mice that express green fluorescent protein in GABAergic interneurons. *The Journal of Neuroscience*, 20(9):3354–68 (2000).

Packer, A. M. and Yuste, R. Dense, unspecific connectivity of neocortical parvalbumin-positive interneurons: a canonical microcircuit for inhibition? *The Journal of Neuroscience*, 31(37):13260–71 (2011).

Parsons, J. A., Erlandsen, S. L., Hegre, O. D., McEvoy, R. C., and Elde, R. P. Central and peripheral localization of somatostatin. Immunoenzyme immunocytochemical studies. *Journal of Histochemistry & Cytochemistry*, 24(7):872–82 (1976).

Paul, A., Crow, M., Raudales, R., He, M., Gillis, J., and Huang, Z. J. Transcriptional architecture of synaptic communication delineates GABAergic neuron identity. *Cell*, 171(3):522–539.e20 (2017).

Peschanski, M. Trigeminal afferents to the diencephalon in the rat. *Neuroscience*, 12(2):465–87 (1984).

Petersen, C. C. and Sakmann, B. The excitatory neuronal network of rat layer 4 barrel cortex. *The Journal of Neuroscience*, 20(20):7579–86 (2000).

Petreanu, L., Mao, T., Sternson, S. M., and Svoboda, K. The subcellular organization of neocortical excitatory connections. *Nature*, 457(7233):1142–45 (2009).

Pfeffer, C. K., Xue, M., He, M., Huang, Z. J., and Scanziani, M. Inhibition of inhibition in visual cortex: the logic of connections between molecularly distinct interneurons. *Nature Neuroscience*, 16(8):1068–76 (2013).

Pi, H.-J., Hangya, B., Kvitsiani, D., Sanders, J. I., Huang, Z. J., and Kepecs, A. Cortical interneurons that specialize in disinhibitory control. *Nature*, 503(7477):521–24 (2013).

Pierret, T., Lavallée, P., and Deschênes, M. Parallel streams for the relay of vibrissal information through thalamic barreloids. *The Journal of Neuroscience*, 20(19):7455–62 (2000).

Porter, J. T., Cauli, B., Staiger, J. F., Lambolez, B., Rossier, J., and Audinat, E. Properties of bipolar VIPergic interneurons and their excitation by pyramidal neurons in the rat neocortex. *The European journal of neuroscience*, 10(12):3617–28 (1998).

Porter, J. T., Johnson, C. K., and Agmon, A. Diverse types of interneurons generate thalamus-evoked feedforward inhibition in the mouse barrel cortex. *The Journal of Neuroscience*, 21(8):2699–710 (2001).

Prönneke, A. *Untangling neuronal diversity : a quantitative electrophysiological and morphological characterization of VIP expressing interneurons*. Ph.D. thesis (2016).

Prönneke, A., Scheuer, B., Wagener, R. J., Möck, M., Witte, M., and Staiger, J. F. Characterizing VIP neurons in the barrel cortex of VIPcre/tdTomato mice reveals layer-specific differences. *Cerebral Cortex*, 25(12):4854–68 (2015).

Prönneke, A., Witte, M., Möck, M., and Staiger, J. F. Neuromodulation leads to a burst-tonic switch in a subset of VIP neurons in mouse primary somatosensory (barrel) cortex. *Cerebral Cortex*, (Advance Access Publication):1–17 (2019).

Ramón y Cajal, S. *Comparative study of the sensory areas of the human cortex*. Clark University, Worcester (1898).

Ramon y Cajal, S. Estudio sobra la corteza cerebral humana. *Rev. Trim. Microscopia*, 4:1–63. (1899).

Ramón y Cajal, S. *Histologie du système nerveux de l'homme & des vertébrés*. Maloine, Paris, 2nd edition (1911).

Reyes, A., Lujan, R., Rozov, A., Burnashev, N., Somogyi, P., and Sakmann, B. Target-cell-specific facilitation and depression in neocortical circuits. *Nature Neuroscience*, 1(4):279–85 (1998).

Ribak, C. E. Aspinous and sparsely-spinous stellate neurons in the visual cortex of rats contain glutamic acid decarboxylase. *Journal of Neurocytology*, 7(4):461–78 (1978).

Rogers, J. H. Immunohistochemical markers in rat cortex: co-localization of calretinin and calbindin-D28k with neuropeptides and GABA. *Brain Research*, 587(1):147–57 (1992).

Runyan, C. a., Schummers, J., Van Wart, A., Kuhlman, S. J., Wilson, N. R., Huang, Z. J., and Sur, M. Response features of parvalbumin-expressing interneurons suggest precise roles for subtypes of inhibition in visual cortex. *Neuron*, 67(5):847–57 (2010).

Safari, M.-S., Mirnajafi-Zadeh, J., Hioki, H., and Tsumoto, T. Parvalbumin-expressing interneurons can act solo while somatostatin-expressing interneurons act in chorus in most cases on cortical pyramidal cells. *Scientific Reports*, 7(1):12764 (2017).

Scala, F., Kobak, D., Shan, S., Bernaerts, Y., Laturnus, S., Cadwell, C. R., Hartmanis, L., Froudarakis, E., Castro, J. R., Tan, Z. H., Papadopoulos, S., Patel, S. S., Sandberg, R., Berens, P., Jiang, X., and Tolias, A. S. Layer 4 of mouse neocortex differs in cell types and circuit organization between sensory areas. *Nature Communications*, 10(1):4174 (2019).

Schneggenburger, R. and Neher, E. Intracellular calcium dependence of transmitter release rates at a fast central synapse. *Nature*, 406(6798):889–893 (2000).

Schneider, C. A., Rasband, W. S., and Eliceiri, K. W. NIH Image to ImageJ: 25 years of image analysis. *Nature Methods*, 9(7):671–75 (2012).

Schubert, D., Kötter, R., and Staiger, J. F. Mapping functional connectivity in barrel-related columns reveals layer- and cell type-specific microcircuits. *Brain structure & function*, 212(2):107–119 (2007).

Schuman, B., Machold, R. P., Hashikawa, Y., Fuzik, J., Fishell, G. J., and Rudy, B. Four Unique Interneuron Populations Reside in Neocortical Layer 1. *The Journal of Neuroscience*, 39(1):125–139 (2019).

Schwartzkroin, P. A. and Prince, D. A. Microphysiology of human cerebral cortex studied in vitro. *Brain Research*, 115(3):497–500 (1976).

Seung, H. S. and Sümbül, U. Neuronal cell types and connectivity: lessons from the retina. *Neuron*, 83(6):1262–72 (2014).

Sharp, F. R. Regional (14C) 2-deoxyglucose uptake during forelimb movements evoked by rat motor cortex stimulation: Cortex, diencephalon, midbrain. *Journal of Comparative Neurology*, 224(2):259–85 (1984).

Sholl, D. A. Dendritic organization in the neurons of the visual and motor cortices of the cat. *Journal of Anatomy*, 87(4):387–406 (1953).

Silberberg, G. and Markram, H. Disynaptic inhibition between neocortical pyramidal cells mediated by Martinotti cells. *Neuron*, 53(5):735–46 (2007).

Simons, D. J. Response properties of vibrissa units in rat SI somatosensory neocortex. *Journal of Neurophysiology*, 41(3):798–820 (1978).

Simons, D. J. and Carvell, G. E. Thalamocortical response transformation in the rat vibrissa/barrel system. *Journal of Neurophysiology*, 61(2):311–30 (1989).

Simons, D. J. and Woolsey, T. A. Morphology of Golgi-Cox-impregnated barrel neurons in rat SmI cortex. *The Journal of Comparative Neurology*, 230(1):119–32 (1984).

Skrede, K. K. and Westgaard, R. H. The transverse hippocampal slice: a well-defined cortical structure maintained in vitro. *Brain Research*, 35(2):589–93 (1971).

Slézia, A., Hangya, B., Ulbert, I., and Acsády, L. Phase advancement and nucleus-specific timing of thalamocortical activity during slow cortical oscillation. *The Journal of Neuroscience*, 31(2):607–17 (2011).

Sohya, K., Kameyama, K., Yanagawa, Y., Obata, K., and Tsumoto, T. GABAergic neurons are less selective to stimulus orientation than excitatory neurons in layer

II/III of visual cortex, as revealed by in vivo functional Ca2+ imaging in transgenic mice. *The Journal of Neuroscience*, 27(8):2145–49 (2007).

Srinivas, S., Watanabe, T., Lin, C.-S., William, C. M., Tanabe, Y., Jessell, T. M., and Costantini, F. Cre reporter strains produced by targeted insertion of EYFP and ECFP into the ROSA26 locus. *BMC Developmental Biology*, 1(1):4 (2001).

Staiger, J. F., Zilles, K., and Freund, T. F. Distribution of GABAergic elements postsynaptic to ventroposteromedial thalamic projections in layer IV of rat barrel cortex. *The European Journal of Neuroscience*, 8(11):2273–85 (1996a).

Staiger, J. F., Zilles, K., and Freund, T. F. Innervation of VIP-immunoreactive neurons by the ventroposteromedial thalamic nucleus in the barrel cortex of the rat. *Journal of Comparative Neurology*, 367(2):194–204 (1996b).

Staiger, J. F., Flagmeyer, I., Schubert, D., Zilles, K., Kötter, R., and Luhmann, H. J. Functional diversity of layer IV spiny neurons in rat somatosensory cortex: quantitative morphology of electrophysiologically characterized and biocytin labeled cells. *Cerebral Cortex*, 14(6):690–701 (2004a).

Staiger, J. F., Masanneck, C., Schleicher, A., and Zuschratter, W. Calbindin-containing interneurons are a target for VIP-immunoreactive synapses in rat primary somatosensory cortex. *Journal of Comparative Neurology*, 468(2):179–89 (2004b).

Stosiek, C., Garaschuk, O., Holthoff, K., and Konnerth, A. In vivo two-photon calcium imaging of neuronal networks. *Proceedings of the National Academy of Sciences of the United States of America*, 100(12):7319–24 (2003).

Straus, E., Muller, J. E., Choi, H. S., Paronetto, F., and Yalow, R. S. Immunohistochemical localization in rabbit brain of a peptide resembling the COOH-terminal octapeptide of cholecystokinin. *Proceedings of the National Academy of Sciences*, 74(7):3033–34 (1977).

Stuart, G. and Spruston, N. Determinants of voltage attenuation in neocortical pyramidal neuron dendrites. *The Journal of Neuroscience*, 18(10):3501–10 (1998).

Sun, Q.-Q., Huguenard, J. R., and Prince, D. A. Barrel cortex microcircuits: thalamocortical feedforward inhibition in spiny stellate cells is mediated by a small number of fast-spiking interneurons. *The Journal of Neuroscience*, 26(4):1219–30 (2006).

Swadlow, H. A. Efferent neurons and suspected interneurons in S-1 vibrissa cortex of the awake rabbit: receptive fields and axonal properties. *Journal of Neurophysiology*, 62(1):288–308 (1989).

Szentágothai, J. The 'module-concept' in cerebral cortex architecture. *Brain Research*, 95(2-3):475–96 (1975).

Talbot, S. and Marshall, W. Physiological studies on neural mechanisms of visual localization and discrimination. *American Journal of Ophthalmology*, 24(11):1255–64 (1941).

Tamamaki, N., Yanagawa, Y., Tomioka, R., Miyazaki, J.-I., Obata, K., and Kaneko, T. Green fluorescent protein expression and colocalization with calretinin, parvalbumin, and somatostatin in the GAD67-GFP knock-in mouse. *The Journal of Comparative Neurology*, 467(1):60–79 (2003).

Tamás, G., Buhl, E. H., and Somogyi, P. Massive autaptic self-innervation of GABAergic neurons in cat visual cortex. *The Journal of Neuroscience*, 17(16):6352–64 (1997).

Tan, Z., Hu, H., Huang, Z. J., and Agmon, A. Robust but delayed thalamocortical activation of dendritic-targeting inhibitory interneurons. *Proceedings of the National Academy of Sciences of the United States of America*, 105(6):2187–92 (2008).

Taniguchi, H., He, M., Wu, P., Kim, S., Paik, R., Sugino, K., Kvitsiani, D., Kvitsani, D., Fu, Y., Lu, J., Lin, Y., Miyoshi, G., Shima, Y., Fishell, G., Nelson, S. B., and Huang, Z. J. A resource of Cre driver lines for genetic targeting of GABAergic neurons in cerebral cortex. *Neuron*, 71(6):995–1013 (2011).

Tasic, B., Menon, V., Nguyen, T. N., et al. Adult mouse cortical cell taxonomy revealed by single cell transcriptomics. *Nature Neuroscience*, 19(2):335–46 (2016).

Tebaykin, D., Tripathy, S. J., Binnion, N., Li, B., Gerkin, R. C., and Pavlidis, P. Modeling sources of interlaboratory variability in electrophysiological properties of mammalian neurons. *Journal of Neurophysiology*, 119(4):1329–39 (2018).

Thomson, A. M., West, D. C., Hahn, J., and Deuchars, J. Single axon IPSPs elicited in pyramidal cells by three classes of interneurones in slices of rat neocortex. *The Journal of Physiology*, 496(1):81–102 (1996).

Thomson, A. M., West, D. C., Wang, Y., and Bannister, A. P. Synaptic connections and small circuits involving excitatory and inhibitory neurons in layers 2-5 of adult rat and cat neocortex: triple intracellular recordings and biocytin labelling in vitro. *Cerebral Cortex*, 12(9):936–53 (2002).

Tomioka, R., Okamoto, K., Furuta, T., Fujiyama, F., Iwasato, T., Yanagawa, Y., Obata, K., Kaneko, T., and Tamamaki, N. Demonstration of long-range GABAergic connections distributed throughout the mouse neocortex. *The European Journal of Neuroscience*, 21(6):1587–600 (2005).

Tremblay, R., Lee, S., and Rudy, B. GABAergic Interneurons in the neocortex: from cellular properties to circuits. *Neuron*, 91(2):260–92 (2016).

Tripathy, S. J., Burton, S. D., Geramita, M., Gerkin, R. C., and Urban, N. N. Brain-wide analysis of electrophysiological diversity yields novel categorization of mammalian neuron types. *Journal of Neurophysiology*, 113(10):3474–3489 (2015).

Tuncdemir, S. N., Wamsley, B., Stam, F. J., Osakada, F., Goulding, M., Callaway, E. M., Rudy, B., and Fishell, G. Early somatostatin interneuron connectivity mediates the maturation of deep layer cortical circuits. *Neuron*, 89(3):521–35 (2016).

Urbain, N., Salin, P. A., Libourel, P.-a., Petersen, C. C. H., Urbain, N., Salin, P. A., Libourel, P.-a., Comte, J.-c., Gentet, L. J., and Petersen, C. C. H. Whisking-related changes in neuronal firing and membrane potential dynamics in the somatosensory thalamus of awake mice report whisking-related changes in neuronal firing and membrane potential dynamics in the somatosensory thalamus of awake mice. *Cell Reports*, 13(4):1–10 (2015).

van Brederode, J., Helliesen, M., and Hendrickson, A. Distribution of the calcium-binding proteins parvalbumin and calbindin-D28k in the sensorimotor cortex of the rat. *Neuroscience*, 44(1):157–71 (1991).

Van Der Loos, H. Barreloids in mouse somatosensory thalamus. *Neuroscience Letters*, 2(1):1–6 (1976).

Veinante, P. and Deschênes, M. Single- and multi-whisker channels in the ascending projections from the principal trigeminal nucleus in the rat. *The Journal of Neuroscience*, 19(12):5085–95 (1999).

von Economo, C. *L'architecture cellulaire normale de l'ecorce cérébrale*. Masson, Paris (1927).

Vucurovic, K., Gallopin, T., Ferezou, I., Rancillac, A., Chameau, P., Van Hooft, J. A., Geoffroy, H., Monyer, H., Rossier, J., and Vitalis, T. Serotonin 3A receptor subtype as an early and protracted marker of cortical interneuron subpopulations. *Cerebral Cortex*, 20(10):2333–47 (2010).

Wahle, P. Differential regulation of substance P and somatostatin in martinotti cells of the developing cat visual cortex. *The Journal of Comparative Neurology*, 329(4):519–38 (1993).

Walker, F., Möck, M., Feyerabend, M., Guy, J., Wagener, R. J., Schubert, D., Staiger, J. F., and Witte, M. Parvalbumin- and vasoactive intestinal polypeptide-expressing neocortical interneurons impose differential inhibition on Martinotti cells. *Nature Communications*, 7(1):13664 (2016).

Wall, N. R., De La Parra, M., Sorokin, J. M., Taniguchi, H., Huang, Z. J., and Callaway, E. M. Brain-wide maps of synaptic input to cortical interneurons. *The Journal of Neuroscience*, 36(14):4000–09 (2016).

Wang, X.-J. and Yang, G. R. A disinhibitory circuit motif and flexible information routing in the brain. *Current Opinion in Neurobiology*, 49:75–83 (2018).

Wang, Y., Toledo-Rodriguez, M., Gupta, A., Wu, C., Silberberg, G., Luo, J., and Markram, H. Anatomical, physiological and molecular properties of Martinotti cells in the somatosensory cortex of the juvenile rat. *The Journal of Physiology*, 561(1):65–90 (2004).

Wehr, M. and Zador, A. M. Balanced inhibition underlies tuning and sharpens spike timing in auditory cortex. *Nature*, 426(27):860–63 (2003).

Welker, C. Receptive fields of barrels in the somatosensory neocortex of the rat. *The Journal of Comparative Neurology*, 166(2):173–89 (1976).

White, E. L. and Rock, M. P. A comparison of thalamocortical and other synaptic inputs to dendrites of two non-spiny neurons in a single barrel of mouse SmI cortex. *The Journal of Comparative Neurology*, 195(2):265–77 (1981).

Wilent, W. B. and Contreras, D. Dynamics of excitation and inhibition underlying stimulus selectivity in rat somatosensory cortex. *Nature Neuroscience*, 8(10):1364–70 (2005).

Williams, L. E. and Holtmaat, A. Higher-order thalamocortical inputs gate synaptic long-term potentiation via disinhibition. *Neuron*, 101(1):91–102.e4 (2018).

Williams, S. R. and Mitchell, S. J. Direct measurement of somatic voltage clamp errors in central neurons. *Nature Neuroscience*, 11(7):790–98 (2008).

Wilson, N. R., Runyan, C. A., Wang, F. L., and Sur, M. Division and subtraction by distinct cortical inhibitory networks in vivo. *Nature*, 488(7411):343–48 (2012).

Wimmer, V. C., Bruno, R. M., De Kock, C. P. J., Kuner, T., and Sakmann, B. Dimensions of a projection column and architecture of VPM and POm axons in rat vibrissal cortex (2010).

Woolsey, T. A. and Van der Loos, H. The structural organization of layer IV in the somatosensory region (S I) of mouse cerebral cortex. *Brain Research*, 17(2):205–42 (1970).

Wu, G. K., Arbuckle, R., hua Liu, B., Tao, H. W., and Zhang, L. I. Lateral sharpening of cortical frequency tuning by approximately balanced inhibition. *Neuron*, 58(1):132–43 (2008).

Xu, H., Jeong, H.-Y., Tremblay, R., and Rudy, B. Neocortical somatostatin-expressing GABAergic interneurons disinhibit the thalamorecipient layer 4. *Neuron*, 77(1):155–67 (2013).

Xu, X., Roby, K. D., and Callaway, E. M. Mouse cortical inhibitory neuron type that coexpresses somatostatin and calretinin. *The Journal of Comparative Neurology*, 499(1):144–60 (2006).

Xue, M., Atallah, B. V., and Scanziani, M. Equalizing excitation–inhibition ratios across visual cortical neurons. *Nature*, 511(7511):596–600 (2014).

Yizhar, O., Fenno, L. E., Davidson, T. J., Mogri, M., and Deisseroth, K. Optogenetics in neural systems. *Neuron*, 71(1):9–34 (2011).

Yoshimura, Y. and Callaway, E. M. Fine-scale specificity of cortical networks depends on inhibitory cell type and connectivity. *Nature Neuroscience*, 8(11):1552–59 (2005).

Yu, C., Derdikman, D., Haidarliu, S., and Ahissar, E. Parallel Thalamic Pathways for Whisking and Touch Signals in the Rat. *PLoS Biology*, 4(5):e124 (2006).

Zaitsev, A., Gonzalez-Burgos, G., Povysheva, N., Kröner, S., Lewis, D., and Krimer, L. Localization of calcium-binding proteins in physiologically and morphologically characterized interneurons of monkey dorsolateral prefrontal cortex. *Cerebral Cortex*, 15(8):1178–86 (2005).

Zhang, S., Xu, M., Kamigaki, T., Hoang Do, J. P., Chang, W.-C., Jenvay, S., Miyamichi, K., Luo, L., and Dan, Y. Long-range and local circuits for top-down modulation of visual cortex processing. *Science*, 345(6197):660–65 (2014).

Zhang, Z. W. and Deschenes, M. Projections to layer VI of the posteromedial barrel field in the rat: a reappraisal of the role of corticothalamic pathways. *Cerebral Cortex*, 8(5):428–36 (1998).

Zhou, X., Rickmann, M., Hafner, G., and Staiger, J. F. Subcellular targeting of VIP boutons in mouse barrel cortex is layer-dependent and not restricted to interneurons. *Cerebral Cortex*, 27(11):5353–68 (2017).

Zhu, J. J. and Connors, B. W. Intrinsic firing patterns and whisker-evoked synaptic responses of neurons in the rat barrel cortex. *Journal of Neurophysiology*, 81(3):1171–83 (1999).

Zhu, Y. and Zhu, J. J. Rapid arrival and integration of ascending sensory information in layer 1 nonpyramidal neurons and tuft dendrites of layer 5 pyramidal neurons of the neocortex. *The Journal of Neuroscience*, 24(6):1272–79 (2004).

List of Figures

Appendix A

Materials

A.1 Mouse lines

- Reporter: Gt(ROSA)26Sor$^{tm9(CAG\text{-}tdTomato)Hze}$, JAX Stock No. 007905
  Reference: Madisen et al. (2010)
- VIP-cre: Vip$^{tm1(cre)Zjh}$, JAX Stock No. 010908
  Reference: Taniguchi et al. (2011)
- SST-Cre: Sst$^{tm2.1(cre)Zjh}$, JAX Stock No. 028864
  Reference: Taniguchi et al. (2011)

A.2 Viruses

- AAV5.hSyn.hChR2(H134R)-eYFP.WPRE.hGH, addgene plasmid id: 26973P
  original titer: 8.62×10^{12} GC ml^{-1}
- AAV9.hSyn.hChR2(H134R)-eYFP.WPRE.hGH, addgene plasmid id: 26973P
  original titer: 1.42×10^{13} GC ml^{-1}

A.3 Solutions used in-vitro electrophysiology experiments

- High sucrose cutting solution: NaCl 87 mM, NaH_2PO_4 1.25 mM, KCl 2.5 mM, glucose 10 mM, sucrose 75 mM, $CaCl_2$ 0.5 mM, $MgCl_2$ 7 mM, $NaHCO_3$ 26 mM
- recording solution/ACSF: NaCl 125 mM, NaH_2PO_4 1.25 mM, KCl 2.5 mM, glucose 25 mM, $CaCl_2$ 2 mM, $MgCl_2$ 1 mM, $NaHCO_3$ 26 mM
- K^+-based intracellular solution: K-Gluconat 135 mM, KCl 5 mM, EGTA (ethylene glycol-bis((β-aminoethyl ether)-N,N,N',N'-tetraacetic acid), 0.5 mM, HEPES (4-(2-hydroxyethyl)-1-piperazineethanesulfonic acid) 10 mM, Mg-ATP (adenosine triphosphate) 4 mM, Na-GTP (guanosine triphosphate) 0.3 mM, Na-P-creatin 10 mM
- C^+-based intracellular solution: $CsMeSO_4$ 135 mM, CsCl 5 mM, EGTA 0.5 mM, HEPES 10 mM Mg-ATP 4 mM, Na-GTP 0.3 mM, Na-P-creatin 10 mM

A.4 Buffers used for histology

- PB buffer 0.1 M, pH 7.4 : 14.42 g Na_2HPO_4 + 2.62 g NaH_2PO_4, dissolved in 1 l ultra pure water
- Fixative: PB buffer with 4 m/v % PFA + 15 v/v % saturated picric acid
- TB buffer 0.05 M, pH 7.6: 6.06 g tris(hydroxymethyl)aminomethane hydrochloride + 1.39 g tris(hydroxymethyl)aminomethane base, dissolved in 1 l ultra pure water
- TBS buffer: TB buffer + 0.9 m/v % NaCl
- TBST buffer: TBS + 0.05 v/v % Triton-X 100
- Blocking solution: TBST + 0.25 m/v % bovine serum albumin and 10 v/v % normal donkey serum

Michael Feyerabend

Curiculum Vitae

Gutenbergstraße 3
37075 Göttingen
Germany
+49 1575 8845268
michael.feyerabend@hotmail.com

Education

2015–now **Ph.D. student**, *International Max Planck Research School for Neurosciences*, Institute of Neuroanatomy, University of Göttingen, Germany.
Title of thesis: "Thalamocortical Innervation of Neocortical GABAergic Interneurons in the Mouse Vibrissal Somatosensory Cortex" Principal thesis advisor: Prof. Dr. Jochen Staiger.

2013–2015 **Master of Science**, *International Max Planck Research School for Neurosciences*, University of Göttingen, Germany.

2010–2014 **Student of psychology**, *Long Distance University of Hagen*, No degree, earning 115 of 180 ECTS.
Covered courses: general, social, developmental and personality pyschology; quantitative and qualitative methods, practical-empirical psychological research, test theory and psychometrics.

2010–2013 **Bachelor of Science**, *Program in Neuroscience of the Faculty of Medicine, University of Cologne*, Cologne, Germany.

2000–2009 **High school**, *Luitpold Gymnasium*, Munich, Germany.

Laboratory Experience

2014–2015 **Master's thesis**, *Institute of Neuroanatomy, University of Göttingen*, Germany.
Title: "Characterizing Cell-Type Specific Inhibitory Input onto Martinotti Cells in Mouse Vibrissal Somatosensory Cortex"
Principal thesis advisor: Prof. Dr. Jochen Staiger.

2014 **Laboratory rotations**, *in context of Master's curriculum*, Göttingen, Germany.

- Single Cell Loading and Calcium Imaging of Mitral Cells with Multiple Glomeruli
  Department of Neurophysiology and Cellular Biophysics, University of Göttingen
  Advisor: Prof. Dr. Dr. Detlev Schild.
- Genetic Invesigation of Sleep-like Behavior in *Ceanorhabitis Elegans*
  Max-Planck-Institute of Biophysical Chemistry
  Advisor: Dr. Hendrik Bringmann.
- Characterizing the Effect of the $GABA_B$-Agonist Baclofen onto Neocortical Inhibitory Interneurons
  Institute of Neuroanatomy, University of Göttingen
  Advisor: Prof. Dr. Jochen Staiger.

2013 **Bachelor's thesis**, *Interfaculty Institute for Biochemistry, University of Tübingen*, Tübingen, Germany.
Titel: "Analysis of Neural cGMP Signaling Using FRET-based Live Cell Imaging"
Advisor: Prof. Dr. Robert Feil

2012 **Internship semester**, *Zhang Group, The Jackson Laboratory*, Bar Harbor, Maine, USA.
Investigating neocortical inhibitory input onto L5 pyramidal cells using whole cell recordings in conditional knock-out mice.

2011 **Internship**, *Institute of Biochemistry, University of Cologne*, Cologne, Germany.
Helping in creation of a monoclonal antibody with the hybridoma fusion technique.

Selected Conferences

2014 **Attendance without contribution**, *9th FENS Forum of Neuroscience*, Milan, Italy.

2016 **Attendance without contribution**, *Barrel Cortex Function*, Amsterdam, Netherlands.

2016 **Coorganizer**, *7th Neuroscience Conference "Neurizons"*, Göttingen, Germany.

2017 **Poster**, *12th Meeting of the German Neuroscience Society*, Göttingen, Germany.

2018 **Poster**, *Barrels and Beyond*, Göttingen, Germany, 1st prize in poster competition.

Teaching

2014 – 2018 **Teaching assistent**, *Annual method course in electrophysiolgy*.
Instructing Master's students in whole-cell patch clamp recording.

2016 – 2019 **Supervisor**, *Training and supervising student assistans*.
Guiding new students in manual morphological reconstructions of various neocortical neurons.

Publications

F Walker, M Möck, **M Feyerabend**, J Guy, R. J. Wagener, D Schubert, J. F. Staiger, and M Witte. Parvalbumin- and vasoactive intestinal polypeptide-expressing neocortical interneurons impose differential inhibition on Martinotti cells.
Nature Communications, 7(1):13664, 2016.

Relevant Skills

Methods whole-cell patch clamp in acute brain slices, flourescence microscopy, neurohistology, optogenetics, advanced statistical analysis, mouse genetics.

IT proficient in Adobe Illustrator and InDesign, ImageJ, Neurolucida, LaTeX, OriginLab.
basic knowledge of MATLAB, R, Python, SPSS, SigmaPlot, Adobe Photoshop.

Languages native speaker of German, fluent in English, intermediate in Spanish.

Other laboratory animal science certification FELASA B.

Miscellaneous and Volunteer Work

2007–2014 **Camp counselor, coordinator and trainer**, *non-profit youth travel operator "Fahrten-Ferne-Abenteuer gGmbH"*.
Taking care of children and young adults, organizing and conducting public camps and tours, supervising staff, training new team members of all positions in weekend seminars.

2009–2010 **National civil service**, *Social psychiatric center of the charity association "the Paritätische"*, Munich, Germany.
Supporting and supervising people with a history of mental illness.

2010–2015 **Scholarship holder**, *Friedrich-Naumann-Stiftung für die Freiheit*.
Participating in regular seminars and events on science, ethics and public policy.

2010–2013 **Member, treasurer and co-founder of the neuroscience student council**, *University of Cologne*, Germany.
Conducting the business of the elected representation of the student body, organizing events for incoming students and promoting exchange among the different cohorts.

2013–2014 **Speaker of first year's students**, *International Max-Planck Research School for Neurosciences*, Göttingen, Germany.
Mediating between students and program administration, being contact for concerns broadly related to student life in the program and Germany in general.

Acknowledgements

I want to thank all current and former colleagues, I had the pleasure to share my working space with. In particular I want to thank Kamila Kiszka and Georg Hafner, for support in various ways: be it the sharing of expertise, the discussion of ideas, just listening to my issues and providing perspective. In addition, I want to thank Julien Guy and Alvar Pröneke for further tangible support in analysis and data visualization. Also many thanks to Patricia Sprysch, who did the major part of the histological preparations. Thanks also to Pavel Truschow for help with image acquisition and post-processing. Some of the reconstructions were made by Nicolas Zdun and Lejla Sahovic. Also a lot of thanks to Martin Möck for spending many hours in explaining me the particularities of different types of analysis and acquisition protocols. Furthermore, I want to thank Mirko Witte for inducting me to the laboratory and most of the techniques used in this work; for creating the conditions, that made my work possible by organizing animal breedings, providing support in IT and, generally, having my back as a supervisor. Last but not least, I want to thank Prof. Jochen Staiger for giving me the opportunity to learn and grow.

Funding was provided by the German Research Society (DFG) via the Sonderforschungsbereich 889. In the first three months, I was generously supported by a bridging gant of the Graduate School for Neurosciences, Biophysics, and Molecular Biosciences (GGNB). My greatest gratitude goes also to administration of my program, the International Max-Planck Research School (IMPRS) for Neurosciences, namely Prof. Michael Hörner and Sandra Drube for timely assistance and support in bureaucratic matters and beyond.